

UNIVERSITÀ DEGLI STUDI DI PAVIA

DIPARTIMENTO DI CHIMICA

CORSO DI LAUREA MAGISTRALE IN CHIMICA



**OPTIMIZATION OF CF₄ RECUPERATION FROM THE
GAS MIXTURE USED IN THE CSC GAS SYSTEM AT
THE COMPACT MUON SOLENOID (CMS) EXPERI-
MENT AT CERN**

**“Ottimizzazione del recupero di CF₄ dalla miscela gassosa impiegata
nei rivelatori CSC presso l’esperimento Compact Muon Solenoid
(CMS) al CERN”**

RELATORE:

Ch.ma Prof.ssa Antonella Profumo

CORRELATORI:

Dott.ssa Beatrice Mandelli

Dott. Roberto Guida

TESI DI LAUREA DI:

Maria Cristina Arena

Anno Accademico 2020/2021



Abstract

Optimization of CF₄ recuperation from the gas mixture used in the CSC gas system at the Compact Muon Solenoid (CMS) Experiment at CERN

Master Thesis by Maria Cristina Arena

The Compact Muon Solenoid (CMS) is one of the four Experiments operating at the Large Hadron Collider (LHC) at CERN. Since Muons represent a very clean probe for many events of interest, the Muon detection system has a fundamental importance for identification and a detailed characterization of particles collision in LHC Experiments.

Each muon station consists of several layers of aluminium drift tubes (DT) in the barrel region and cathode strip chambers (CSC) in the endcap region, complemented by resistive plate chambers (RPC), both in barrel and endcap region. The Muon detector system is based on gaseous detectors, which works through the gas ionization. The main component of gas detectors is the gas mixture that must be correct and stable for the properly functioning of systems and the use of expensive and greenhouse gases cannot be avoided because of physic requirements that impose certain choices on the gas mixture composition.

Therefore, the aim of this thesis consists in a detailed study of the CF₄ recuperation system, used for the CMS CSC detector (that operates with a gas mixture of Ar/CO₂/CF₄ 40/50/10), with the final goal of optimizing its economic and environmental efficiency. Based on warm separation process, the recovery system includes membranes and adsorption modules for CO₂ and CF₄ and an efficient CO₂ removal is mandatory to reach a good CF₄ adsorption capacity. The CF₄ Membrane Module and the CF₄ Absorber Module were studied and optimized in the light of gas chromatography measurements. The effects of experimental parameters affecting the overall functioning of the modules, such as the input flow stream and gas pressure, have been investigated. In the light of the experimental evidence reported in this Thesis, the new

membrane module setup and CF₄ absorber configuration ensure a remarkable increase of the average weekly efficiency from ~45% in the period November 2020-January 2021 to ~66% in the period February-June 2021.

Contents

RIASSUNTO	9
CHAPTER 1.....	25
INTRODUCTION	25
1.1 CERN AT LHC	25
1.2 “LHC EXPERIMENT MUON SYSTEM”	27
1.3 GAS IONIZATION PRINCIPLES	30
1.3.1 <i>Gas multiplication</i>	32
1.3.2 <i>Fill Gases</i>	33
1.3.3 <i>Gaseous ionization detector</i>	33
1.4 THE LHC GAS SYSTEM FOR MUON DETECTORS	36
CHAPTER 2.....	41
MONITORING OF THE CMS GAS SYSTEMS	41
2.1 COMPACT MUON SOLENOID AT LHC.....	41
2.1.1 <i>Drift Tubes</i>	42
2.1.2 <i>Resistive Plate Chambers</i>	42
2.1.3 <i>Cathode Strip Chambers</i>	43
2.1.4 <i>Gas Electron Multiplier detectors</i>	43
2.2 GAS CHROMATOGRAPHY AT THE LHC	44
2.3 GAS ANALYSIS WITH GAS CHROMATOGRAPH.....	46
2.4 ENVIRONMENTAL IMPACT OF GASEOUS DETECTOR OPERATION	50
2.4.1 <i>CERN strategies to reduce the emissions of Greenhouse gases from particle detection....</i>	52
CHAPTER 3.....	57
CF₄ RECUPERATION PLANT IN CMS-CSC GAS SYSTEM.....	57
3.1 CSC GAS SYSTEM.....	57
3.2 CF ₄ RECUPERATION PLANT	59
3.2.1 <i>CF₄ Membrane Module</i>	62
3.2.2 <i>CO₂ Absorber Module</i>	64
3.2.3 <i>CF₄ Absorber Module</i>	67
3.2.4 <i>CF₄ Storage and reuse</i>	68
3.3 PRINCIPLES OF MEMBRANES TECHNOLOGY	72
CHAPTER 4.....	76
OPTIMIZATION OF THE “CF₄ MEMBRANE MODULE” IN THE CF₄ RECOVERY PLANT (CSC-CMS)	76
4.1 MEMBRANES FOR CF ₄ SEPARATION	76
4.2 EXPERIMENTAL SETUP	80
4.2.1 <i>Test 1: E-Type Membrane</i>	82
4.2.2 <i>Test 2: CO-C10 Membrane</i>	86
4.2.3 <i>Test 3: CO-C10A Membranes</i>	89
4.2.4 <i>Test 4: C07FS Membrane</i>	93
4.2.5 <i>Test 5: Membrane CO-C410</i>	96
4.2.6 <i>Membranes tests: overview</i>	100
4.3 FLOW TEST ON THE CF ₄ MEMBRANE MODULE	101
4.3.1 <i>Flow Test: Overview</i>	106
4.4 PRESSURE TEST FOR THE CF ₄ MEMBRANE MODULE.....	106
4.4.1 <i>Pressure Test: Overview</i>	113

CHAPTER 5.....	116
OPTIMIZATION OF THE “CF₄ ABSORBER MODULE” IN THE CF₄ RECOVERY PLANT (CMS-CSC)	116
5.1 CF ₄ ABSORBER MODULE: OVERVIEW	116
5.2 STRUCTURE AND FUNCTIONING OF MOLECULAR SIEVE	118
5.3 WEEKLY ANALYSIS OF THE CF ₄ ABSORBER MODULE	119
5.3.1 <i>Analysis of complete cycle of CF₄ absorber module</i>	122
5.4 ANALYSIS OF THE RECUPERATED CF ₄ CONTAINED IN THE STORAGE BATTERIES	125
CONCLUSIONS	128
BIBLIOGRAPHY	132
ACKNOWLEDGEMENTS	137

Riassunto

Il lavoro di tesi è stato svolto presso il CERN (European Organization for Nuclear Research) di Ginevra nel dipartimento EP-DT-FS (Experimental Physics -Detector Technologies-Fluidic Systems) sotto la supervisione del Dottor Roberto Guida e della Dottoressa Beatrice Mandelli. Lo scopo del lavoro di tesi è stato quello di studiare, caratterizzare e ottimizzare i moduli dell'impianto di recupero del tetrafluorometano (CF_4) presso l'esperimento Cathode Muon Solenoid (CMS).

CMS è uno dei quattro grandi esperimenti situati lungo l'anello del Large Hadron Collider (LHC) che è l'acceleratore di particelle più grande e potente finora realizzato. È costruito all'interno di un tunnel sotterraneo di 27 km di circonferenza, a circa 100 m di profondità. Si tratta di un acceleratore di tipo circolare che può accelerare adroni (protoni e ioni pesanti) fino al 99,9999991% della velocità della luce e farli successivamente scontrare, con un'energia che ha raggiunto, nel centro di massa, i 13 TeV, molto vicina al limite teorico della macchina di 14 TeV. La macchina accelera due fasci di particelle che circolano in direzioni opposte, ciascuno contenuto in un tubo a vuoto. Questi collidono in quattro punti lungo l'orbita, in corrispondenza di caverne nelle quali il tunnel si allarga per lasciare spazio a grandi sale sperimentali. Qui si trovano i quattro principali esperimenti di fisica delle particelle: ATLAS (A Toroidal LHC Apparatus), CMS, LHCb (LHC-beauty) e ALICE (A Large Ion Collider Experiment) (Figura 1). Essi sono costituiti da numerosi rivelatori che utilizzano diverse tecnologie e operano intorno al punto in cui i fasci collidono. I numerosi rivelatori che costituiscono ciascun esperimento LHC sono suddivisi in tre principali categorie:

- Rivelatori interni (Inner Detectors): si trovano vicino ai punti di collisione, consentendo il rilevamento e la misurazione del momento delle particelle cariche.
- Calorimetro Adronico ed Elettromagnetico (HCAL/ECAL): misurano l'energia e direzione degli adroni (adronico), dei fotoni e degli elettroni (elettromagnetico).
- Spettrometro muonico: I muoni (rappresentati con il simbolo μ), sono delle particelle elementari molto simili agli elettroni ma con massa circa 207 volte superiore. Essi provengono dal decadimento delle particelle che si formano a

seguito della collisione dei due fasci di protoni (o fasci di ioni Pb nell'esperimento ALICE). Poiché i muoni sfuggono ai rivelatori più interni (inner detectors e calorimetri), per rivelarli è necessario utilizzare un sistema specifico e dedicato. All'interno dello spettrometro muonico è presente un sistema di tracker (Muon Tracker) che consente di registrare il percorso delle particelle e un sistema di trigger (Muon Trigger) che permette di identificare muoni che presentano un certo momento trasverso. In particolare, in questo lavoro di tesi è stato ottimizzato il recupero del componente della miscela gassosa impiegata in uno di questi rivelatori, Cathode Strip Chambers (CSC) di CMS.

Dal momento che nel punto di interazione tra i due fasci si generano circa ventidue collisioni a ogni incrocio e un incrocio si verifica ogni venticinque miliardesimi di secondo, il rivelatore utilizza un sistema di "trigger" per selezionare in tempo reale, tra questi milioni di eventi, i più significativi che più identificano i fenomeni fisici in esame.

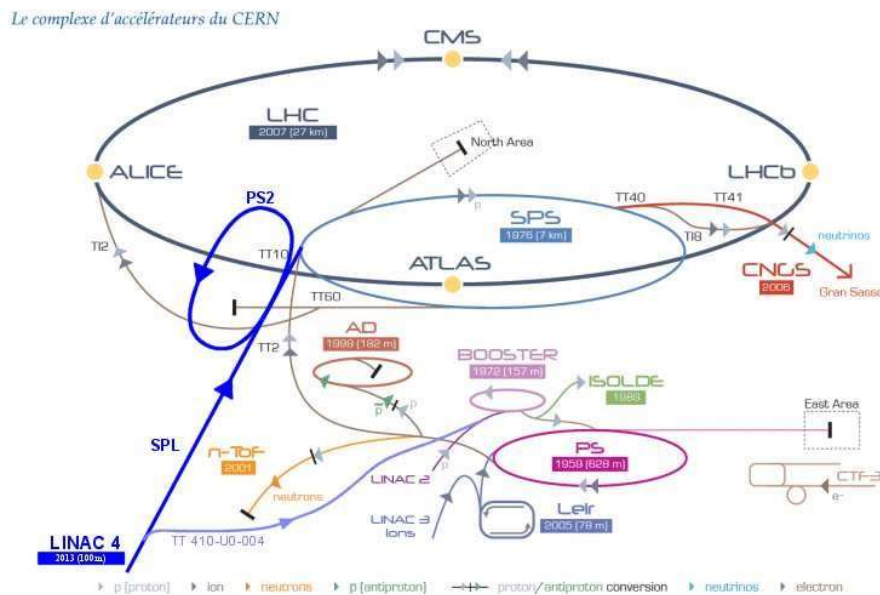


Figura 1: il Large Hadron Collider con i suoi punti sperimentali e i pre-acceleratori. I fasci di protoni e ioni pesanti cominciano il percorso agli acceleratori lineari (LINAC 4). Continuano il loro cammino nel Proton Synchrotron (PS), nel Super Proton Synchrotron (SPS) e giungono nell'anello esterno. Durante il percorso si trovano i quattro punti sperimentali in cui i fasci vengono fatti collidere: ATLAS, CMS, LHCb, ALICE.

Le CSC, dove è impiegato il CF_4 , sono rivelatori a gas specializzati nel rivelare muoni. In generale, un rivelatore a gas è un dispositivo che rivela la presenza di particelle: se una particella che attraversa un gas ha un'energia sufficiente per ionizzarlo vengono prodotte delle coppie elettrone-ione lungo la sua traccia. Queste coppie possono essere raccolte e ulteriormente moltiplicate usando un campo elettrico sufficientemente intenso che fa migrare gli elettroni verso l'anodo positivo e gli ioni positivi verso il catodo negativo.

Le CSC sono impiegate nella regione terminale dell'esperimento CMS, dove il campo magnetico è così intenso e disomogeneo da impedire di ottenere informazioni spaziotemporali precise. Esse sono costituite da filamenti (anodi) carichi positivamente che intersecano strisce di rame cariche negativamente (catodi), normalmente riempiti con una miscela di Ar (40%), CO_2 (50%) e CF_4 (10%). Tuttavia, per ridurre il consumo del CF_4 durante i periodi di manutenzione del sistema, le CSC sono riempite con una miscela Ar (40%), CO_2 (55%) e CF_4 (5%), che è stata la composizione della miscela durante lo svolgimento del lavoro di tesi. Quando un muone passa nella camera, questo ionizza il gas e induce la formazione della coppia elettrone-ione al suo interno. Gli elettroni si dirigono verso gli anodi creando la cosiddetta valanga (avalanche), gli ioni positivi si dirigono verso i catodi, inducendo una carica pulsata nelle strisce catodiche. Vengono, quindi, registrate le due coordinate spaziali per ciascuna particella.

In generale, la miscela gassosa impiegata nei rivelatori riveste un ruolo di primaria importanza poiché è responsabile del corretto funzionamento dei sistemi e della loro longevità. Il monitoraggio delle miscele risulta, quindi, fondamentale per verificare lo stato del sistema. A questo scopo, lo strumento normalmente scelto è il micro-GC, una versione compatta del classico gas-cromatografo, creato combinando le varie micro-componenti (micro-iniettore, colonne capillare, TCD). Con questo tipo di strumento si possono utilizzare colonne più corte di quelle del classico GC che garantiscono l'esecuzione dell'analisi nell'arco di pochi minuti. Accanto all'ottimizzazione del sistema di recupero del CF_4 , sono state anche condotte analisi bisettimanali presso l'esperimento CMS, per monitorare lo stato del modulo "Mixer" ed "Exhaust to Distribution" per i rivelatori DT (Drift Tubes: Ar (85 %), CO_2 (15%)), CSC e RPC (Resistive Plate Chambers; $\text{C}_2\text{H}_2\text{F}_4$ (95.2%), $\text{i-C}_4\text{H}_{10}$ (4.5%), SF_6 (0.3%)) (Figura 2).

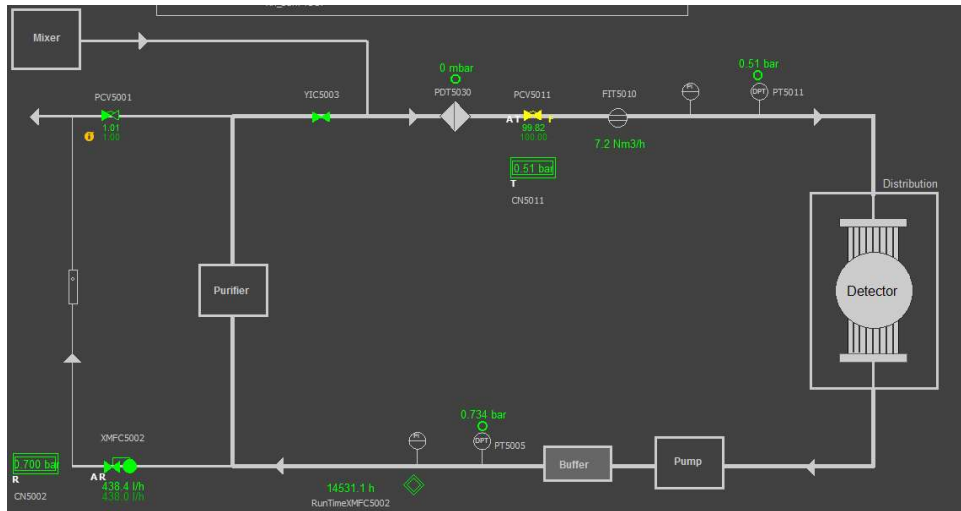


Figura 2: Schema del modulo Exhaust del rivelatore CSC: Mixer, Distribution, Pump, Buffer, Purifier.

Come appena visto, molti dei rivelatori degli esperimenti del LHC impiegano gas effetto serra (GHG) costosi, ma ciò non può essere evitato poichè la fisica dei dispositivi impone che vengano utilizzati specifiche miscele gassose. Un gas effetto serra (greenhouse gas - GHG) è definito come un gas che quando si trova in atmosfera assorbe ed emette radiazioni nel range dell'infrarosso. L'indice di Potenziale di Riscaldamento Globale (Global Warming Potential - GWP) dà una misura del calore che un gas effetto serra riesce a trattenere nell'atmosfera per un certo intervallo di tempo e definisce quanta energia può assorbire l'emissione di 1×10^3 kg di un certo gas per un periodo di tempo, confrontato con l'emissione di 1×10^3 kg di CO_2 . In particolare, gli idrofluorocarburi (CF_4 , $\text{C}_2\text{H}_2\text{F}_4$, ecc.), gli idrofluoroclorocarburi e l'esafluoruro di zolfo (SF_6) hanno un GWP migliaia di volte più elevato di quello della CO_2 .

Ridurre l'utilizzo di questi gas effetto serra costituisce uno degli obiettivi principali del CERN e in quest'ottica sono state sviluppate diverse strategie:

- Sistemi di ricircolo del gas
- Sistemi di recupero di gas
- Ricerca di nuovi gas con bassi GWP
- Costruzione di impianti per lo smaltimento di GHG per decomposizione in composti non pericolosi.

In seguito al grande volume del detector (100 m^3) e all'impiego del costoso CF_4 , il sistema a gas delle CSC era stato progettato per lavorare in ricircolo con meno del 5% di miscela fresca iniettata nel sistema. Tuttavia, dopo alcuni mesi, è stata rilevata un'importante presenza di aria all'interno della miscela in uscita dal detector, che ha costretto a portare al 10% la percentuale di miscela fresca da iniettare. In questo modo i livelli di O_2 risultano accettabili, grazie anche alla presenza di molecular sieve che ne permettono una quasi totale eliminazione, mentre N_2 non potendo essere rimosso, si accumula nel sistema fino a raggiungere concentrazioni dell'1%. Successivamente si è sviluppato un sistema di recupero per il CF_4 , il composto più pericoloso per l'ambiente e più costoso della miscela.

Il sistema di recupero si trova in superficie, nella gas room dell'esperimento CMS ed è costituito da quattro moduli (Figura 3):

1. Modulo membrane per la separazione della CO_2 .
2. Molecular Sieve 4\AA per la rimozione della restante CO_2 .
3. Molecular Sieve 13X per l'adsorbimento e il recupero del CF_4 .
4. Modulo di compressione e stoccaggio del CF_4 recuperato.

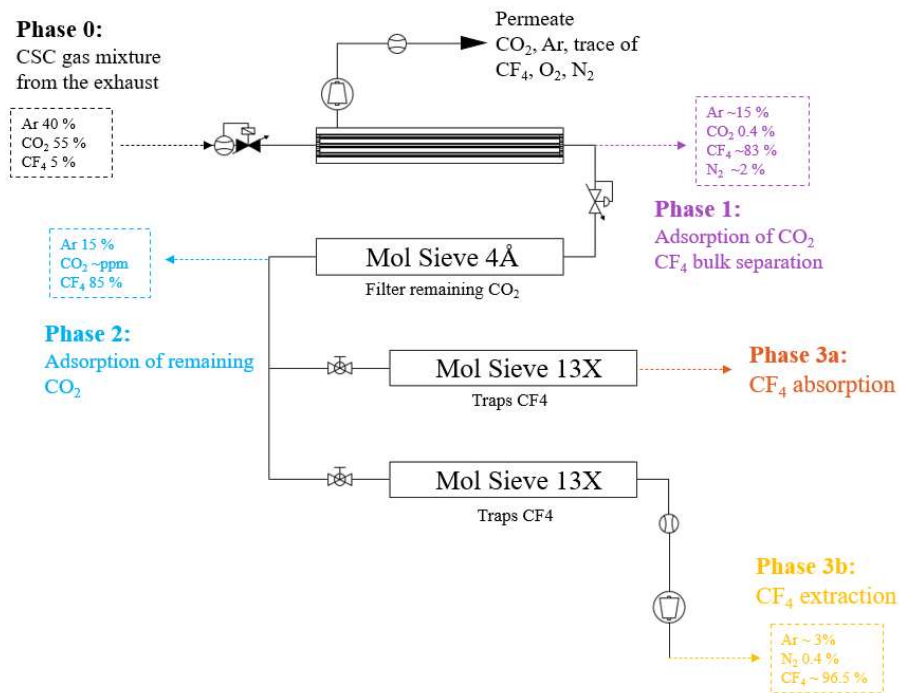


Figura 3: Schema dell'impianto di recupero del CF_4

Dal 2012 (anno della sua costruzione) ad oggi, l'efficienza globale del sistema dal 20% passando per il 50% (fine 2020), ha raggiunto il 65% nel periodo Febbraio-Giugno 2021.

La prima parte del lavoro di tesi ha riguardato lo studio e la caratterizzazione delle membrane del primo modulo dell'impianto e la caratterizzazione di nuovi modelli di membrane al fine di trovare la configurazione migliore del modulo per massimizzare l'efficienza di recupero del CF₄. Il rack è progettato per lavorare con 4 membrane, collegate in parallelo, della tipologia "*Hollow fiber membranes of polyimide Matrimid®5218*". Le fibre all'interno delle membrane sono costituite da multistrati (Kapton, Al, C, Molecular Sieve, polimeri) permeabili, nello specifico, alla CO₂. Tre delle quattro membrane hanno buone efficienze per flussi fino a 300 l/h, mentre la quarta presenta alta efficienza per flussi superiori a 600 l/h.

Il flusso in ingresso nella membrana viene diviso in due parti: Permeati (P) e Non Permeati (NP). I primi sono i componenti gassosi in grado di permeare la struttura della membrana e sono di solito i composti di interesse nella separazione, mentre i NP sono quei composti della miscela che vengono trattenuti dalla membrana. Nel caso specifico, il flusso di interesse è quello in uscita ai NP, dove appunto si ritrova il CF₄, dal momento che le membrane impiegate sono ottimizzate per la separazione della CO₂. Da una parte è cruciale che il gas in uscita ai non permeati contenga la massima quantità di CF₄, ma è anche importante che solo una minima quantità di CF₄ venga perso ai P. Ovvero, si potrebbe avere un CF₄ molto puro ai NP ma avendone perso una grande frazione ai P.

È necessario che ci sia un bilanciamento tra purezza e frazione e recuperata e in base a ciò, l'efficienza di separazione (ϵ) del CF₄ è espressa come:

$$\epsilon(CF_4) = \frac{volume(CF_4^{Output})}{volume(CF_4^{Input})}$$

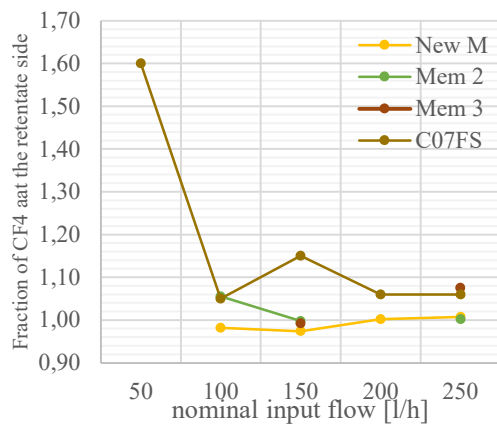
Durante ogni test le membrane sono state installate in un sistema progettato per poter controllare tutti i parametri fondamentali come il flusso in ingresso alla membrana, il flusso e la pressione in uscita ai P e ai NP. Il gradiente di pressione negativo ai P è stato mantenuto con l'ausilio di una pompa a vuoto e la composizione dei flussi ai P e

NP è stata monitorata tramite analisi gas cromatografiche, in base alle quali è stata valutata l'efficienza di ciascuna membrana.

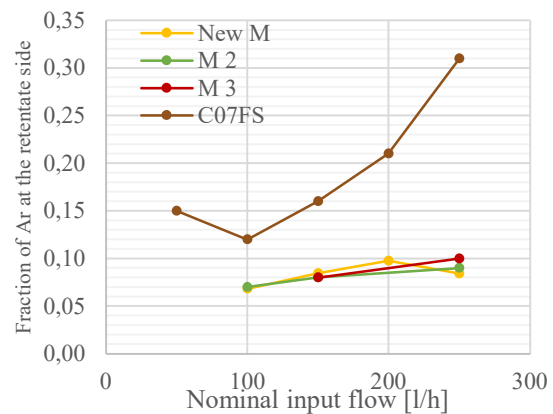
Nome	Modello	Flusso di lavoro	Caratteristiche
Vecchia membrana 1	E-type	Fino a 300 l/h	Elevato spessore e nessun gradiente di densità
Nuova Membrana 1	CO-C10	Fino a 300 l/h	Elevato spessore e gradiente di densità
Membrana 2	CO-C10A	Fino a 300 l/h	Elevato spessore e gradiente di densità
Membrana 3	CO-C10A	Fino a 300 l/h	Elevato spessore e gradiente di densità
M. Altamente selettiva	CO-C07FS	Fino a 300 l/h	Ridotto spessore e gradiente di densità
Membrana 4	CO-C410A	> 600 l/h	Elevato spessore e gradiente di densità

Tabella 1: Membrane testate e loro caratteristiche fondamentali.

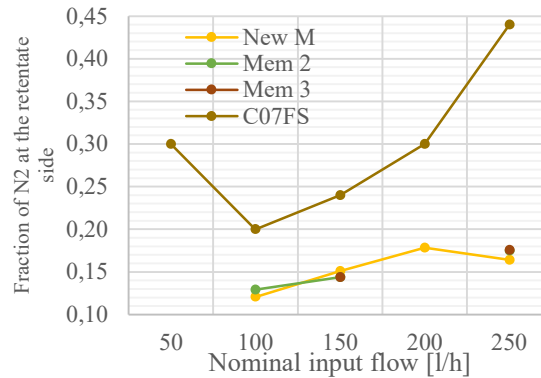
In Tabella 1 sono riassunti i risultati ottenuti per le membrane testate.



a)



b)



c)

FIGURE 1: Confronto tra le membrane testate (ad esclusione della E-Type e della CO-C410); a) Frazione di CF_4 ai Non permeati; b) Frazione di Ar ai Non permeati; c) Frazione di N_2 ai Non permeati.

I risultati dei test hanno mostrato che il vecchio modello di membrana E-Type ha un'efficienza molto bassa, come già riscontrato durante altri test negli anni precedenti, ed è stato confermato che non può essere utilizzata nel modulo a causa dell'elevata frazione di CF_4 persa ai P. Per questo motivo non è stata inclusa nel confronto con le altre membrane testate. Le membrane 2, 3 (modello CO-C10A) e la nuova membrana CO-C10 hanno un comportamento simile nell'intervallo di flusso testato. Con queste membrane si ottiene una buona separazione dei componenti della miscela gassosa, una buona qualità di CF_4 in uscita ai NP anche a elevati flussi in ingresso alla membrana (200-250 l/h), con una piccola frazione di contaminanti (Ar e N_2) che viene parzialmente ridotta nei moduli successivi. La membrana altamente sensibile CO-C07FS ha una buona efficienza di separazione, anche se una grossa frazione di Ar e N_2 (~ 30%) permea la membrana, e di conseguenza il CF_4 recuperato presenta un elevato grado di contaminazione. Ne segue che questo tipo di membrana non è la soluzione migliore per il sistema di recupero poiché inciderebbe sulla qualità del gas recuperato.

La migliore configurazione del modulo membrane del CF_4 , considerando le attuali condizioni di lavoro, prevede l'impiego delle due membrane CO-C10A e della membrana più grande, la CO-410A. Per una portata media in ingresso di 600 l/h, le 3 membrane lavorano rispettivamente a 150 l/h e 300 l/h, flussi ai quali le membrane presentano buone efficienze di separazione.

<i>Composizione del gas in uscita ai NP</i>						<i>Frazione [%] ai NP</i>				
<i>Flusso nominale [l/h]</i>	<i>CF₄ [%]</i>	<i>CO₂ [%]</i>	<i>Ar [%]</i>	<i>O₂ [ppm]</i>	<i>N₂ [ppm]</i>	<i>CF₄</i>	<i>CO₂</i>	<i>Ar</i>	<i>O₂</i>	<i>N₂</i>
400	91.0	0.4	8.0	22	7301	69.2	0.03	0.78	0.3	1.9
500	83.0	0.4	15.3	77	19000	74.0	0.03	1.81	0.3	4.5
600	74.0	0.5	23.4	83	26700	77.5	0.05	3.26	0.3	7.4
700	65.5	0.4	31.2	100	31825	80.7	0.04	5.09	0.4	10.3
800	57.2	0.8	39.4	50	26242	86.5	0.11	7.67	1.5	13.7

Tabella 2: Riassunto dei test effettuati con variazione del flusso all'input del modulo membrane

In Tabella 2 sono riassunti i dati relativi al test effettuato sull'intero modulo membrane in cui sono stati valutati gli effetti dovuti alla *variazione di flusso* in ingresso al modulo. È chiaro come all'aumentare del flusso di input, la composizione del gas in uscita ai NP cambi, arricchendosi in contaminanti come Ar e N₂ con conseguente diminuzione della concentrazione di CF₄ (evidenziato in blu).

$$Frazione\ del\ componente\ X\ in\ NP\ (o\ P) = \frac{Flusso\ di\ X\ ai\ NP\ (o\ P)}{Flusso\ input \times X[\%]}$$

Tuttavia, nella seconda parte della Tabella 2 (Frazione [%] ai NP) si può notare come la *frazione* del CF₄, calcolata come sopra, aumenti all'aumentare del flusso, indicando quindi un aumento dell'efficienza di separazione. Ne segue che l'ideale è lavorare a flussi elevati oppure diminuire il numero di membrane per lavorare nel range di flusso ottimale per ciascuna membrana.

<i>Composizione del gas in uscita ai NP</i>							
<i>[l/h]</i>	<i>P [bar]</i>	<i>CF₄ [%]</i>	<i>CO₂ [%]</i>	<i>Ar [%]</i>	<i>O₂ [ppm]</i>	<i>N₂ [ppm]</i>	<i>Frazione di CF₄ [%]</i>
418	-0.45	79.6	1.2	17.8	61	12421	70.8
418	-0.6	89.9	0.6	8.5	42	6504	67.5
626	-0.35	64.8	0.6	33.2	58	22052	81.9
626	-0.44	72.7	0.5	24.8	43	18157	78.5
626	-0.6	86.5	0.2	12.6	22	10470	75.9
835	-0.45	70.4	0.13	28.4	26	18836	82.4
835	-0.6	83.9	0.05	15.3	21	13520	79.0

Tabella 3: Riassunto dei test effettuati con variazione della pressione ai Permeati nel modulo membrane

L'ultimo test effettuato nell'ambito della prima parte del lavoro di tesi è riassunto in Tabella 3. In questo caso è stato valutato l'effetto della *variazione di pressione ai Permeati* sulla composizione della miscela in uscita ai NP e sulla frazione di CF₄ recuperato. Sono stati testati i flussi 400, 600 e 800 l/h e per ciascuno di essi è emerso che in seguito alla diminuzione di pressione ai Permeati, ai NP si ottiene un gas ricco in CF₄ con una drastica diminuzione della contaminazione di Ar e N₂ (Es. dati evidenziati in rosso in Tabella 3). Per quanto concerne invece la frazione di CF₄ recuperata ai NP, si può chiaramente vedere come questa non subisca modificazioni significative in conseguenza della diminuzione della pressione ai Permeati.

In seguito a questo test è stata messa in funzione una seconda pompa a vuoto nel modulo membrane, per garantire una pressione intorno a -0.6 bar per un flusso di input di circa 600 l/h.

La seconda parte del lavoro di tesi ha riguardato l'ottimizzazione del modulo "CF₄ Absorber", contenente due colonne riempite con setacci molecolari, il molecular sieve 13X, caratterizzato da un diametro dei pori di 10Å, in grado di adsorbire solo il CF₄ (che ha un diametro cinetico di 4.8Å), lasciando liberi Ar e N₂ (con diametri cinetici di 3.4 e 3.64Å, rispettivamente).

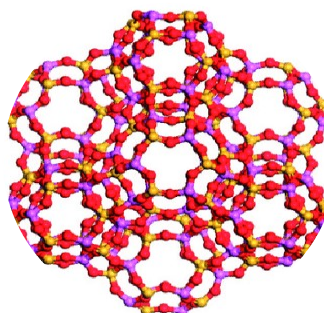


Figura 4: Layout della struttura del molecular sieve 13X

L'adsorbimento è basato sul metodo della Pressure Swing Adsorption: parte dal vuoto e si arresta quando la pressione relativa all'interno della cartuccia è pari a zero o alla pressione nella linea del supply.

Il contaminante principale in seguito alla fase di separazione resta N₂, a una concentrazione di circa 0,9%.

A seguito del test effettuato sul modulo membrane, è stato possibile trovare una correlazione tra il flusso in ingresso nel primo modulo e l'efficienza dell'intero sistema di recupero del CF₄. Per monitorare lo stato del sistema, oltre a tenere conto dei parametri sul software WinCCOA, si è deciso di effettuare le analisi GC del modulo CF₄ Absorber una volta alla settimana. Nella Tabella 4 sono riassunte alcune delle analisi effettuate durante i mesi.

Date	Ar [%]	CF₄ [%]	CO₂ [%]	O₂ ppm	N₂ ppm
07/10/2020	2.22	97.23	0.016	400	3860
13/11/2020	1.13	97.41	0.066	175	2175
10/12/2020	21.03	78.00	0.054	420	24766
14/01/2021	17.14	80.95	0.014	458	37625
08/02/2021	2.09	97.38	0.020	628	4996
10/03/2021	2.88	95.37	0.004	111	4460
09/04/2021	3.85	94.49	0.019	137	5095
11/05/2021	2.05	97.67	0.016	179	2881
08/06/2021	1.78	97.16	0.006	173	2646

Tabella 4: Riassunto dei test settimanali del gas proveniente dal modulo "CF₄ absorber"

Negli ultimi mesi l'andamento della contaminazione di Ar e N₂ e la concentrazione di CF₄ sono rimasti stabili ad eccezione dei mesi di dicembre e gennaio (evidenziati in rosso in tabella) durante i quali le analisi hanno mostrato un andamento anomalo, raggiungendo una contaminazione del ~20%, probabilmente per l'ampia fluttuazione del flusso dal modulo Exhaust all'impianto di recupero.

La concentrazione di Ar è stata calcolata sottraendo la concentrazione di N₂, poiché il picco di N₂ è visibile anche nella colonna PPU dove questi sono sovrapposti (Figura 5).

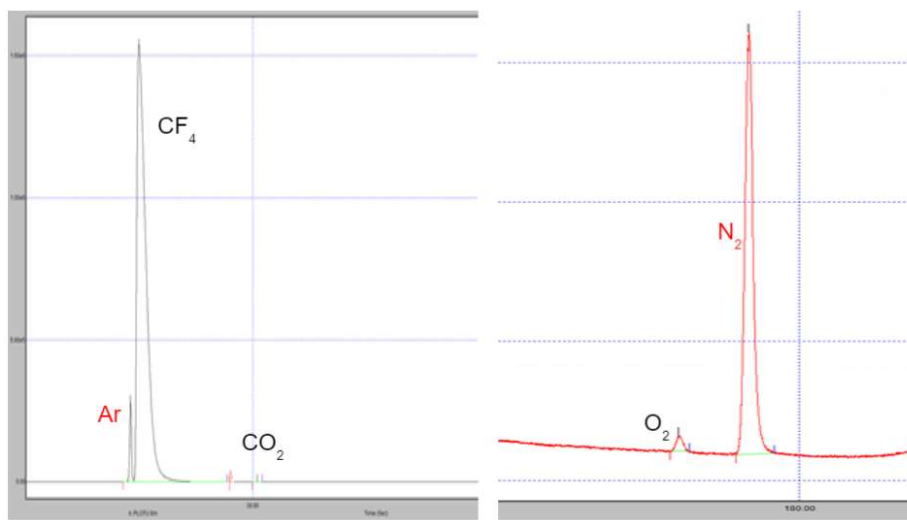


Figura 5: Tipico esempio di cromatogramma del gas in uscita dal modulo CF₄ absorber

Inizialmente la fase di recupero del CF₄ dal setaccio molecolare iniziava ad una pressione nella colonna di -0,7 bar, con un'efficienza totale del sistema molto bassa. Di conseguenza, in seguito ai test effettuati si è deciso di modificare i parametri di pressione di svuotamento della colonna, aumentando la pressione iniziale della fase di recupero da -0,7 bar a -0,45 bar. È stata poi monitorata la variazione di efficienza totale del sistema ed è stato verificato se ci fosse una sostanziale perdita di CF₄ nelle condizioni precedenti. In seguito a questa modifica si è riscontrato un effettivo aumento dell'efficienza globale del sistema senza perdite in termini di purezza del CF₄ recuperato, come riscontrabile dalla Tabella 4.

Inoltre, durante le analisi μ GC sono stati monitorati i parametri del modulo CF_4 absorber, ed è stata osservata una variazione della concentrazione di Ar alle diverse pressioni all'interno della colonna.

Si è quindi reso necessario eseguire delle analisi durante l'intero ciclo di separazione per comprendere meglio l'andamento della concentrazione del CF_4 e dell'Ar. I risultati ottenuti sono di seguito riportati.

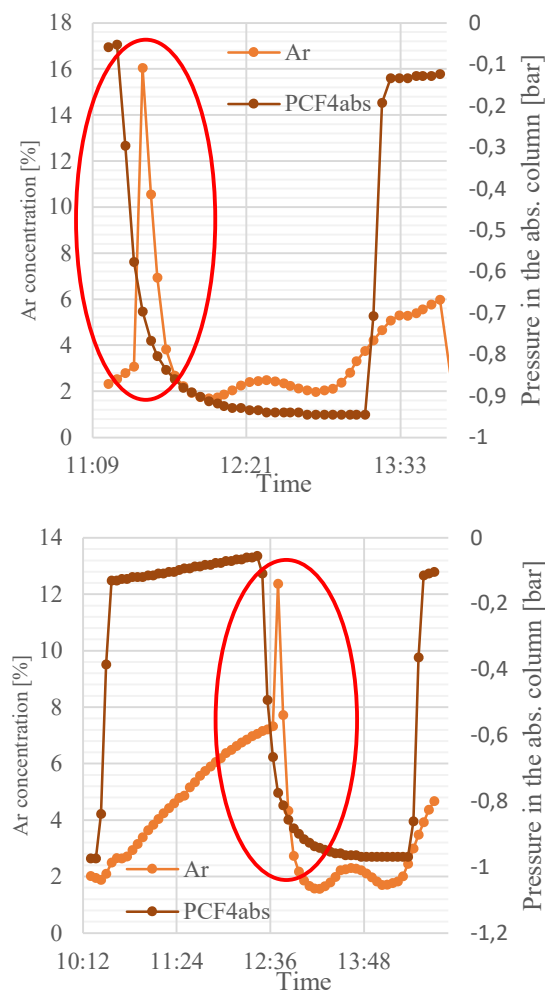


Figura 6: Focus sul trend della concentrazione di Ar vs pressione nella colonna dell'absorber

Come si può vedere dalla Figura 6, la concentrazione di Ar presenta un picco in prossimità della pressione alla quale inizia il recupero del CF₄ dalla colonna. Ciò è probabilmente dovuto alla bassa velocità di mescolamento dei componenti in uscita dalla colonna stessa durante le diverse fasi del modulo.

Al fine di comprendere meglio l'andamento della concentrazione di Ar, le possibili cause derivanti dal sistema (come valvole o perdite) e per quantificare il contenuto di Ar nel CF₄ recuperato, sono state eseguite delle analisi del gas recuperato nella batteria utilizzata per ri-iniezione del CF₄ nel detector. Le analisi, riassunte nella tabella successiva, sono state eseguite sia prima che dopo la modifica dei parametri di svuotamento della colonna.

Analysis	Date	Ar [%]	CF ₄ [%]	CO ₂ [%]	O ₂ ppm	N ₂ ppm
1	27/01/2021	8.6	90.4	0.002	81	9053
2	16/02/2021	8.7	90.8	0.010	86	9168
3	24/02/2021	10.3	88.9	0.012	251	13205
4	20/05/2021	7.0	92.3	0.015	99	7800
5	29/06/2021	7.0	93.9	0.020	90	7377

Tabella 5: Riassunto delle analisi del CF₄ nel modulo batteria

Dalla Tabella 5 si evince come la composizione del gas recuperato sia nettamente migliorata in seguito alla modifica della pressione alla quale ha inizio il recupero del CF₄, confermando quanto precedentemente visto con le analisi settimanali. Il miglior risultato si è ottenuto nell'analisi numero 5 dove è stata raggiunta la minima contaminazione di Ar e N₂ e la massima concentrazione di CF₄.

Questi risultati confermano che la nuova configurazione del modulo membrane per la separazione del CF₄ e i nuovi parametri del modulo absorber consentono di ottenere un CF₄ più puro senza sostanziali perdite di CF₄ e senza compromettere l'efficienza globale del sistema.

A seguito di questi test, la frazione di CF₄ recuperato reiniettato nel sistema CSC è stata modificata per la prima volta dal 50% al 60%, anche per via della grande quantità di gas recuperato nelle batterie.

Infine, le modifiche apportate al sistema hanno portato ad un miglioramento dell'efficienza media settimanale dal ~45% nel periodo novembre 2020-gennaio 2021, al ~66% nel periodo febbraio- giugno 2021.

Per migliorare ulteriormente l'impianto e ottenere un CF₄ più puro, potrebbe essere utile testare le membrane in serie per ottenere un CF₄ più puro e testare membrane basate su nuove tecnologie per una migliore rimozione di Ar e N₂.

Chapter 1

Introduction

1.1 CERN at LHC

The European Organization for Nuclear Research (CERN) carries on physics program based on the studies of the Standard Model as well as to the search of New Physics and, to fulfil its requirement, the Large Hadron Collider (LHC) has been made.

The LHC is the world's largest and most powerful particle accelerator, and it consists of a 27-kilometre ring of superconducting magnets, lying 100m underground, with several accelerating structures to boost the energy of the particles along the way.

The functioning of the accelerator is based on two high-energy particle beams traveling at close to the speed of light before they are made to collide. The beams travel in opposite directions in separate beam pipes kept under ultra-high vacuum. They are guided around the accelerator ring by a strong magnetic field ensured by superconducting electromagnets.

The working temperature of this magnets is -271.3°C (1.8 K) – a temperature colder than outer space.

Primary protons are obtained from Helium, and they are accelerated in a first linear collider (LINAC), to be then injected in the chain of circular accelerators that allows the achievement of their maximum energy (6.5TeV). Protons pass through the Proton Synchrotron (PS, 25GeV), the Super Proton Synchrotron (SPS, 450GeV) and finally are injected in the LHC (Figure 1).

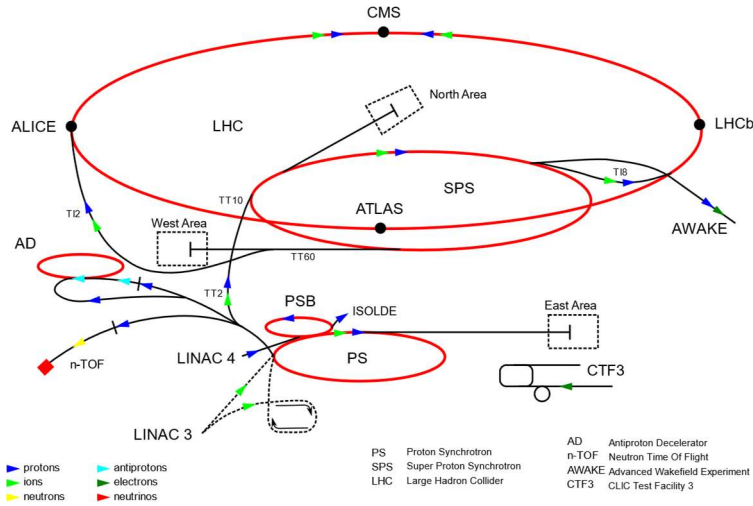


FIGURE 2: Schematic drawing of the LHC complex layout, with accelerators and experiments

The beams inside the LHC are made to collide at four locations around the accelerator that correspond to the four Experiments: ATLAS, CMS, ALICE and LHCb [1]. The CERN accelerator complex accelerates protons, but also nuclei of ionized atoms (ions), such as the nuclei of lead (Pb), argon (Ar) or xenon (Xe) atoms. Some LHC runs are thus dedicated to lead-ion collisions.

ATLAS (A Toroidal LHC apparatus) and CMS (Compact Muon Solenoid) are the two general purpose Experiments that were developed for exploring all the possible aspects of the LHC physics (from the search for the Higgs boson to extra dimensions and particles that could make up dark matter) and for searching new particles. ALICE (A Large Ion Collider) Experiment is designed to study the physics of strongly interacting matter at extreme energy densities, while LHCb (Large Hadron Collider beauty) Experiment specializes in investigating the differences between matter and antimatter by studying a type of particle called the "beauty quark", or "b quark".

Even if each Experiment has a specific purpose, the requirements on the detectors of which they are made are quite the same. Their main aim is to identify charged particles and measure particles momentum with high resolution, and it is possible identifying three main different parts of LHC Experiments:

- Inner Detectors:

Located close to the collision points, they allow the tracking and momentum measurement of charged particles, as well as Interaction Point and vertices reconstruction.

- Hadronic and Electromagnetic Calorimeters:

They measure the energy of hadrons, photons and electrons crossing their volume, based on the energy loss of emerging particles.

- Muon systems:

Since Muons escape the electromagnetic calorimeter, a dedicated Muon system is used to detect them. Typically placed at the outermost layers of the experiments, it allows to unambiguously detect the signature of many relevant events. These systems will be discussed later since gas analysis for gaseous detectors is the focus of this thesis.

1.2 “LHC Experiment Muon System”

Muon detection is fundamental for a complete identification and characterization of particles collision in LHC Experiments since Muons represent a very clean probe for many events of interest. For this reason, each Experiment is equipped with a Muon detector system, made of detectors capable of identifying and tracking these particles.

- **ALICE [2]**

To fulfil the ALICE physics program requirements, the Muon spectrometer is located downstream of the ALICE detector, covering the angular range $171^\circ < \theta < 178^\circ$. It consists of three absorbers, a Muon magnet, a trigger system and a tracking system, shown in Figure 2. The trigger system (Muon Trigger system, MTR) allows to efficiently trigger high pT Muons, exploiting the full luminosity¹ potential of the LHC heavy ion beams.

¹ In accelerator physics, the *luminosity* is a measure of the performance of the accelerator and describes how many events N are occurring in a certain time t with an interaction cross-section σ as: $\frac{dN}{dt} = L \cdot \sigma$. The integrated luminosity instead expresses the cumulative luminosity over a given time period and it

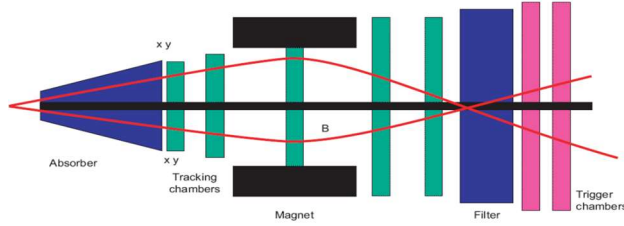


FIGURE 3: ALICE Muon System

The system consists of 4 planes of 18 Resistive Plate Chamber detectors (RPCs) each, operating in avalanche saturated mode. Signals are collected by individual strips along the RPCs length and treated by a dual threshold discriminator. Information from the 4 trigger planes is processed by the local hardware cards, determining roughly the transverse momentum of the Muon track.

- **ATLAS [3]**

The ATLAS Muon spectrometer forms the outer part of the Experiment, and it is designed to detect charged particles exiting the barrel and end-cap calorimeters.

The subsections of the Muon System are

- Thin Gap Chambers, located in the end-cap region, are capable of delivering track information within a few tens of nanoseconds after the passage of the particle (trigger system).
- Resistive Plate Chambers, located in the barrel region, are used for the same purpose of TGC.
- Monitored Drift Tubes, provide the measurement of the precision momentum and consist of three to eight layers of drift tubes, operated at an absolute pressure of 3 bar, which achieve an average resolution of $80 \mu\text{m}$ per tube, or about $35 \mu\text{m}$ per chamber. To reach such resolution, a high-precision optical alignment system monitors the positions and internal deformations of the MDT chambers.
- Cathode Strip Chambers, used in the innermost tracking layer due to their higher rate capability and time resolution.

gives a measure of the total amount of events. The High-Luminosity Large Hadron Collider (HL-LHC) project aims to increase the integrated luminosity by a factor of 10.

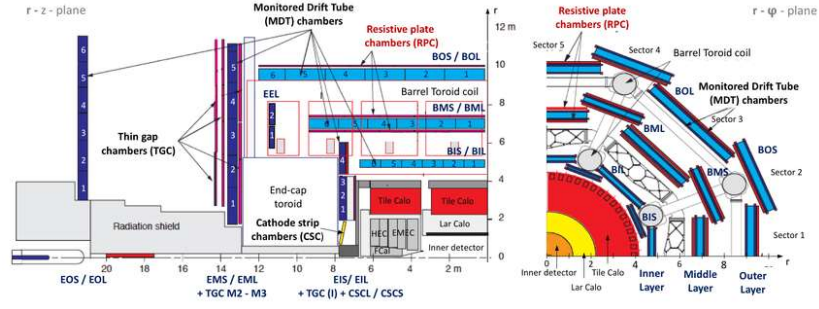


FIGURE 4: ATLAS muon system layout

- CMS [4]

The CMS experiment structure is based on a super-conducting solenoid, that produces a 3.8 T magnetic field. The iron yoke is equipped with a Muon spectrometer for identification, triggering and momentum measurement. To fulfil its requirement, the Experiment is equipped with three types of detectors that use different technologies. DT (Drift Tubes) measure muon positions in the barrel part of the detector, RPC (Resistive Plate Chambers) give a quick measure of the muon momentum, which is then used by the trigger to make immediate decisions about whether the data are worth keeping. RPCs combine a good spatial resolution with a time resolution of just one nanosecond and CSC (Cathode strip Chambers) are used in the endcap disks where the magnetic field is uneven and particle rates are high. Because the strips and the wires are perpendicular, we get two position coordinates for each passing particle.

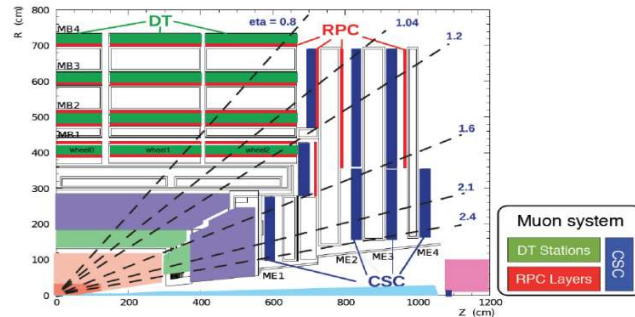


FIGURE 5: CMS muon system layout

- **LHCb [5]**

The Muon detection system is fundamental in the LHCb Experiment since Muons are present in the final states of many CP-sensitive B decays. The system provides fast information for high pT Muon trigger at the earliest level of online event selection, as well as Muon identification for the high-level trigger and offline analysis.

The Muon system is composed of five stations (M1-M4) and each station is equipped with 276 Multi Wire Proportional Chambers (MWPCs, 5 mm gas gap), except for the high-rate region, where 12 double layers of Triple Gas Electron Multipliers (GEMs) were installed until Run 2. The stations consist of two mechanically independent parts, side A and C, that can be horizontally moved to access the beam pipe and the chambers for maintenance, and each of them is divided into four regions (R1-R4) with increasing distance from the beam axis.

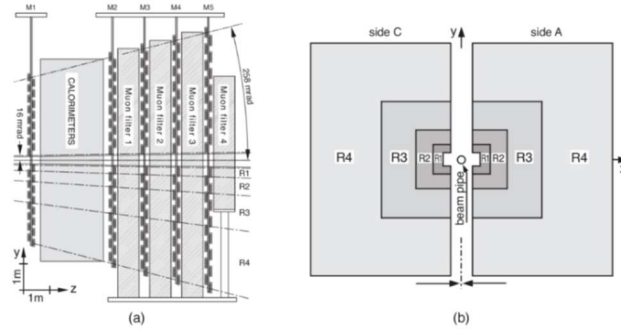
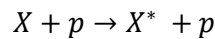


FIGURE 6: LHCb muon system layout

1.3 Gas ionization principles

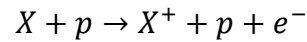
The Muon detector system is based on gaseous detectors, which works through the gas ionization.

When a charged particle passes through a gas causes a series of inelastic interactions that result in excitation and ionization of molecules or atoms. The schematic reaction of the X species' excitation is:



where p is the charged particle. In atoms, the excitation energy is absorbed by the orbiting electrons that are raised to higher distinct energy levels while in a molecule, the energy is absorbed not only by the electrons, which are excited to higher energy levels, but also by the whole molecule, which is excited to discrete modes of vibration and rotation [6].

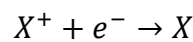
The schematic reaction of the X species' ionization is:



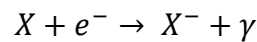
in this process is necessary that the energy of charged particle is higher than ionization potential of the X species. This interaction is known as *primary ionization* and an electron-ion pair is created. The electron produced in this process can have enough energy to ionize another molecule producing a secondary ion pair. The sum of the two contributions takes the name of *total ionization*.

These reactions affect the efficiency and the energy resolution of the detector. In fact, it is important that the produced pairs remain separate so long as they are collected by the detector readout system since their recombination and electron attachment does not permit this operation.

If not under the effect of an electrical field they recombine because of their electrical attraction:



Electronegative species can capture free electrons to form negative ions:



If any electronegative gases are present, for ex. O_2 , H_2O or SF_6 , the efficiency of the ion-electron collection diminishes. On the contrary, noble gas have negative electron affinity [7].

1.3.1 Gas multiplication

When a low electric field is applied in a gas volume, electrons and ions created by an incident radiation simply drift to their collecting electrodes and when the field is properly increased, there is an intensification of the gas multiplication process.

Free electrons are easily accelerated by the applied field, gaining kinetic energy. When this energy is greater than the ionization energy of the gas molecules, secondary ionization can occur in the collision between the free electron and neutral gas molecules, producing an additional ion pair. The electron from secondary ionization can be accelerated by the field, undergoing collisions during its subsequent drift, and thus creating additional ionization. The gas multiplication process takes the form of a cascade, the so-called Townsend avalanche. Each free electron created can potentially create more free electrons. Under proper conditions, the amount of secondary ionization events can be multiplied by a factor of many thousands.

For a particular value of the applied voltage, hence of the electric field inside the gas volume, the collected charge begins to multiply, and the observed pulse amplitude increases (proportional region). Over most of this region, the gas multiplication is linear, and the collected charge is then proportional to the number of original ion pairs created by the incident radiation. The region of true proportionality represents the usual operation mode of gas-filled proportional counters. If the applied voltage is further increased, non-linear effects occur, drifting in a limited-proportionality region [8].

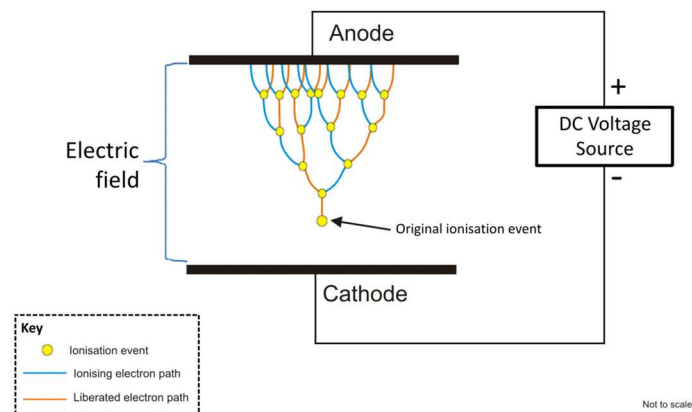


FIGURE 7: Visualisation of a Townsend Avalanche

1.3.2 Fill Gases

Argon is the noble gas most commonly used in gaseous detector due to its chemical properties and a generally limited cost. It has a very low *electron attachment coefficient*, allowing for most of the free electrons to reach the multiplication region without significant interference. However, it should be considered that, besides to a simple ionization, the collision between electrons and neutral gas molecules may give rise to excitation, without the creation of a secondary electron. The excited molecules decay to their ground state, through the emission of a visible or ultraviolet photon, that may create additional ionization elsewhere in the gas. These events are normally undesirable since they may reduce the proportionality. Furthermore, they cause the avalanche to spread.

It has been found that the addition of a certain quantity of polyatomic gas, such as Carbon Dioxide (CO_2) or the $\text{i-C}_4\text{H}_{10}$, can suppress the photon-induced effects by absorbing the photons in a way that does not lead to further ionization. The polyatomic component is usually present in some concentration with the monatomic one, as a stabilizing additive and each muon detectors work with different nominal gas mixture. Another crucial point is to maintain the purity of the chosen gas, that can be obtained with a continuous flow through the chamber. It can be a once-through type, in which the gas simply exhausted to atmosphere, or a recirculation type, with the purification of the gas before re-injection. Traces of oxygen or other impurities must be removed since they can cause significant losses of free electrons [8].

1.3.3 Gaseous ionization detector

Gaseous detectors used in the Muon system exploit the gaseous ionization capability for detecting the presence of particle.

This type of detectors consists of a gas volume structured in such a way that a continuous gas flow can pass and fill the system. Since gas has a great mobility of ions and electrons, it is used as medium for the collection of ionization from radiation.

At the beginning were widely used gas ionization counters, those with a cylindrical system, also called “counting tubes”.

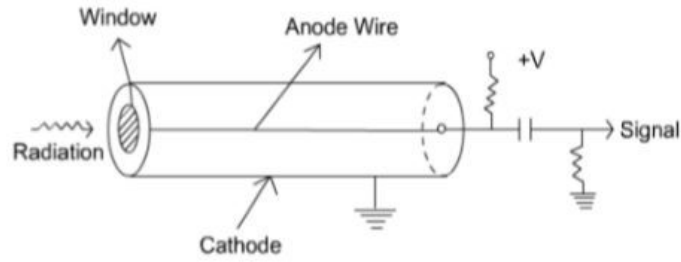


FIGURE 8: Wire chambers detectors layout

The structure of a wire chamber gaseous detector is shown in Figure 7: the outer wall serves as the cathode (positive charged electrode), while a rod, a grid or a plate in the middle of the gas volume serves as the anode. An electric field is applied to the electrodes and consequently in the gas volume.

However, if an electric field is applied, the positive and negative specimens are attracted respectively to cathode and anode while, if the electric field is absent, ions and electrons move away from the point of creation by diffusion.

If the electric field has properly strength, the applied voltage prevents the ions-electrons recombination and these specimens arrive at the electrodes to be collected.

The signal is produced by the drift of electrons and ions (not by the collection of charge at the electrodes) [9] and the gas parameters influencing the ionization detectors performance are:

- Ionisation potential (eV)
- Energy loss required to produce an electron ion pair (eV). Part of the energy is lost to excite the medium. Noble gases are preferred due to the absence of vibration and rotation states, so ionisation dominates.
- Number of primary electrons reduced by:
 - Recombination: $X^+ + e^- \rightarrow X + \gamma$
 - e^- attachment: $X + e^- \rightarrow X^- + \gamma$

Gas counters may be operated in different operation modes depending on the applied high voltage:

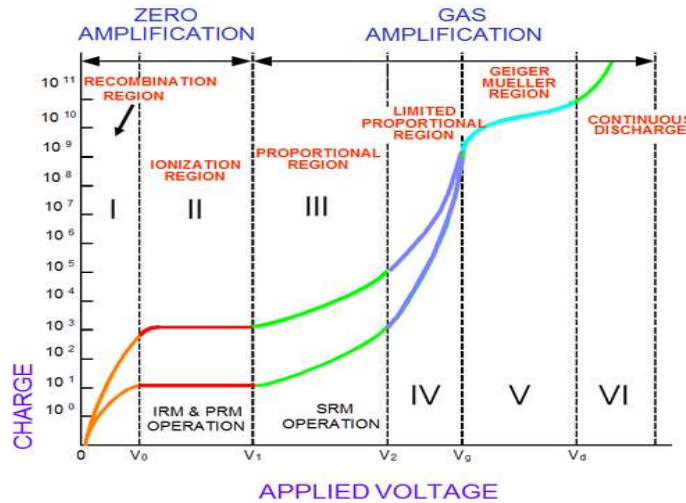


FIGURE 9: Relationship between the pulse size produced and the potential applied across the electrodes

- The *Ionization Region* operates at a voltage which allows full collection of charges, but it is not high enough for the amplification of signal. This means that electric field has not the strength to accelerate the electrons and no secondary ions are created. All created pairs are collected and a further increase in the applied voltage shows no effect.
- In the *Proportional region* the voltage applied produces an electric field strong enough to accelerate free electrons. At this point free primary electrons have enough energy to ionise again gas molecules producing secondary electrons. The electrons released in these secondary ionizations are accelerated to produce still more ionization giving rise to a cascade of electrons known as “avalanche”. The result is a proportional amplification of the current. The number of electron-ion pairs in the avalanche is directly proportional to the number of primary electrons.
- In the *Limited proportional Region and Geiger Muller region* the voltage is increased, ionization becomes sufficiently large that the charge created warps the electric field about the anode. As a result, proportionality is lost. Continuing to increase voltage, the energy becomes so large that a discharge occurs in the gas and chain reaction of many avalanches takes place all along the anode. These secondary avalanches are caused by photons emitted by de-energised

molecules. The output current becomes saturated and gives the same amplitude regardless of the energy of the initial event. To stop the discharge a quenching gas must be present to absorb the photons.

1.4 The LHC Gas System for Muon detectors

The main component of gaseous detectors is the gas mixture that must be correct and stable for the properly functioning of systems. Each detector system, regardless of its aim, has its own gas system.

The role of the gas systems is to mix the different component of the gas mixture in the right proportion and to distribute the resulting mixture to the corresponding detectors. High reliability is necessary to guarantee the stability and quality of gas mixture, since it is the primary element influencing the detector performance. The LHC gas systems are characterized by a common structure that, if needed, can be adapted to each gas detector requirements; it is made of many modules, each of which has its own function and their pipes extension can reach several hundreds of meters.

The modules are associated with a Programmable Logic Controller (PLC) unit, that manages and controls the units. The software used for controlling the system is based on the WinCC-OA SCADA tool, where is possible finding information about the status of the system and, in general, it is possible to control the device and have information about the interactions between two modules. The collected data are stored in a database and is possible to consult them through a custom graphical user interface [10].

The gas system modules of LHC Experiments are located in three different places: in the Surface room (SG), in the Underground service room (US) and in the Experimental cavern (UX). From the surface gas room, the gas mixture is sent to the Underground gas room where there is the pre-distribution system as well as part of the gas system parameters regulation. The latter part of gas distribution takes place in the UX, from the service gas balcony racks. The figure below reports a schematic layout of an LHC gas system.

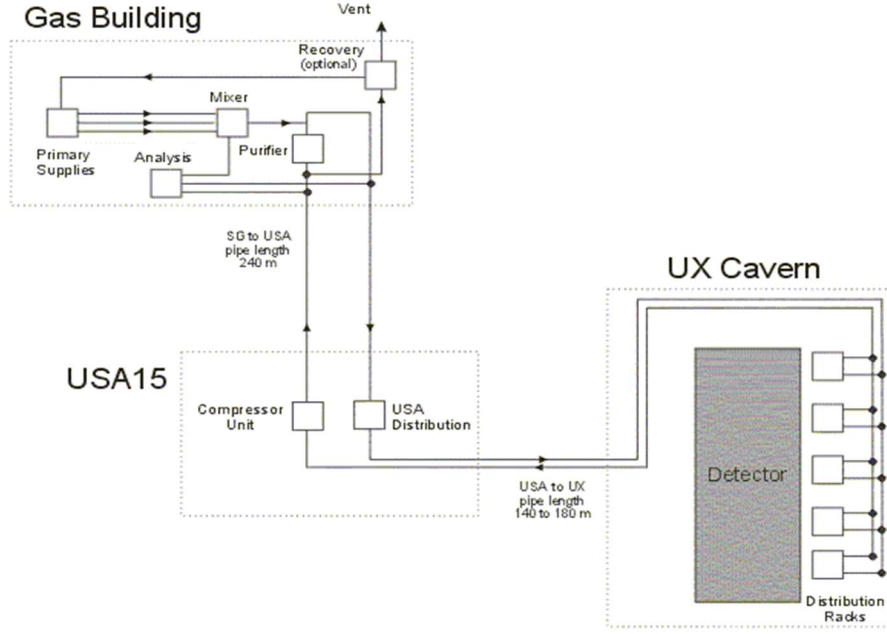


FIGURE 10: Layout of basic modules of an LHC gas system

The single modules are briefly described in the followings.

- **Primary Gas Supply:**

For each gas there are two independent supply sources, one in use and one in stand-by, that can compensate when there is a failure in the main one and during replacement of the storage tanks.

- **Mixer Module:**

Primary gases are used to prepare the gas mixture for each detector. Mixer modules have up to four input lines, equipped with Mass Flow Controllers (MFCs), controlled via the software control system to set the correct concentration of each component of the gas mixture. In particular, for each fresh gas, two MFCs are installed with different volume flow ranges, since the gas systems needs different flows according to the operation status (run, fill, purge). The gas mixture is prepared with a precision given by the MFCs which is: $0.5\% Rd \pm 0.1\% FS$.

- **Gas Distribution:**

Several steps are needed to distribute the gas mixture to each detector, with precise gas volume flow and pressure. Pre-distribution modules are located in

the US, and they are related to different detector sectors of the Detector System. The gas is sent from the US to the UX, where the final distribution modules are located, and each gas line is split into several smaller lines, to distribute the gas with the required granularity. The UG and US distribution levels can be accessed and controlled during LHC runs if necessary. The gas mixture coming from the exhaust of the chambers is re-grouped into return modules.

- **Pump Module:**

Once the gas has flown from the UX into the return modules, the pump module compresses the gas to a higher pressure in way to send it back to the surface.

- **Exhaust Module:**

In the basic gas systems, the gas passes through the exhaust module, where volume flow and pressure regulations allow to manage the gas emission in relation to the gas system parameters which are subject to specific requirements, for example the chamber pressure stability.

- **Purifier Module:**

In the recirculation gas systems, the return gas is re-injected in the system and a purifier module allows to remove or reduce the impurities typically accumulated along the gas path, in the gas system elements or directly in the detectors volume. Impurities can be originated in various ways from leaks to chemical reaction happening when the gas is subject to irradiation and electric field (creation of avalanche, which creates further e- that can break easily the molecules). The most common impurities are N₂, O₂ and H₂O, but only the last two can be easily removed through adsorption filters.

The purifier module consists of two 24-liters cartridges, filled with suitable material that interacts with the specific impurity such as Molecular sieves used for H₂O removals and metallic catalysts for O₂ absorption.

- **Gas Analysis Module:**

The gas analysis module allows a continuous monitoring of the gas mixture quality in the critical gas system points (after mixer, exhaust, after purifier). Normally, O₂, H₂O and InfraRed (iC₄H₁₀, CO₂) analysers are present, to measure the concentration of impurities and relevant mixture components. In some

cases, the analysis module has an integrated system to perform Gas Chromatograph analysis on selected sample lines, in a way to obtain a more complete measurement of all the gas mixture components.

Chapter 2

Monitoring of the CMS Gas Systems

2.1 Compact Muon Solenoid at LHC

The Compact Muon Solenoid (CMS) is one of the four Experiments operating at the Large Hadron Collider (LHC). It is a multi-purpose detector located 100 metres underground with a cylindrical symmetry and it is composed of 4 different types of detectors:

- Tracking system provides for a precise and efficient measurement of the trajectories of charged particles emerging from the LHC collisions
- Electromagnetic calorimeter (ECAL) for measuring the energies of photons and electrons
- Hadronic calorimeter (HCAL) measures the energy of hadrons
- Muon system, to detect muon particles, which are 200 times heavier than electrons and escape from calorimeters

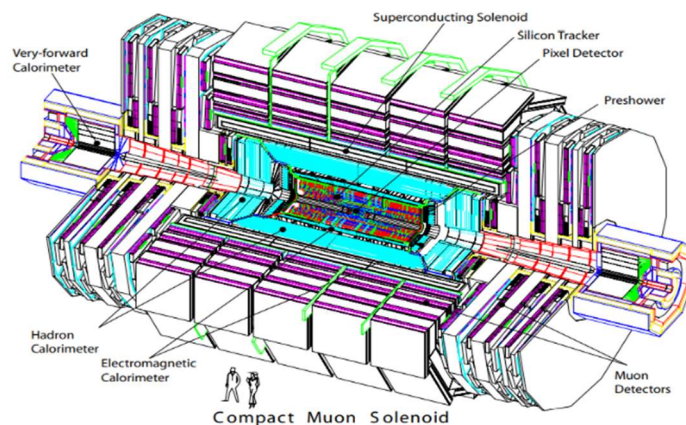


FIGURE 11: CMS overall layout

The core of CMS is a 13-m-long, 6-m-inner-diameter, 4-T superconducting solenoid providing a large bending power (12 Tm) before the muon bending angle is measured

by the muon system. The return field is large enough to saturate 1.5 m of iron, allowing 4 muon stations to be integrated to ensure robustness and full geometric coverage. Each muon station consists of several layers of aluminium drift tubes (DT) in the barrel region and cathode strip chambers (CSC) in the endcap region, complemented by resistive plate chambers (RPC), both in barrel and endcap reg [11].

2.1.1 Drift Tubes

Drift Tubes are used for the Muon's path reconstruction and they are located in the Barrel region. Each tube contains a wire with large pitch and the tubes are arranged in layers.

When a muon passes through the DT, it forms electron-ion pairs inside the gas mixture, the electrons follow the electric field and end up at the positively charged wire.

The DTs operate with a gas mixture of 85% Ar and 15% CO₂ that has good quenching properties.

Since electron drift velocity² is one of the most important parameters for DT detectors, a definite precision on the gas mixture supplied to the chamber must be ensured [12].

2.1.2 Resistive Plate Chambers

Resistive Plate Chambers are gaseous detectors which aim to provide a muon trigger in both the barrel and end cap regions. They are characterized by fast response, good time resolution, flexibility in segmentation, robustness and by the relative low cost of production.

The RPCs use a constant and uniform electric field produced by two resistive parallel electrode plates. The 2mm thick gap between these two plates is filled with a gas mixture of Freon R134a (C₂H₂F₄) 95.2%, isobutane 4.5% and SF₆ 0.3%, that has high

² In the absence of electric field, electrons move randomly in all direction having an average thermal energy $3/2 KT$. In presence of an electric field, the electrons start to drift along the field direction with mean drift velocity v_d (the average distance covered by the drift electron per unit time). The drift velocity depends on the pressure, temperature and could be affected by the presence of pollutants like water or oxygen. Electronegative pollutant depletes the gas of electrons.

absorption coefficient to ultraviolet light. When charged particles pass through the gas, the gas atoms ionize and form electron-ion pairs. The electron goes to the positive electrode and discharge is originated by the electric field. The discharge is prevented from propagation through the whole gas by the high resistivity of the electrodes [12].

2.1.3 Cathode Strip Chambers

Cathode strip chambers are employed in the end cap regions where the magnetic field is very intense (up to several Tesla) and very inhomogeneous to provide precise space and time information. It consists of positively charged wires (anode) crossed with negatively charged copper strips (cathode) filled with a gas mixture of Ar 40%, CO₂ 50%, CF₄ 10%. To reduce the waste of CF₄ during maintenance periods, the CSCs are filled with a gas mixture of Ar 40%, CO₂ 55%, CF₄ 5%. When a muon passes through the chamber it ionizes the gas and forms electron-ion pairs inside it. The electrons go to the anode wires creating an avalanche, the positive ions move toward the copper cathode strips, inducing a charge pulse in the strip. Two position coordinates for each particle are recorded.

In addition to providing precise space and time information, the closely spaced wires (2mm) make the CSC a fast detector suitable for triggering [12].

2.1.4 Gas Electron Multiplier detectors

GEMs belong to the class of Micro-Pattern Gaseous Detectors. Their basic element is an electrode made with a 5 μm Kapton film, covered with a Copper coating. The electrode is covered in bi-conical holes, of 70 μm diameter and with 140 μm pitch. When an electric field is applied across the foil, each hole acts locally as a proportional amplifier for the electrons created by charged particle ionization in the drift.

GEMs are currently installed in LHCb Muon System, and they are planned to be installed in CMS Endcaps during the upgrades taking place in LS2. GEMs are useful in high-rate regions, as they have better performance than other gaseous chambers. GEMs standard gas mixture is composed by 70% of Argon and 30% of CO₂. Alternative mixtures have been studied, finding advantages in the addition of CF₄ to the standard one. In particular, the mixture Ar/CO₂/CF₄ in proportions 45/15/40 was found to be a good choice. It allows to reach a sufficiently high gain without excessive high

voltage on the foils, while the presence of CF_4 significantly enhances the time resolution of the detector [13].

2.2 Gas Chromatography at the LHC

For the proper functioning of the LHC Experiments gas systems, the monitoring of the gas mixture is fundamental since it allows to have constant information about the status of the system. For this purpose, the instrument of choice is generally a micro-GC, a compact Gas Chromatograph created by the integration of micro-fabricated components. The basic elements of the instrument are a micro injector, one or more analytical columns and dedicated Thermal Conductivity Detectors (TCDs). The advantage of this type of device is to have analytical columns that are much shorter than the ones of a standard Chromatograph, allowing to perform analysis in the time span of some minutes.

For what concerning the analyses performed at the CMS experiment, the status of Mixer module and Exhaust to Distribution Module is bi-weekly monitored for DT, CSC and RPC detectors. For each detector mixture was developed a dedicated “method” in the μGC , in which temperatures and pressures are set to ensure the best components separation.

Analytical parameters

Method: C:\Soprane\Method\DT

Module: ☒ Module A (PPU) ☒ Module B (MSSA) ☐ Module C ☐ Module D

Inlet temp. (°C) ☒ 100.00

Inject temp. (°C) ☒ 75.00 ☒ 85.00 ☐ ☐

Column temp. (°C) ☒ 65.00 ☒ 115.00 ☐ ☐

Pump (sampling time) (s) Pump1: 60.00 Pump2: 60.00

Sampling time (s) 60.00 60.00

Inject time (ms) 25.00 100.00

Backflush time (s)

Run time (s) 240.00 240.00

Column pressure (psi) ☒ 28.00 ☒ 33.00 ☐ ☐

Detector ☒ ON ☒ ON ☐ OFF ☐ OFF

Sensitivity Standard Standard

Progr. Temp./ Press. Prog. A Prog. B Prog. C Prog. D

New Save as Print Send meth. chromat. Param. Cancel OK

a)

Analytical parameters

Method: C:\Soprane\Method\RPC_Mix_ON

Module A ☒ Module B ☒ Module C ☐ Module D ☐

Module PPU MS5A

Inlet temp. (°C) ☒ 100.00

Inject temp. (°C) ☒ 80.00 ☒ 85.00 ☐ ☐

Column temp. (°C) ☒ 95.00 ☒ 105.00 ☐ ☐

Pump (sampling time) (s) Pump1: 60.00 Pump2: 60.00

Sampling time (s) 60.00 60.00

Inject time (ms) 25.00 100.00

Backflush time (s)

Run time (s) 240.00 240.00

Column pressure (psi) ☒ 28.00 ☒ 33.00 ☐ ☐

Detector ☒ ON ☒ ON ☐ OFF ☐ OFF

Sensitivity Standard Standard

Progr. Temp./ Press. Prog A Prog B Prog C Prog D

New Save as Print Send meth. chromat. Param. Cancel OK

b)

Analytical parameters

Method: C:\Soprane\Method\CSC_onCold

Module A ☒ Module B ☒ Module C ☐ Module D ☐

Module PPU MS5A

Inlet temp. (°C) ☒ 100.00

Inject temp. (°C) ☒ 60.00 ☒ 85.00 ☐ ☐

Column temp. (°C) ☒ 45.00 ☒ 115.00 ☐ ☐

Pump (sampling time) (s) Pump1: 10.00 Pump2: 10.00

Sampling time (s) 10.00 10.00

Inject time (ms) 25.00 100.00

Backflush time (s)

Run time (s) 210.00 210.00

Column pressure (psi) ☒ 28.00 ☒ 33.00 ☐ ☐

Detector ☒ ON ☒ ON ☐ OFF ☐ OFF

Sensitivity Standard Standard

Progr. Temp./ Press. Prog A Prog B Prog C Prog D

New Save as Print Send meth. chromat. Param. Cancel OK

c)

FIGURE 12: μ GC methods for a) DT, b) RPC and c) CSC mixtures analyses

As shown in FIGURE 12, each gas mixture needs an analytical method to ensure the separation of the components in the mixture and the importance of these parameters will be explained in the next paragraphs.

2.3 Gas Analysis with Gas Chromatograph

For what concerns gas analysis in the LHC Experiments gas systems, the instrument of choice is generally a micro-GC, a compact Gas Chromatograph created by the integration of micro-fabricated components. The basic elements of the instrument are a micro injector, one or more analytical columns and dedicated Thermal Conductivity Detectors (TCDs). The advantage of this type of device is to have analytical columns that are much shorter than the ones of a standard Chromatograph, allowing to perform analysis in the time span of some minutes.

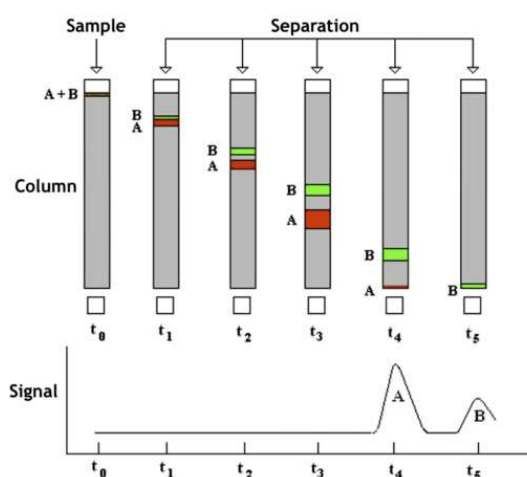


Figure 13: Schematic representation of the separation process inside a μ Gc column

The gas mixture under analysis is injected into the micro-GC through a micro injector, along with a carrier gas which can be Ar, He, H₂ or N₂, depending on the specific properties of the column type of choice and the analysed mixture. The column temperature is controlled by an oven and separates the mixture into its component gases in typically less than 180 s. The separation occurs thanks to the specific chemical species that coats the inside surface of column which has different interaction strength with the mixture components.

There are two types of columns, the capillary and the packed ones. The GC at CMS is a μ GC Agilent R3000 equipped only with capillary columns of two different types:

- **PPlotU:** Porous Layer Open Tubular column. Stationary phase is Divinylbenzene/Ethylen glycoldimethacrylate. It separates C₁ to C₄ hydrocarbons, CO₂, CH₄, H₂O, H₂S, SO₂, and N₂O.

- **MolSieve:** 5Å zeolite molecular sieve. It separates permanent and noble gases: Ne, H₂, O₂, Ar, N₂, CH₄, CO.
- **OV1:** made of 100% Polydimethylsiloxane, designed to separate hydrocarbons from C₄ to C₁₂, BTEX, and VOC.

Basically, achieving quality separations involves understanding and optimizing the effect of many variables including column type and length, choice of the carrier gas and temperature of the column.

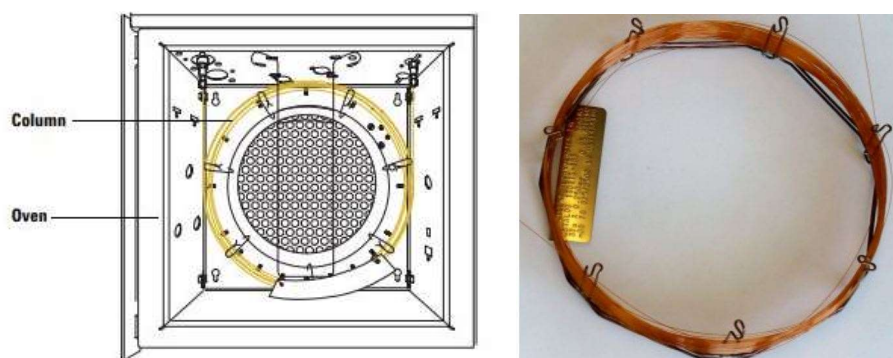


FIGURE 14: Drawing of a capillary column in an oven: a typical uGC column

The different components are detected by a Thermal Conductivity Detector (TCD), which output signal is proportional to the amount of gas exiting from the column. The plot over time of the electrical signal is a chromatogram, where each peak represents a different component. The peak retention time is used to identify each component while the peak size (height or area) is a measurement of the concentration.

It consists of electrically heated filaments in a temperature-controlled cell. The filaments change their resistance according to the different thermal conductivities of different compounds. The change in resistance is then measured with a Wheatstone bridge circuit, which produces a voltage signal. One way of the Wheatstone bridge is reserved to the reference gas (pure carrier gas). The second way is reserved to the analytical column flow. This flow is constituted by pure carrier gas or contains molecules from the sample. When the analytical way flow is pure carrier gas, bridge is equilibrated and signal is zero. When the analytical flow contains other molecules, the heat capacities of the polyatomic sample molecules cause fluctuations in the filament

temperature. The bridge is unbalanced and the signal is amplified by the electronics to get the chromatogram. The reference gas (carrier gas) passes through R1 filaments (FIGURE 15). Analytical flow from the column passes through the S1 filaments. Pins 1 and 3 give the measurement of the signal. Pins 2 and 4 are for the electrical supply of the bridge.

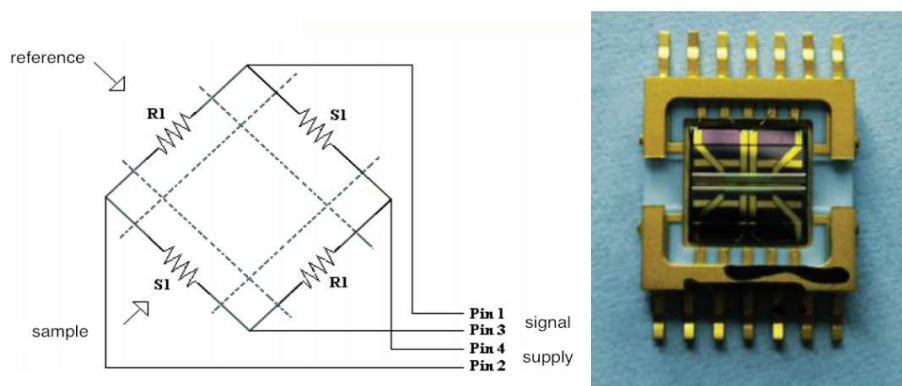


FIGURE 15: Wheatstone bridge scheme (left); universal detector based on Micro Electro-Mechanical System (MEMS) 10 times more sensitive than conventional Thermal Conductivity Detectors (right).

Once the chromatogram is obtained, it is processed offline. The voltage signal produced by the TCD is then proportional to the concentration of the analyte: the dynamic response starts from few ppm to 100%, with a proportionality area-concentration that is linear for concentrations in the range 0-20% but flattens above the 20-30%. A proper calibration is needed to be able to compute the concentration value from the raw signal (measured in μV).

FIGURE 16 reports an example of a chromatogram, where there CMS CSC gas mixture was analysed. The analysis refers to the PPU column, where the three mixture components, Ar/CO₂/CF₄ are present and the peaks are well separated.

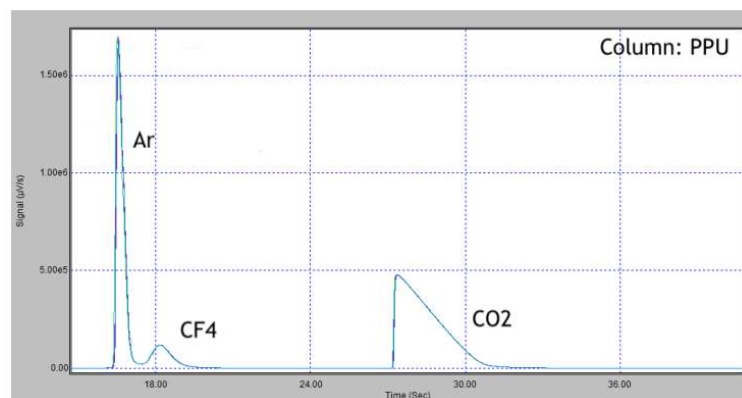


FIGURE 16: Chromatogram of the CMS CSC gas mixture from the PPU analysis column

As regards the MolSieve column, the analyses of the CMS CSC gas system are reported in FIGURE 17. The chromatograms are useful to detect and quantify O_2 and N_2 , well separated into two distinct peaks. It can be seen how the mixture composition at mixer level is very pure, while impurities are measured in the sample returning from the system, which is then purified of the accumulated O_2 by the action of the Purifier material.

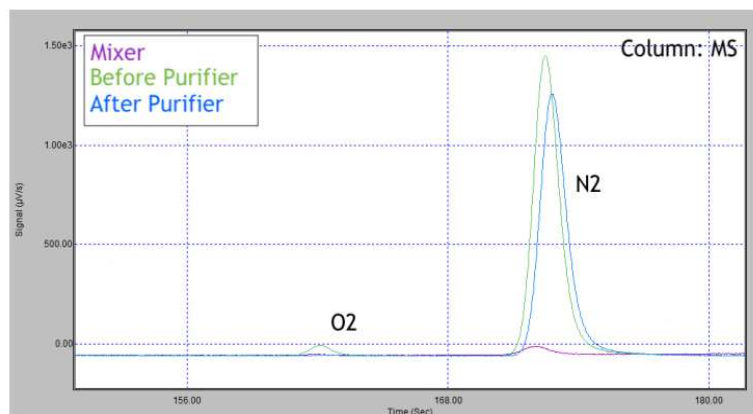


FIGURE 17: Chromatogram of the CMS CSC gas mixture in three different analysis points, from the MolSieve column

Finally, the FIGURE 18 reports the calibration measurements realized for the CMS CSC gas mixture, the one concerning the CF_4 concentration. The plot shows the trend of the conversion factor variation obtained measuring the area of CF_4 peaks in reference mixtures of increasing nominal CF_4 content (5% - 100%). It can be seen how the trend is approximately linear for lower concentration values, but then the curve slope

progressively decreases. It is therefore fundamental to have a calibration with a reference mixture in which the concentration of the relevant component is as close as possible to the one of the sample mixtures, to avoid inaccuracies in the concentration calculation.

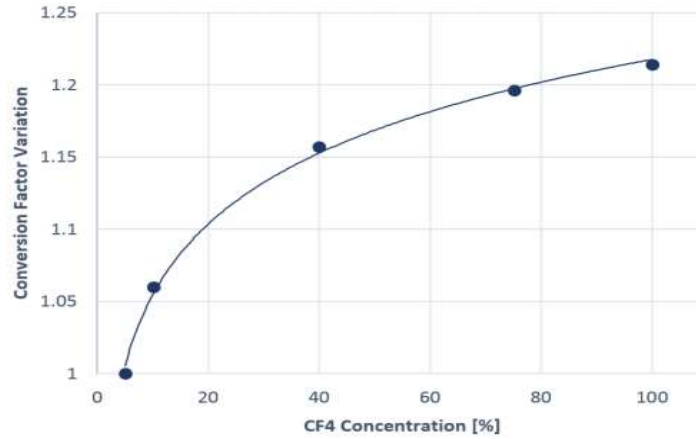


FIGURE 18: Example of CF_4 calibration curve, obtained analysing mixture with known concentration of CF_4 [14]

2.4 Environmental impact of gaseous detector operation

Over the 4 experiments (ALICE, ATLAS, CMS and LHCb) taking data at the CERN Large Hadron Collider (LHC) more than 28 gas systems are delivering the proper gas mixture to the corresponding detectors. In some cases, the use of expensive and greenhouse gases cannot be avoided because of physics requirements that impose certain choice on the gas mixture. A Greenhouse gas (GHG) is defined as a gas that, when in atmosphere, absorbs and emits radiation within the thermal infrared range [14]. A measure of how much heat a GHG traps in the atmosphere in a fixed time span is the Global Warming Potential (GWP) index. The GWP defines how much energy the emission of 1×10^3 kg of a gas would absorb over a period of time, relative to the emission of 1×10^3 kg of CO_2 . The GWP index strongly depends both on his radiation absorption spectrum in the infrared (radiative activity) and on lifetime of the gas in the atmosphere. In particular, hydrofluorocarbons (HFCs), hydro-chlorofluorocarbons (HCFCs), and sulphur hexafluoride (SF_6) have high GWP as, for a given amount of mass, they trap thousands or tens of thousands times more heat than CO_2 .

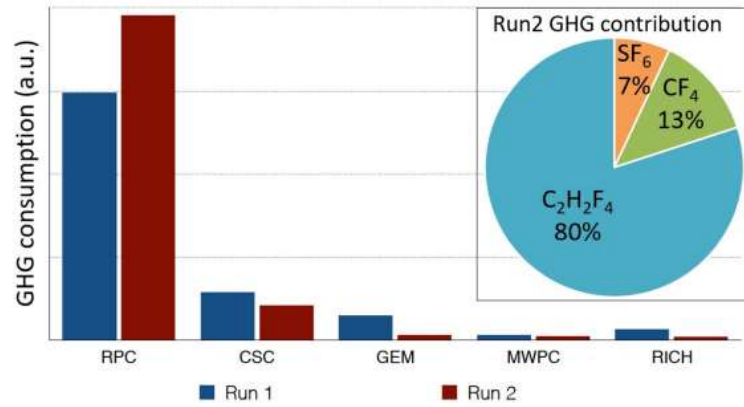


FIGURE 19: GHG emissions from detector systems at the LHC experiments [15]

Reducing the use of GHGs is a worldwide objective to which CERN wants to contribute. ATLAS and CMS experiments are the main contributors due to their large detector volumes (up to 100 m³) while ALICE and LHCb contributes about 12% each one [16]. The overall GHG contribution comes from C₂H₂F₄ (71%), CF₄ (20%) and SF₆ (9%), which are widely employed at the four LHC experiments mainly for the RPC, Cathode Strip Chambers (CSC) and Gas Electron Multiplier (GEM) detectors during Run 2.

In a very basic gas system, the gas mixture is prepared and it is sent to the detector. After the detector, the gas mixture is vented to atmosphere. This type of gas system is characterized by simplicity and standard monitoring system is required. However, this approach is not sustainable due to the very high GHG emission to atmosphere.

Several approach with different level of complexity can be adopted to control the gas consumption. In particular, four types of intervention were identified and they will be described in the following [17].

2.4.1 CERN strategies to reduce the emissions of Greenhouse gases from particle detection

Four different strategies have been identified to optimize the gas usage [15]:

- Gas recirculation systems
- Gas recuperation systems
- Search for new environmentally friendly gases for particle detectors
- Development of plants for the disposal of greenhouse gases by decomposition in harmless compounds

The first three approaches in the list will be briefly described and their application on LHC experiments will be explained while the last one, the development of plants for the disposal of greenhouse gases by decomposition in harmless compounds is nowadays discarded. Systems for the disposal of GHG have been developed by industry, but GHGs are normally very stable compounds hence very difficult to treat. This option would come at great infrastructure cost and complexity, as well as it would lack on addressing the GHGs unavailability and price increase.

- ***Gas recirculation system***

In the first phases of LHC gas systems design, the possibility of re-using the gas mixture multiple times was considered in case of large detector volumes or usage of expensive gases to limit their consumption. When a gas system is operated in recirculation mode, the gas mixture is collected after being used in the detector, passed through the Purifier module to undergo purification processes and be re-injected in the system. The maximum recirculation rate is fixed by detector leak or need of controlling impurities that cannot be filtered (i.e., N_2).

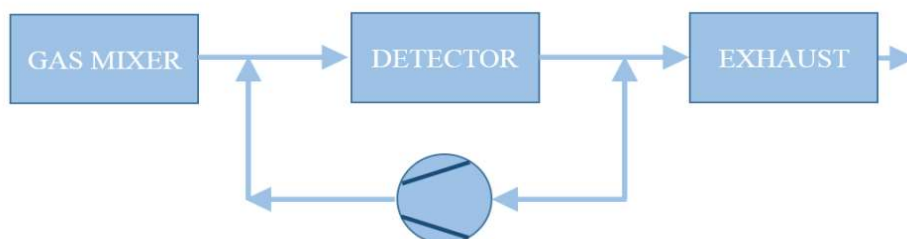


FIGURE 20: Schematic view of the gas recirculation system

The advantage of using this gas system is that the gas consumption can be drastically reduced since the fraction of recirculated gas can be above the 99% level.

In the LHC Run 1 the total gas emission from gas recirculation systems accounts for about 85% of the total CO₂ equivalent. Most of the gas systems have recirculation efficiency higher than 90%. However, given the high circulation flow used, the remaining 10% of fresh injection contributes significantly to the overall emission. Unfortunately, 75% of these emissions were due to leaks in the detectors and, therefore, they cannot be easily repaired [17].

Moreover, the disadvantages of the gas recirculation systems are related to their complexity. A constant monitoring of the mixture composition and of the presence of impurities is mandatory. Also the detector pressure regulation and the gas system in general are much more complex with respect to an open mode basic gas system.

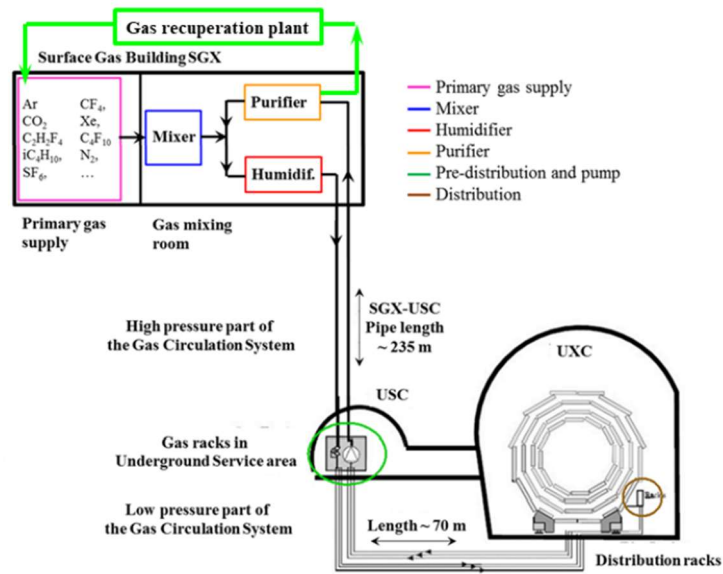


FIGURE 21: CMS closed loop gas system [18]

- **Gas recuperation system**

In some cases, the recirculation gas system is not sufficient due to the impurities that accumulate in the gas stream. However, in principle the gas mixture can be recuperated from the exhaust of the gas recirculation system and sent to dedicated separation plant able to extract a specific mixture component. This approach is useful for the possibility

to achieve a further reduction in gas emission but it introduces a second level of complexity in addition to the gas recirculation system and for this reason it requires a dedicated R&D studies depending on the specific gas mixture components to separate.

Different recuperation systems were developed since the start of LHC gas systems operation, and CMS-CSC gas system is a typical example of this approach: both for requirements and complexity aspects related to operation. The CMS-CSC muon detector used a gaseous mixture of Ar/CO₂/CF₄ (40/50/10) and, despite the detector is tight, it has been discovered that due to gas diffusion mechanism the gas mixture is contaminated by air. Some contaminants, as H₂O or O₂, can be removed by the purifier modules, but unfortunately N₂ cannot be removed and it tends to accumulate. In order to overcome this issue without making compromises on the gas mixture quality, a CF₄ recuperation plant has been developed. The CF₄ recuperation plant is operational since June 2012 and allows a further reduction in the GHG emission.

- *Search for new environmentally friendly gases for particle detectors*

A third field of research is focused on the replacement of the current GHGs used in gaseous detectors. Despite the recent EU F⁺ gas regulation, GHGs would remain available for research applications but their price could raise possibly making gas detectors operation very costly. Environmentally friendly alternatives are being searched for R134a, SF₆ and CF₄. As different compounds have been developed in industry to replace R134a as refrigerant, these candidates are being looked into as possible replacements in the RPCs gas mixture. The aim is to find a new eco-friendly mixture that is able to reproduce the same detector performance as it is observed with the current gas mixture. Good results have been obtained with the use of mixture containing HFO-1234ze (C₃H₂F₄), that is a hydrofluoroolefin with a GWP < 1 for 100-year time horizon, and a neutral gas.

A definitive solution is not still achieved and further R&D studies will be needed.

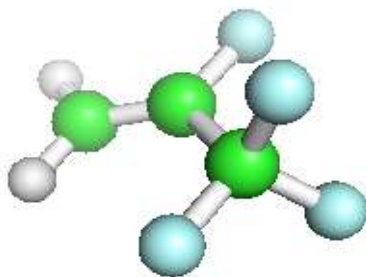


FIGURE 22: Optimized ground state geometries of HFO1234ze gas molecule

Chapter 3

CF₄ Recuperation Plant in CMS-CSC Gas System

3.1 CSC gas system

Cathode Strip Chambers (CSCs) are used in the end-cap regions of the Muon Spectrometer for the Compact Muon Solenoid (CMS) experiment at the Large Hadron Collider (LHC) [19]. The CMS endcap muon chambers are basically classic multi-wire proportional chambers consisting of 6 anode wire planes interleaved among 7 trapezoidal cathode panels, albeit with a huge scale of the overall system (2.000.000 wires and 6000 m² of sensitive area), high precision requirements (~ 200 μm spatial resolution per plane), and sophisticated trigger capabilities [20]. In the regions where the CSC detectors are employed, the magnetic field is very intense (up to several Tesla) and inhomogeneous. Moreover, the background particle rate is very high.

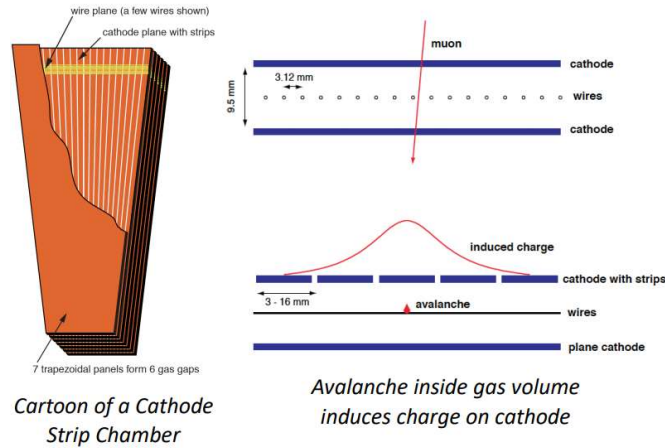


FIGURE 23: Layout of a Cathode Strip Chambers

The current CSC gas mixture used is 40% Ar, 50% CO₂, 10% CF₄. In particular, Ar provides the necessary gas gain for desired HV settings, CO₂ is used for quenching of spurious pulse to enhance time response and CF₄ has anti-aging properties preventing wire etching and polymerization [21].

Due to the very large detector volume (90 m^3) and the use of the expensive and greenhouse gas CF_4 , the CSC gas system has been designed to operate in closed loop mode with less than 5% of fresh mixture injected. However, after some months of operation it has been detected an important presence of air into the return mixture from the detector. All tests have proven that both the detector and the gas system are gas tight and in fact, the source of contamination was identified as a diffusion leak resulting from components used for the construction of the detectors. For this reason, nowadays the percentage of fresh mixture injected is set to 10% and N_2 and O_2 concentrations stay within reasonable limits to allow good operation of the chambers. O_2 is removed from the gas stream using a purifier module filled with an $\text{Ni-Al}_2\text{O}_3$ catalyst, while N_2 cannot be filtered and therefore it accumulates to a concentration of about 1%.

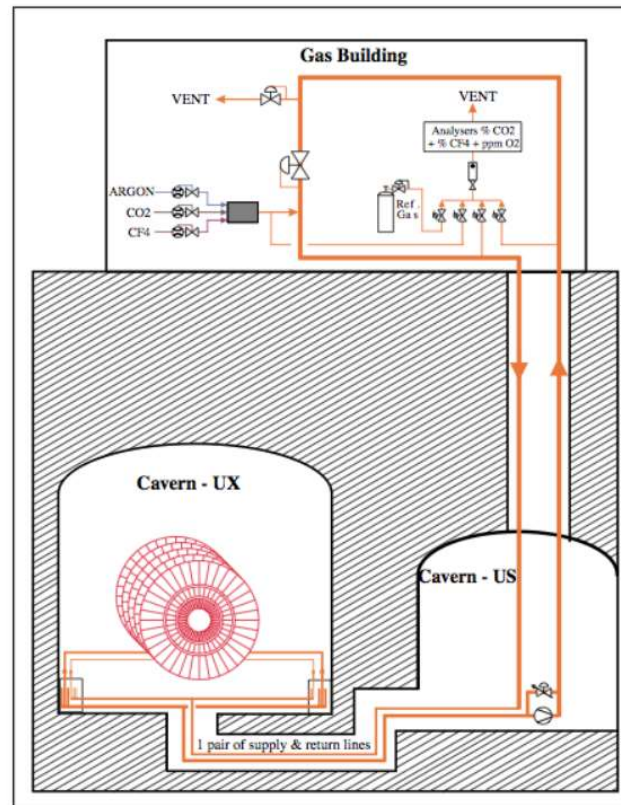


FIGURE 24: Simplified schematics view of gas circulation loop [22]

Since the fraction of recirculated gas cannot be increased due to the N_2 that accumulate, a gas recuperation system for the CF_4 , the most expensive and environmentally harmful component, has been developed. Basically, the gas is recuperated from the

exhaust module (≈ 600 l/h) and sent to dedicated separation plant where the CF_4 is extracted and stored in a battery.

Since CF_4 is not environmentally friendly (GWP of 7390 for 100-year time horizon [23]), in parallel to the gas recuperation system, nowadays there are also studies in trying to reduce the CF_4 concentration or to look for alternative gases: longevity properties of gases with less CF_4 and performance studies with more eco-friendly gases.

3.2 CF_4 Recuperation Plant

When the recuperation plant was projected there were two possible mechanisms to recover the CF_4 : the warm separation by absorption and liquefaction. The adsorption by molecular sieve has been adopted due to the high cost of liquefaction (working temperature below -128°C).

The entire process involves several steps in which membranes and molecular sieve are used.

The input flow to the recuperation plant comes from the closed loop after the purifier module to minimize the presence of O_2 and other contaminants.

Basically, the process can be divided in four steps (FIGURE 25):

5. Membrane module for CO_2 bulk separation.
6. Molecular Sieve 4\AA for CO_2 residual removal.
7. Molecular Sieve 13X for CF_4 adsorption and recuperation.
8. CF_4 compression and storage.

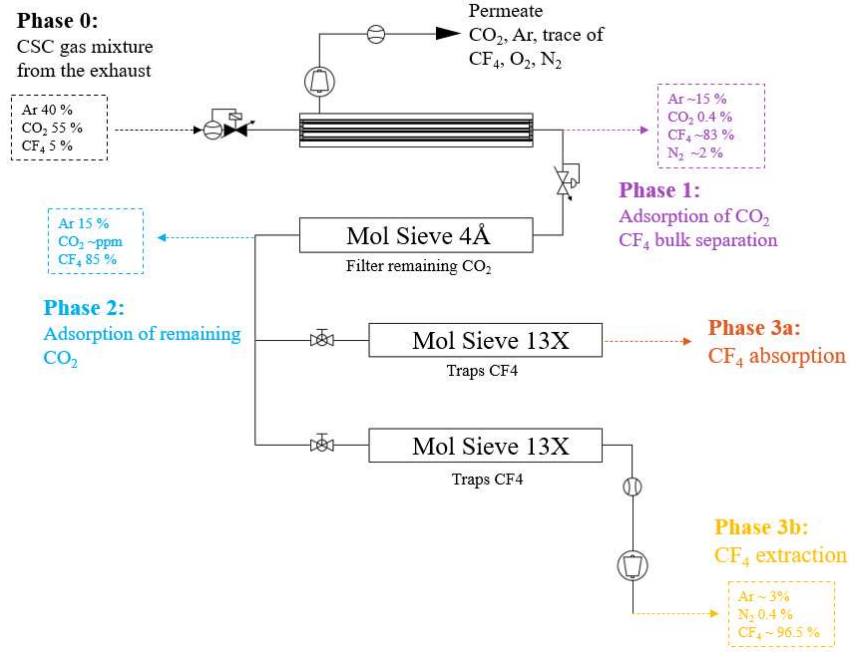


FIGURE 25: Schematic view of the CF₄ recuperation plant. The circles are the points of gas analysis

During the tests performed with the CF₄ recuperation prototype system, the gas composition was measured using a gas chromatograph Agilent-microGC3000 equipped with PoraPlotU and Molecular Sieve 5 Å columns.

The system consists of 5 physical racks and one buffer (FIGURE 26) and it was paid back in about two years of operation (after good efficiency was achieved). Recuperated CF₄ was used for the first time in 2015. Since then, the system has been always operational – at different recuperation efficiencies. The extra-complexity introduced to monitor the CMS-CSC gas systems after the addition of the CF₄ recuperation plant is mainly related to the operation, maintenance, tuning of the plant and to a general reinforcement of the mixture analysis. Indeed, in addition to the standard LHC gas analysis module (common to all the detector of the same experiment) a dedicated infrared analyser has been installed (continuous monitoring of CO₂ and CF₄), gas chromatographic analyses are performed when CF₄ recuperated is injected to fine tune the gas mixture composition and a new gas monitoring system based on single wire detectors has been implemented. Nowadays the tuning of the system is still ongoing as the last

module used to trap the CF_4 from the exhaust gas from the gas recirculation has revealed to be more complex even with respect to the small prototype used to develop the system.



FIGURE 26: Picture of the CF_4 recuperation plant installed in the surface gas building (SGX5) of the CMS experiment

Since 2012 the recuperation efficiency is widely increased, passing from 20% to 50% in 2020. Extensive tests were performed in the last eight months and the efficiency has reached an average value $> 60\%$.

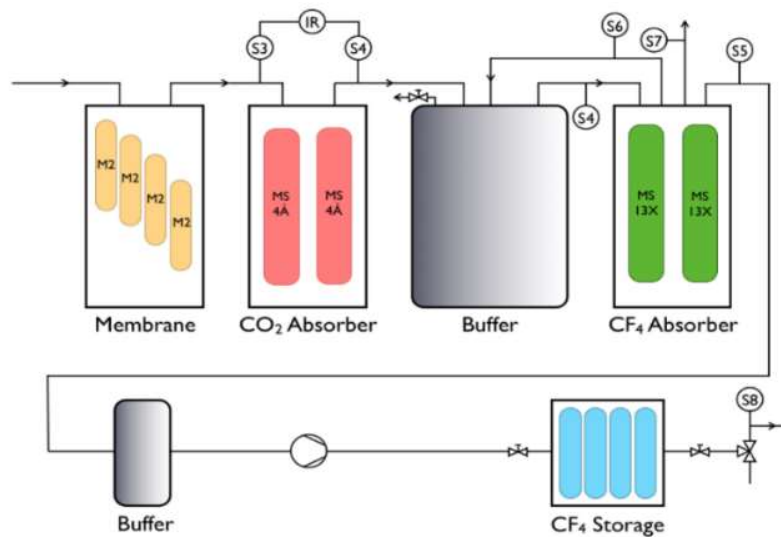


FIGURE 27: Schematic view of the CF_4 recuperation plant. The circles are the point of gas analysis.

In the paragraphs below the single modules illustrated in FIGURE 27 will be briefly described.

3.2.1 CF_4 Membrane Module

The first CF_4 separation step takes place in this module. The gas mixture coming from the Exhaust module in the underground is sent to the surface gas room where it is injected in the membrane module of the recuperation plant (FIGURE 28). The rack contains four membranes connected in parallel and each membrane is made of many little straw tubes. The straw wall is made from a multilayer film (Kapton, Al, C, Molecular Sieve, polymers) which is permeable to specific gases - in our case CO_2 . These membranes are *Hollow fiber membranes of polyimide Matri-mid®5218*, which allows to operate at high input flow (up to 800 l/h). Three membranes work with an input flow up to 300 l/h each, while the fourth has good performance at higher flow as 600 l/h.

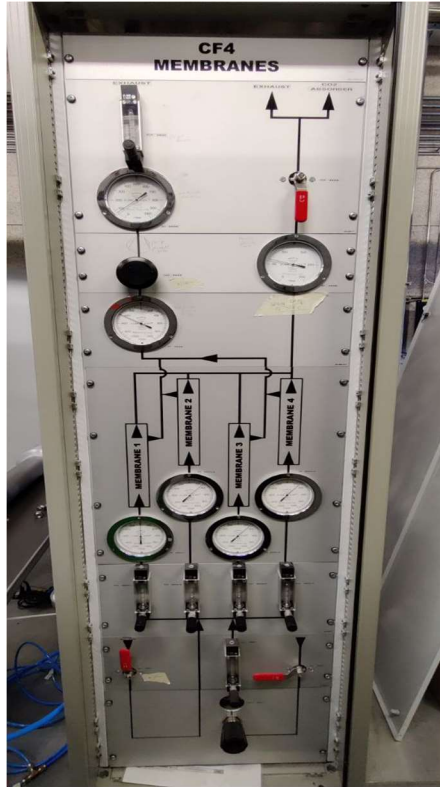


FIGURE 28: Picture of CF₄ Membranes Module

The CO₂ separation effectiveness is a function of the input flow and the remaining CO₂ flow increases as the input flow increases. The input gas flow comes from the exhaust module of the CSC chambers and it is distributed uniformly through the membranes thanks to the rotameters that allows to set the desired flow for each membrane and they can be adjusted only manually.

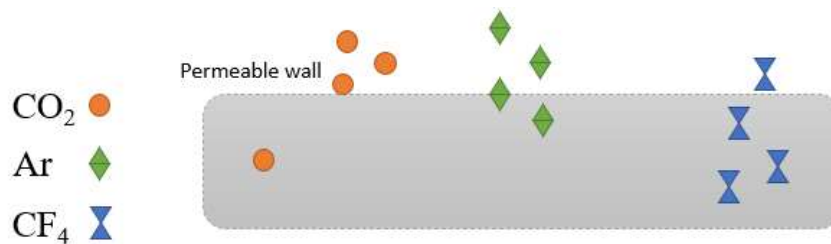


FIGURE 29: Schematic view of the membrane working principle.

At the permeate side are located two pumps to produce the negative pressure needed for the CO₂ extraction. The gas flow at permeate side is sent to the exhaust and it is

mainly composed of CO_2 and Ar while the flow at retentate is sent to the next module, the CO_2 absorber and it is mainly composed of CF_4 ($\approx 75\%$) and Ar ($\approx 25\%$). Nowadays three membranes are in use since one of the membranes with a work up to 300 l/h has a lower efficiency and it was stopped and these three membranes are already enough for the flow needed.

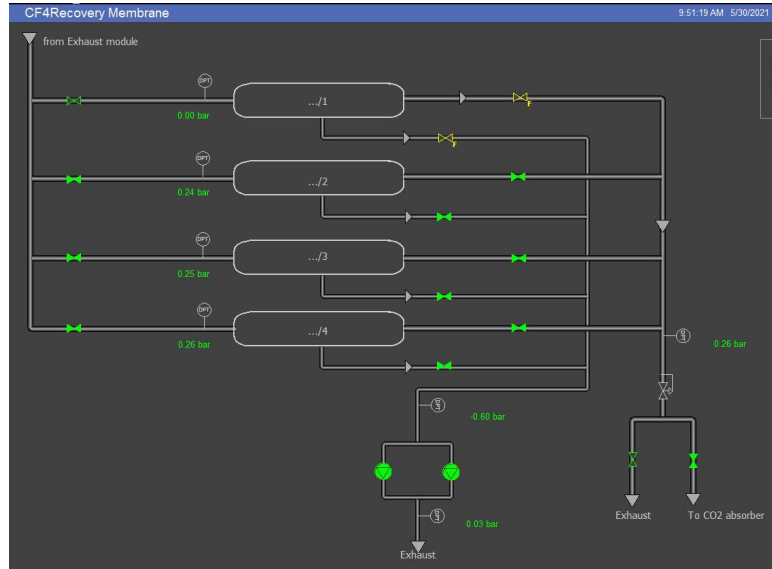


FIGURE 30: Schematic layout of CF_4 membrane module in WinCCOA software

The functioning of membranes and test performed on the module will be explained more in details in the next chapter.

3.2.2 CO_2 Absorber Module

The gas flow coming from the permeate side contains about 1% of CO_2 and this quantity is remarkable because the Molecular Sieve 13X used to trap the CF_4 is also trapping the CO_2 .

Then, in order to ensure the purest possible recuperation of the CF_4 , it is necessary to remove as much as possible the residual CO_2 (that has a kinetic diameter of 3.3\AA). To achieve this purpose, a dedicated CO_2 absorber is installed, which is shown in the second phase of the recuperation plant (FIGURE 32). The absorber used is 4\AA Molecular Sieve, a micro-porous synthetic zeolite with precise and uniform pore size with sodium as the major cation. It is used as adsorber for gaseous and liquid materials, and it is

based on the exclusion size principle: if a molecule is small enough to pass through the pores, it can be adsorbed while larger molecules are not (FIGURE 31).

This behaviour depends on the electrical interactions between the surface of MS and the gaseous molecules due to Van der Waals forces.

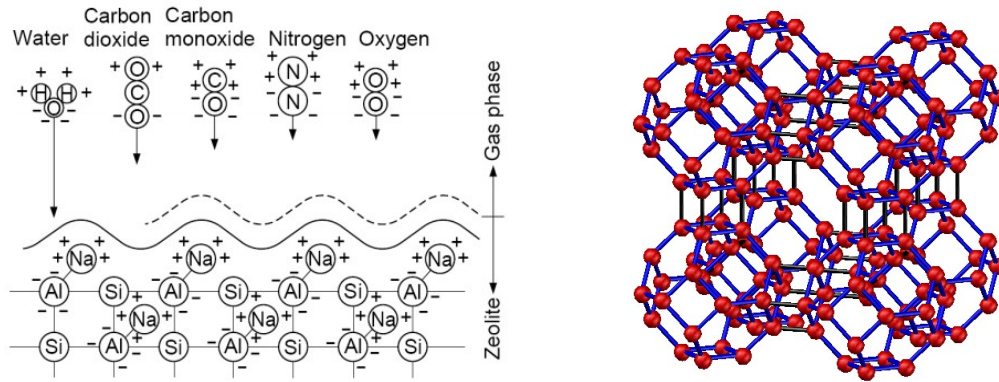


FIGURE 31: Schematic view of the Molecular Sieve working principle (left) and a Structure model of 4Å Molecular Sieve (right) [24]

The purifier module used for the CF₄ recuperation plant contains two columns of 24 l each. During normal operation while one column is in run (i.e. the gas is passing through it and the CO₂ is removed) the other is either in standby or in regeneration (i.e. the column is in preparation for being re-used). During the regeneration phase the column is conditioned at high temperature to recover its adsorbing capacities while during the standby the column waits until the other one gets saturated. This mechanism allows to avoid dead time during the operation of the system. The heating is needed because the CO₂ is strongly retained in the 4Å Molecular Sieve, but it is not a problem since a comparison between the cartridge lifetime (90 h) and the cartridge regeneration time (12 h) shows how the two processes fit well in the system progression.

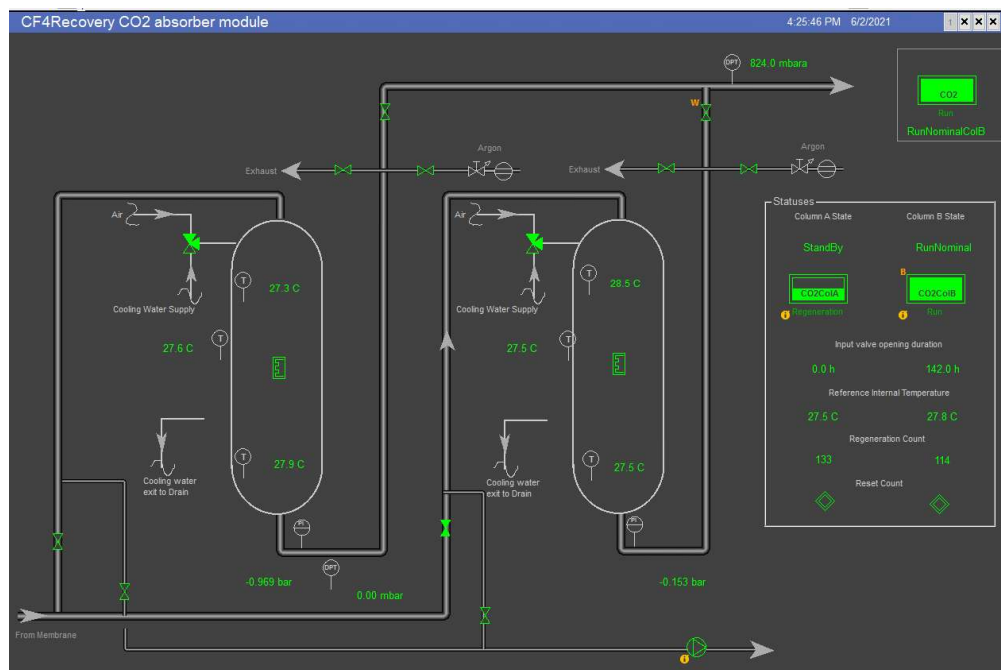
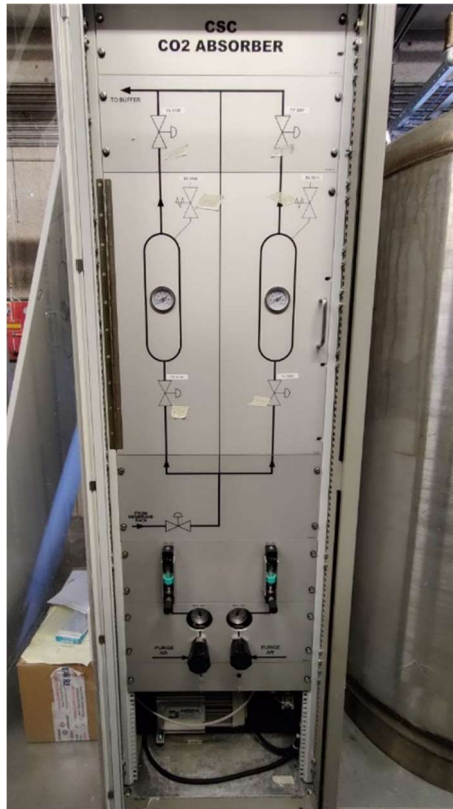


FIGURE 32: Picture of CO₂ Absorber Module and layout of CO₂ absorber module in winCCOA

3.2.3 CF₄ Absorber Module

The gas coming from the CO₂ absorber module contains Ar (15%), CF₄ (85%) and some ppm of N₂. This mixture is sent to a second absorber module containing a 13X Molecular Sieve that is characterized by a pore diameter of 10Å, which absorbs only CF₄ (that has a kinetic diameter of 4.8Å) while the Ar and N₂ (they respectively have a kinetic diameter of 3.4 and 3.64Å) remain volatile and are vented from the cartridge (FIGURE 34). The goal is to absorb and then extract the CF₄ from the Molecular Sieve 13X pores.

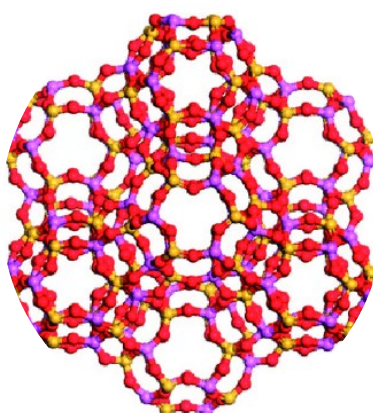


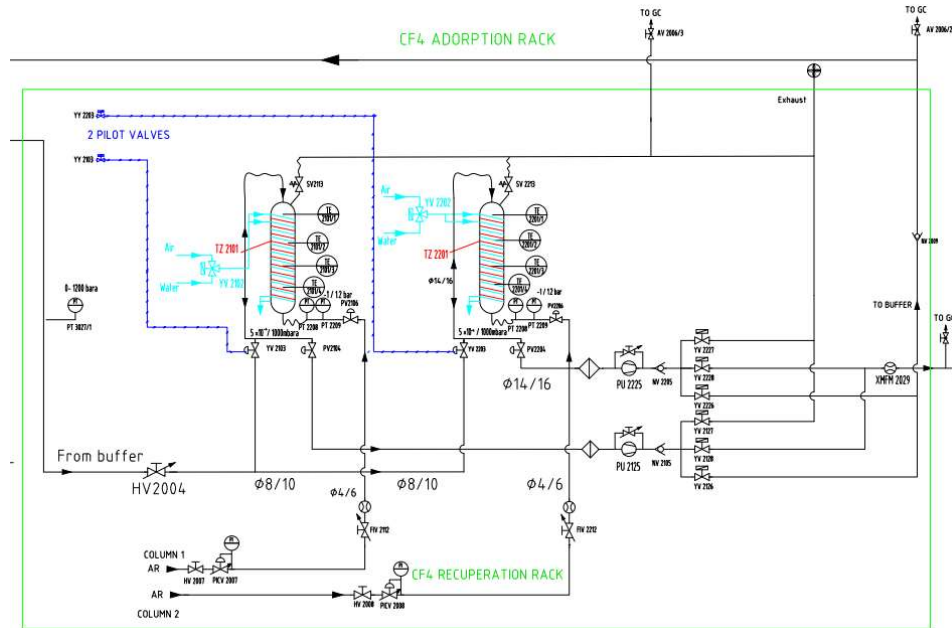
FIGURE 33: Structure model of 13X Molecular Sieve

The adsorption starts from vacuum and stops when the relative pressure inside the cartridge is equal to zero or to the pressure in the supply line to the module. This method is called Pressure Swing Adsorption since also the regeneration is done with pressure cycle only and its advantage is that the Molecular Sieve is not fully saturated and therefore the CF₄ continues to be adsorbed until the end of the cycle, leaving only Argon in the empty space.

The columns in the LHC gas systems are usually heated only from outside but in this case, they are heated also from the inside with a central heating bar in order to decrease the time needed to reach the nominal regeneration temperature and therefore to reduce as much as possible the dead time when a complete thermal regeneration will be needed.

The main contaminant is N₂ with a concentration of about 0.9% and the problem is that N₂ level would increase also in the recuperated CF₄ and, with this injection into the system, it would bring to some higher concentration in the closed loop. Moreover,

preliminary results show how the N₂ concentration in the recuperated gas is not affected by the N₂ concentration in the input stream to the recuperation plant. This result is probably due to the adsorption properties of the 13X molecular sieve for the different gas involved (CF₄, N₂, Ar).



3.2.4 CF₄ Storage and reuse

A gas line is used to supply a second CF₄ Mass Flow Controller (MFC) dedicated to the injection of the recuperated gas into the mixture. Nowadays, it is injected 50% of new CF₄ and 50% of recuperated CF₄.

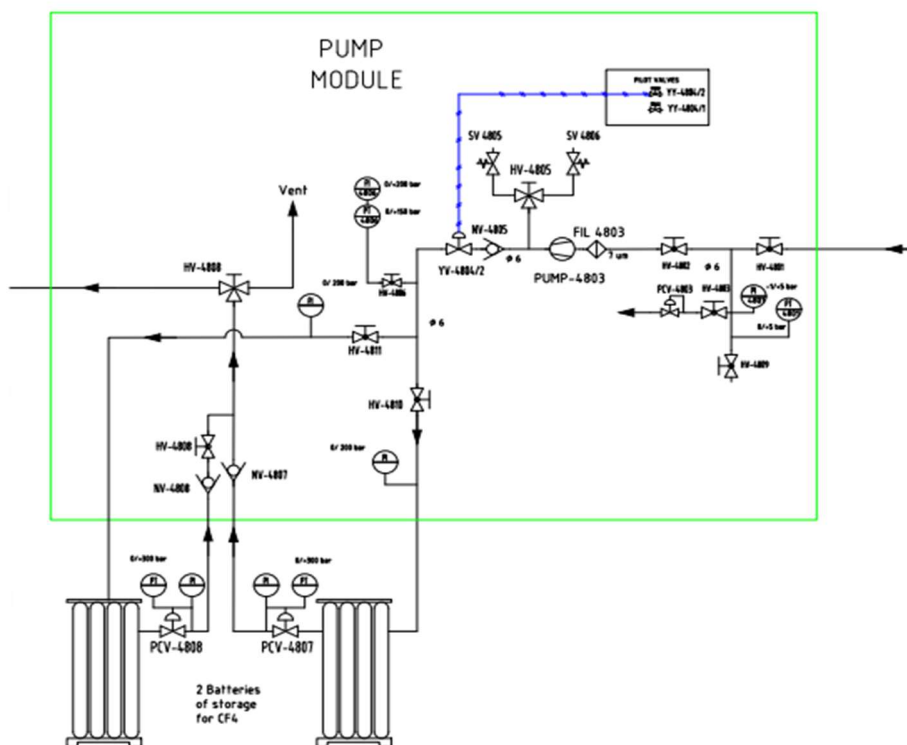


FIGURE 35: Schematic layout of pump module in SGX5

The transition of gas mixture between the modules is managed by software controls, contained in the same infrastructure as the standard gas systems controls. The software controls the full logic of the CF₄ recovery plant as for example opening/closing of valves and start/stop of pumps, according to the values of specific parameters (i.e. columns pressure, temperature), that can be set by the user.

The correct and efficient operation of the full recuperation plant is monitored through gas analyses, realized with the Gas Chromatograph. In FIGURE 36 an example of gas mixture analysed is reported: before the input in the recuperation plant (Exhaust from Buffer, green) and the composition of recuperated gas from the absorber module (Recuperated CF₄, blue). In the PPU column are shown the peaks of Ar, CO₂ and CF₄, while in the Molecular Sieve the N₂ peak is visible and how it is significantly reduced in the recuperated CF₄.

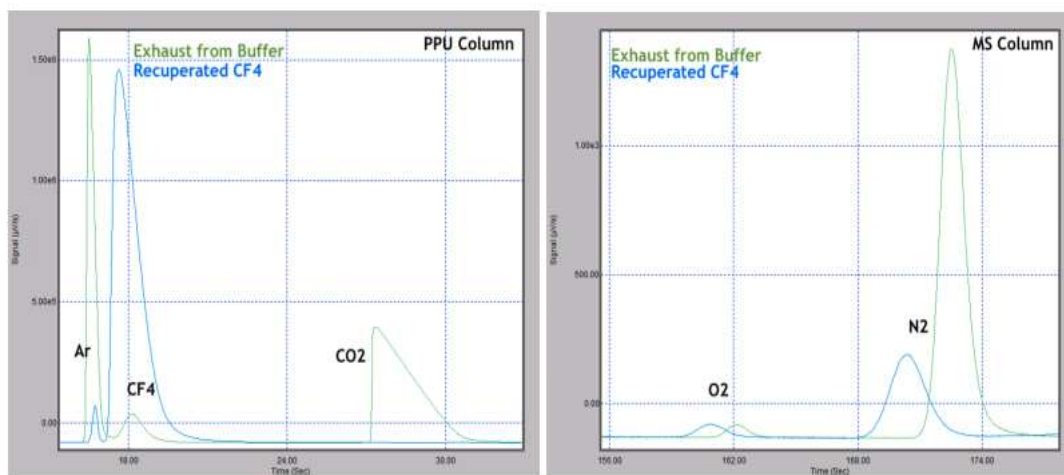


FIGURE 36: Gas chromatograms of input (Exhaust from Buffer, green) and output (Recuperated CF₄, blue) of the CF₄ recuperation plant, for the PPU column (left) and MS column (right)

The daily and weekly CF₄ recuperation efficiency is calculated as the ratio between the CF₄ recuperated volume and the CF₄ volume at the input of the plant.

Despite in the last years many parameters have been improved, the recuperation efficiency oscillated between the 30% and 60% and this depends on many factors as the pressure and volume flow from the exhaust to the input of the plant, the parameters of the different separation steps and the possible development of gas leaks in the path of the recuperated gas. The stability of the input volume flow to the plant, i.e. the exhaust flow from the CSC gas system, is considered to be a key factor determining the final efficiency and recuperated gas quality. In the last months there have been many improvements in the exhaust flow stabilization and consequently also the recuperation efficiency increased from ~ 45% to ~ 60% (March 2021) thanks to the stabilization of flow, whose oscillations passed from 400 l/h to 150 l/h.

Since the construction and commissioning of the plant in 2012, a total of 450 m³ of CF₄ were recuperated, a volume that corresponds to more than 1 year of CF₄ consumption by the CSC gas system (FIGURE 37).

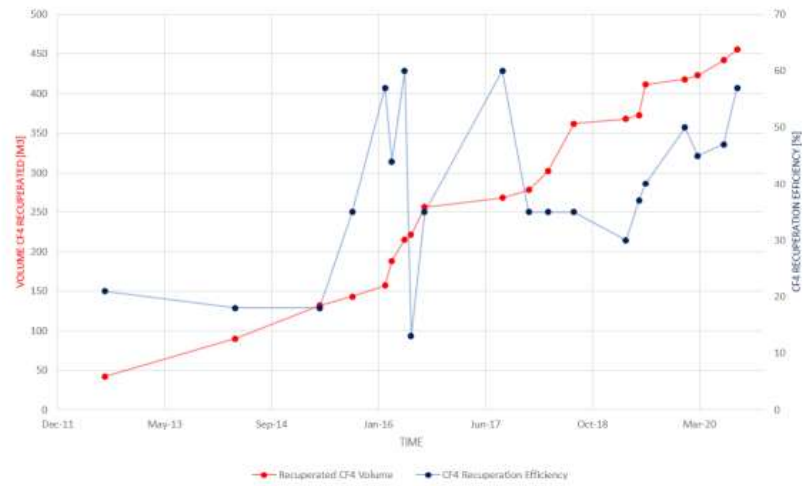


FIGURE 37: Trends of the CF_4 recuperated volume (left axis) and CF_4 recuperation efficiency (right axis) along the years of operation of the CSC recuperation plant [14].



FIGURE 38: Picture of the Storage module

3.3 Principles of membranes technology

Given its multidimensional character, which involves rapid mass transfer rate and high selectivity towards a specific gas, Membrane Technology represents the perfect technique for gaseous separation in the CF_4 recovery plant as seen in the previous paragraphs [25].

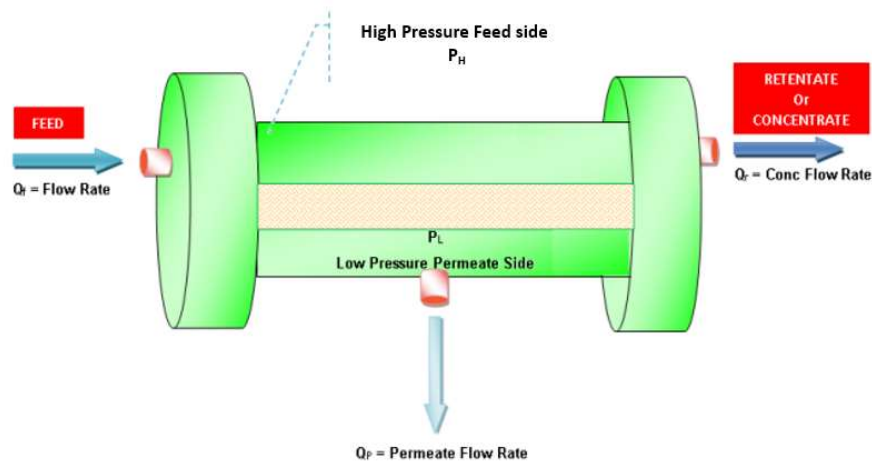


FIGURE 39: Principle of Gas Permeation and Separation in Hollow Fiber membranes

As shown in the FIGURE 39, the feed inlet stream enters the module at a certain composition and a certain flow rate. Because the membrane can transport one component more readily than other, both the feed composition and the flow rate inside the module will change as a function of distance and it depends on different interaction, sorption, diffusivity and kinetic diameter of the molecules. By passage through, the feed is split into permeate stream and retentate stream also known as retentate. Either the permeate and the retentate could be the final product and in our case the product of interest is the second one.

The key area of research in membrane technology is the development of new membranes increasing permeability and selectivity or increasing the permeability without compromising the selectivity or enhancing the selectivity at constant permeability.

The driving force for gas separation is partial pressure gradient which is the product of total pressure and mole fraction but other than driving force, the membrane itself is the principal factor determining the selectivity and flux. The nature of the membrane

determines the type and application, ranging from the separation of microscopic particle to the separation of molecules of an identical size or shape. In fact, membranes are prepared from different polymers such as polycarbonates, polyimides, polyamides, polyetherimides or polysulfones and most membranes used for gas separation are non-porous.

Transport of gases through nonporous polymeric membranes is usually described by solution–diffusion mechanism which consists of three steps: 1) sorption of preferential permeate (solubility) at the upstream surface of the membrane, 2) activated diffusion through the membrane and 3) desorption at the downstream side. Solution-diffusion mechanism is driven by a difference in thermodynamic activities existing across the membrane and interacting forces working between membrane material and permeating molecules. The activity difference causes a concentration gradient that leads to diffusion in the direction of decreasing activity.

To describe the fundamentals of gas separation, however, other factors relating to the nature of the polymer (i.e. chemical structure) need to be considered and in this context two parameters are important: the glass transition temperature and the crystallinity.

The glass transition temperature determines whether a polymer is in the glassy or in the rubbery state and it is mainly determined by chain flexibility and chain interaction. In general, permeability through a rubbery material (elastomer) is much higher relative to glassy polymers because of the higher mobility of the chain segments. In contrast the selectivity of glassy polymers is higher. In the case of CO₂, the elastomers exhibit high permeabilities and low selectivity whereas glassy polymers show much lower permeabilities but generally high selectivity.

The basic concept of gas separation is governed by *permeability coefficient* (*P*) which is the capability of a membrane to permeate gas molecules and it is used to describe the transport of a gas, vapour or liquid through a dense, non-porous membrane:

$$P = \text{Diffusivity } (D) \times \text{Solubility } (S) \quad (1)$$

Solubility is a thermodynamic parameter and gives a measure of the amount of penetrant absorbed by the membrane under equilibrium conditions, while *diffusivity* is dependent on the geometry of the penetrant, for as the molecular size increases the diffusion coefficient decreases. Permeability coefficient is often given in Barrer units (1

Barrer = $10^{-10} \text{ cm}^3_{\text{STP}} \cdot \text{cm} \cdot \text{cm}^{-2} \cdot \text{s}^{-1} \cdot \text{cmHg}^{-1}$). Gas solubility generally increases with increasing gas condensability (or critical temperature). For example in most polymers, CO_2 is more soluble than CH_4 , O_2 and N_2 .

The ability of a membrane to separate two molecules, A to B, is the ratio of their permeability, called as the membrane *selectivity*:

$$\alpha = \frac{P_A}{P_B}$$

(2)

For a binary gas mixture, the selectivity can also be determined from a molar concentration of the two gases in feed and permeate:

$$\alpha = \frac{y(1-x)}{x(1-y)}$$

(3)

where y is the permeate concentration of the fast-permeating gas and x is its feed concentration.

In the next chapter will be in-depth the membrane functioning principles.

Chapter 4

Optimization of the “CF₄ Membrane Module” in the CF₄ recovery plant (CSC-CMS)

4.1 Membranes for CF₄ separation

The type of membrane chosen for the CF₄ separation processes at CSC-CMS recuperation plant is based on selective gas permeation via diffusion, as most of the membranes for gas separation. For this purpose, were chosen separation membranes commercially available from UBE Industries. Hollow fiber membranes of polyimide Matrimid®5218 (FIGURE 40, UBE Ind.), characterized by high gas selectivity, are specifically designed for CO₂ separation and they are suitable for the extraction of CF₄ from Ar/CO₂/CF₄ gas mixture.

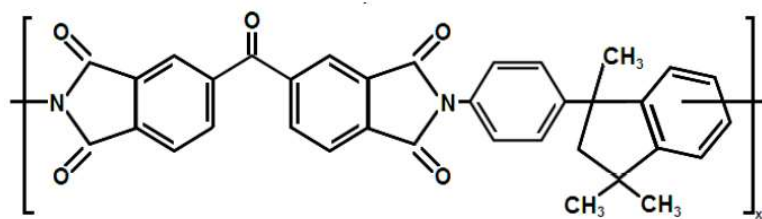


FIGURE 40: Chemical structure of Matrimid® 5218.

Though Argon is present in the gas mixture from which CF₄ needs to be extracted, CO₂ represents the most difficult component to separate as the two molecules have more similar characteristics. CO₂ is by design efficiently separated by the UBE's membrane in the permeate stream, with the remaining components flowing in the retentate stream at a good purity level. The membrane developed by UBE industries is a hollow fiber membrane (HFM) made of capillaries of aromatic polyamide, with symmetrical dense-porous structure in the oldest membrane and asymmetrical dense-porous structure in the newest, achieved thanks to the different length of the polymer chain with variable porosity along the cross-section of the capillary. The first type has a uniform composition and structure over the entire cross section, and the thickness of the entire

membrane determines the flux. These types of membranes are also named homogeneous (dense) membranes.

In dense membranes molecules of the different compounds first dissolve into the membrane matrix and then diffuse through the membrane under a concentration gradient. The permeability of each species is therefore affected by the solubility of each compound into the membrane material (thermodynamic aspect) and by the rate at which each component diffuses through the membrane (kinetics aspect) [26]. The average pore diameter in dense polymer membranes is within the thermal motion of the polymer chains from which the membrane is made of. The asymmetric membrane consists of thin and dense selective layer (skin) supported on a much thicker microporous support layer that provides mechanical support and they are characterised by a unique structure resulting from the different length of the polymer chain with variable porosity in the cross-section [27]. It combines both the high selectivity of a dense membrane with the high permeability of a very thin membrane. Asymmetric dense/porous membrane is obtained by phase inversion in which the polymer is transferred from a solution to a solid state in a controlled manner, most often by precipitation upon immersion. The industrial production of asymmetric membranes has evolved considerably in recent years [28]. It has been reported that PI having high chain stiffness, weak inter-chain interaction and loose chain packing tend to have high gas permeability. This means that both dianhydrides and diamines components of the PI should not contain flexible links. Due to the glassy nature of these polymers, PI tend to thermodynamically rearrange their chains reducing the number and sizes of free volume contributing to gas permeability [29].

The module is placed in a high-pressure steel housing designed for counter-current stream flows.

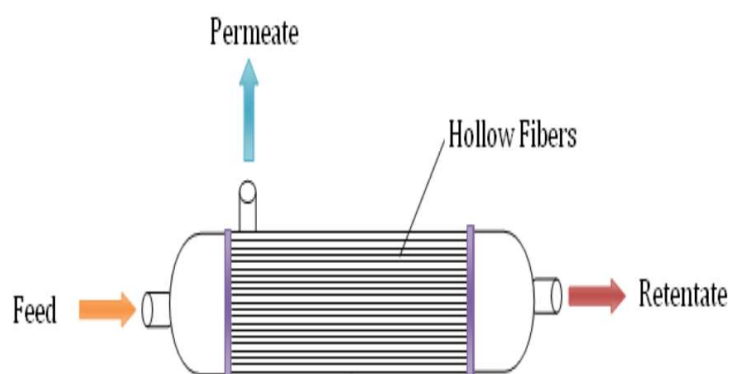


FIGURE 41: Hollow Fiber Membrane Module

The separation is in this case driven by hydrostatic pressure difference, as different species would exert different partial pressures at the two sides of the membrane wall. Capillaries are arranged in a bundle, housed in a case module where gas inlet and outlets are located. The arrangement of the membrane material in capillary straws (FIGURE 42) allows to maximize the material surface that can interact with the feed gas mixture, increasing the membrane selectivity.



FIGURE 42: Picture of the UBE membrane section, with the bundle of straws visible inside the membrane case

If it is considered the three-component separation, specifically $\text{Ar}/\text{CF}_4/\text{CO}_2$ gas mixture, when the gas mixture is introduced into the membrane in the feed stream entrance (FIGURE 43), the CO_2 molecules easily diffuse through the membrane material because of the partial pressure difference between the two sides of membranes. At the permeate stream is located a pump to create a higher-pressure gradient which allows the passage of CO_2 in the Permeate exit.

The retained component, the CF_4 , can flow through the straws and is let out of the membrane body. The third component, Ar, has a particular behaviour because it partially permeates the membrane, but it can also be retained by the module as the CF_4 . The Ar distribution depends on the input stream flow: higher the input flow, higher the Ar [%] at the retentate side (FIGURE 66).

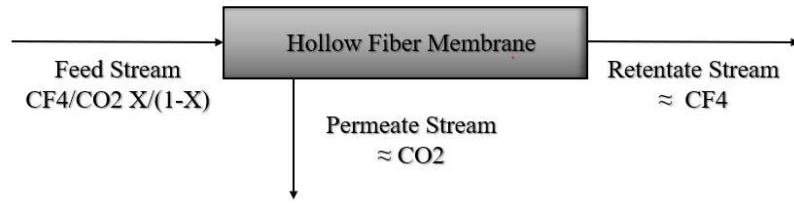


FIGURE 43: Separating process for the $CF_4/CO_2/Ar$ gas mixture.

In an ideal separation process, all the CO_2 and Ar molecules present in the feed mixture would permeate the membrane walls, while all the CF_4 molecules would flow at the retentate output of the membrane. Given the non-ideal nature of the separation process and considering that the membranes used in the CF_4 recuperation plant are optimized for the CO_2 permeation, separation membranes have limitations in their performance, which can be tuned through the accessible parameters depending on the requirements on the separation product.

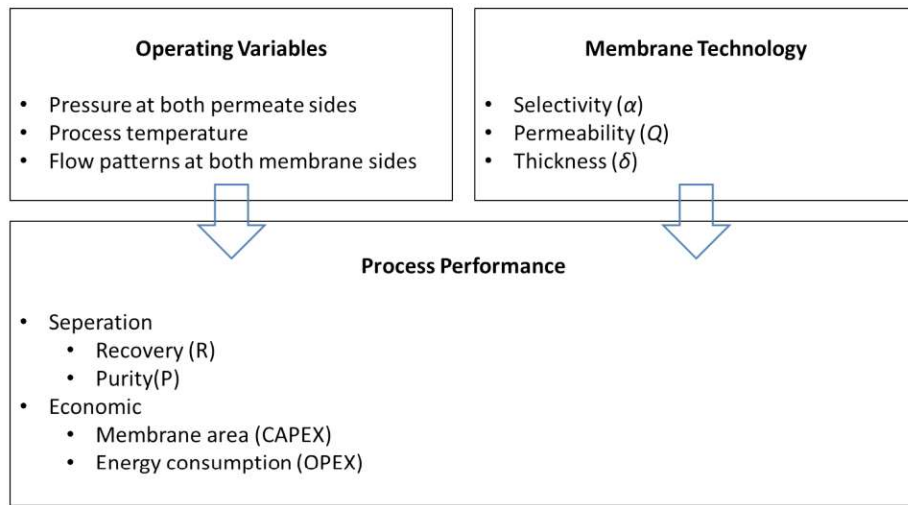


FIGURE 44: Schematic of membrane gas separation process design and evaluation [26]

For this specific case, while on one hand it is crucial that the retained gas contains the highest possible CF_4 fraction, it is also fundamental that the fewer possible CF_4 volume leaves the membrane through the permeated flow. For example, one could have very pure CF_4 in the retentate gas fraction, but then such fraction could contain only half of the total CF_4 present in the input, while the other half would be lost in the permeate stream. Therefore, a balance should be found between having very pure recuperated

CF₄ and recuperating a gas volume that is high enough to make the process worth the costs and efforts.

To tune the balance of the process requirements, membrane performance is evaluated with two parameters: recovered gas quality and CF₄ separation efficiency. The recuperated gas quality is simply expressed with the CF₄ concentration in the gas volume of the retentate stream. The CF₄ separation efficiency (ϵ) is defined as follows:

$$\epsilon(CF_4) = \frac{\text{volume } (CF_4^{Output})}{\text{volume } (CF_4^{Input})} \quad (4)$$

where the output is here the retentate gas stream. It should be considered that CF₄ separation efficiency depends on different factors, such as the input gas pressure, the feed flow rate and mixture composition. For example, for the same type of membrane different versions are produced, each specifically developed to work with a given input flow rate, in way to optimize the separation for such flow range. For this reason, different studies were realized to characterize the UBE membranes to maximize their performance in the CSC-CMS CF₄ recuperation plant.

4.2 Experimental setup

In the followings will be treated the membrane characterization tests studying the efficiency of the single membrane and through which was possible calculating the cumulative efficiency of the entire module. Each test was realized with the membrane installed in a custom-made system where all the parameters can be tuned and measured. The input gas flow (from the exhaust module) was set by the user through the WinCCOA software, the gas flow rates of permeate and retentate were monitored with Flow Calibrator devices that have a precision of 0.5% of reading (MesaLab DryCal [30]), the pressure at the permeate (-400 mbar) and retentate (100 mbar) sides were regulated with manometers to maintain constant the values for all tests. The negative gradient of pressure at the permeate side was allowed by a pump. Finally, the gas mixture concentration at the permeate and retentate sides of the membrane was measured using a Gas-Chromatograph (Paragraph 2.3) that allows to determine the concentration

of the different components, impurities (O_2 , N_2) in the gas streams and allows to calculate the efficiency of the separation.



FIGURE 45: Picture of the membrane test setup

The membrane tested and their specifications are reported in the Table 1. The membranes working up to 300 l/h were tested at 50 l/h, 100 l/h, 150 l/h, 200 l/h and 250 l/h, while the membrane working up to 600 l/h was tested at 300 l/h and 400 l/h.

Name	Model	Flow	Characteristics
Old Membrane 1	E-type	Up to 300 l/h	High thickness and uniform density
New Membrane 1	CO-C10	Up to 300 l/h	High thickness and gradient of density
Membrane 2	CO-C10A	Up to 300 l/h	High thickness and gradient of density
Membrane 3	CO-C10A	Up to 300 l/h	High thickness and gradient of density
M. High selectivity	CO-C07FS	Up to 300 l/h	Small thickness and gradient of density
Membrane 4	CO-C410A	> 600 l/h	High thickness and gradient of density

Table 1: Details of the tested UBE membranes

All tests are realized with the same feed gas mixture Ar/CO₂/CF₄ 40/55/5.

4.2.1 Test 1: E-Type Membrane

The first membrane tested is the E-type, the oldest membrane in the rack. It was tested for the first time in the prototype of recuperation plant and then was moved in the definitive implant. However, some years ago, after some efficiency tests, it showed up that this membrane had an efficiency lower than the three other membranes in the rack and for this reason, it was stopped.

The E-type exploits an old technology based on the high thickness of the fiber and a uniform distribution of chains length of polyimide. This structure has low contact surface and it allows the passage of great percentage of CF₄ in the permeate stream for low feed flows. Consequently, the test confirmed that membrane has a very low efficiency rate which differs from the separation efficiency rate of the other membranes in the rack.

In the following two tables are shown the composition of permeate (Table 2) and retentate (Table 3) streams.

Permeate Stream							
Nominal Flow [l/h]	Measured Flow [l/h]	CF₄ [%]	CO₂ [%]	Ar [%]	CF₄ Volume [l/h]	CO₂ Volume [l/h]	Ar Volume [l/h]
50	50	4.2	54.0	45.3	2	27	23
100	106	3.3	54.7	43.3	4	58	46
150	156	2.0	56.0	43.9	3	87	68
200	205	1.6	56.7	43.6	3	116	89
250	257	1.1	57.6	43.2	3	148	111

Table 2: Composition of Permeate Stream

Retentate Stream							
Nominal Flow [l/h]	Measured Flow [l/h]	CF₄ [%]	CO₂ [%]	Ar [%]	CF₄ Volume [l/h]	CO₂ Volume [l/h]	Ar Volume [l/h]
50	0.5	62.3	5.7	33.6	0.31	0.03	0.17
100	2.0	96.6	0.6	4.5	1.92	0.01	0.09
150	2.3	80.8	0.2	19.3	1.88	0.00	0.45
200	10.9	74.8	0.2	25.8	8.15	0.02	2.81
250	18.8	69.7	0.2	30.6	13.10	0.04	5.75

Table 3: Composition of Retentate Stream

The *nominal flow* is the input flow from the exhaust module to the membrane module set through the WinCCOA software while the *measured flows* are the permeate and retentate streams measured with the DryCal during the tests. The [%] is the concentration of the mixture component analysed by the μ GC and the *volume* of each component is obtained as the product of the percentage of the component in the original mixture and the measured flow at each side of the membrane.

$$Volume\ of\ X = X\ [\%] \times Measured\ Flow\ \left[\frac{l}{h} \right]$$

(5)

In the Table 2 and 3 it is visible how the E-Type membrane is highly dependent from the input flow stream and, in particular, for low flows (from 50 to 150 l/h) most of the gas mixture goes to permeate side, decreasing the efficiency of the system. From input stream as 200 l/h, the behaviour of the membrane is more similar to that of the other membranes and a major part of CF₄ goes to the retentate side. Since the membranes usually work at flow of 100 or 150 l/h and in this range the performance of the membrane is not good, the E-type membrane was stopped some years ago.

To better visualize the distribution of components at each side of the membrane, it was calculated the fraction of each component as following:

$$\text{Fraction of } X \text{ component in NP (or P)} = \frac{X \text{ flow at NP (or P)}}{\text{Input Flow} \times X[\%]} \quad (6)$$

In graphs below the trend of gas mixture components through the membrane.

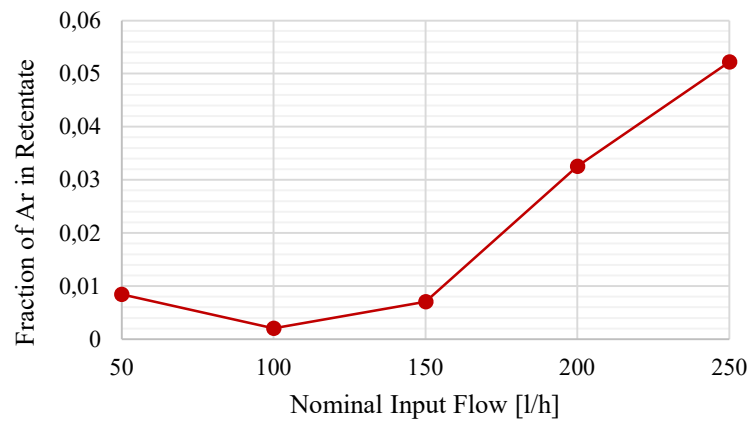


FIGURE 46: Fraction of Argon in Retentate Stream

In the FIGURE 46: Fraction of Argon in Retentate Stream the trend of the fraction of Ar in the retentate stream at different flows is shown and it is visible how the content of Ar is dependent from it: the highest the flow the highest is the content of Ar in retentate stream and less pure is the CF₄ recuperated. For the highest flow, the fraction of Ar is ~ 6% that means, in terms of litres per hour, 34 l/h.

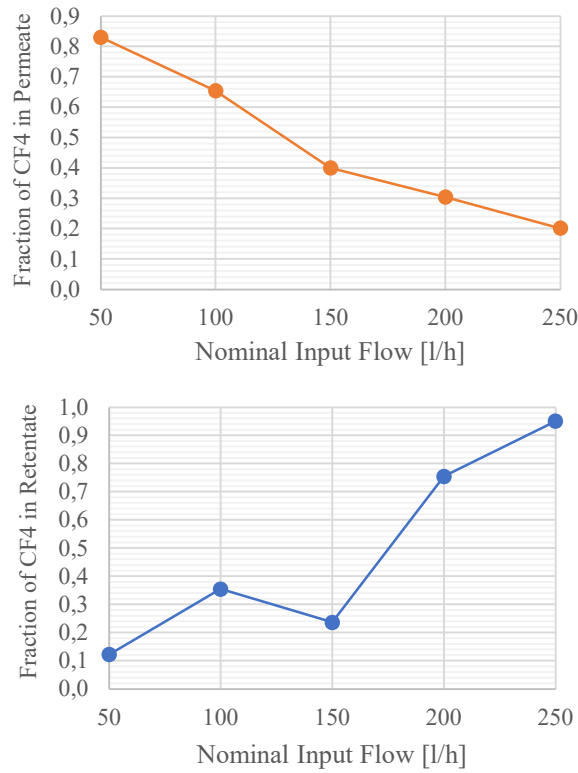


FIGURE 47: Fraction of CF_4 in Permeate (left) and Retentate (right)

Results (FIGURE 47) show the fraction (6) of CF_4 in Permeate and Retentate: for flows up to 150 l/h most of CF_4 is lost at the permeate side due to symmetrical dense-porous structure that allows its permeation. Only for high flows the separation efficiency increases but it does not reach anyway the 100%. However, the fraction of CF_4 in retentate at 150 l/h is an outlier and it cannot be considered in the statistics.

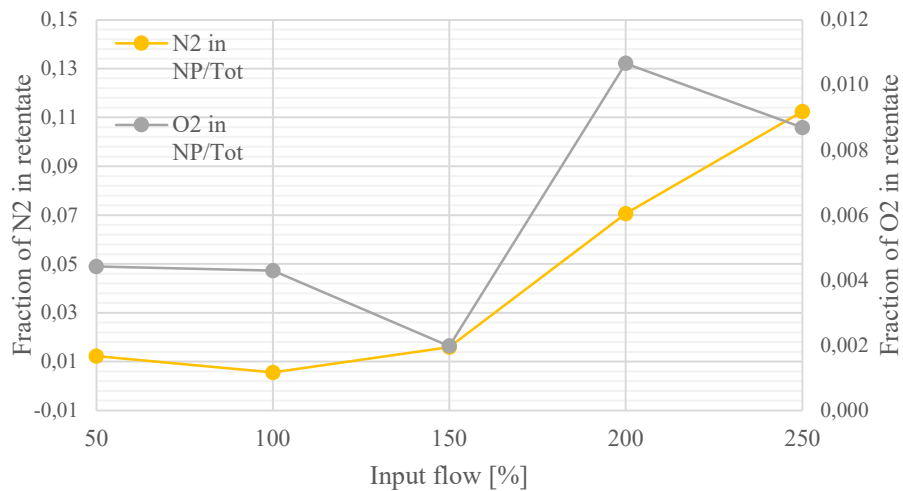


FIGURE 48: Fraction of O_2 (grey) and N_2 (yellow) in Retentate

In the FIGURE 48 the fractions (5) of N₂ (3.64Å Kinetic diameter) and O₂ (3.46Å kinetic diameter) contaminants in the retentate side are shown. It is visible how the oxygen content is overall very low, and it increases at higher flow while the nitrogen contamination is 10 times bigger than that of O₂ and it has its maximum value for the input flow of 200 l/h. The minimum value of O₂ and N₂ content is for an input flow of 150 l/h.

Most of N₂, O₂ and CO₂ molecules go to permeate side because the rigid, highly voided structure with randomly distributed, interconnected pores make only molecules that differ considerably in size to be separated effectively by such membranes.

Basically, Ar, CO₂, N₂ and O₂ have similar kinetic diameters that allow their passage through the membrane's fibers conveying the components at the permeate side while CF₄ which have a bigger kinetic diameter, permeates less the membrane layer and go to the retentate side. The permeability coefficients decreased in the following order: CO₂ > Ar > O₂ > N₂ > CF₄, which is the order of the increase of the kinetic diameters of these gases [31].

4.2.2 Test 2: CO-C10 Membrane

The second membrane tested was the CO-C10 model, that is characterized by high thickness of fibers and a gradient of density. This membrane model is intermediate between that of the E-type and the asymmetric hollow fibers membranes, preferred to others owing to their low production costs, high surface/volume ratios, reduced overall dimensions of the equipment (footprint) and excellent mechanical strength.

In the followings will be shown the results obtained during the performed tests.

<i>Permeate Stream</i>							
<i>Nominal Flow [l/h]</i>	<i>Measured Flow [l/h]</i>	<i>CF₄ [%]</i>	<i>CO₂ [%]</i>	<i>Ar [%]</i>	<i>CF₄ Volume [l/h]</i>	<i>CO₂ Volume [l/h]</i>	<i>Ar Volume [l/h]</i>
100	98	0.05	58.4	41.9	0.0	57.4	41.2
150	150	0.02	58.5	41.6	0.0	87.6	62.2
200	196	0.00	59.1	41.2	0.0	116.1	80.9
250	253	0.00	59.3	41.8	0.0	150.0	105.6

Table 4: Composition of Permeate Stream

<i>Retentate Stream</i>							
<i>Nominal Flow [l/h]</i>	<i>Measured Flow [l/h]</i>	<i>CF₄ [%]</i>	<i>CO₂ [%]</i>	<i>Ar [%]</i>	<i>CF₄ Volume [l/h]</i>	<i>CO₂ Volume [l/h]</i>	<i>Ar Volume [l/h]</i>
100	8	59.1	1.9	35.0	4.9	0.15	2.9
150	14	55.6	0.8	40.0	7.7	0.10	5.5
200	20	53.2	0.5	43.0	10.4	0.10	8.4
250	24	56.5	0.2	39.0	13.5	0.04	9.3

Table 5: Composition of Retentate Stream

The results of performed tests on CO-C10 membrane are summarized in the Table 4 and Table 5 for input flows from 100 to 250 l/h. It can be considered that there is not CF₄ loss at the permeate side also for low input flow (100 l/h). In relation to measured flow at the retentate side, from input stream flow from 150 l/h to 250 l/h the membrane has an efficiency of 100%. Moreover, for the average membranes flow of 150 l/h there is the best trade-off in terms of Ar and CO₂ contamination at the retentate side. The highest contact surface of the membrane due to the gradient of density of fibers allows to reduce the permeate flow without compromising the quality of recuperated CF₄.

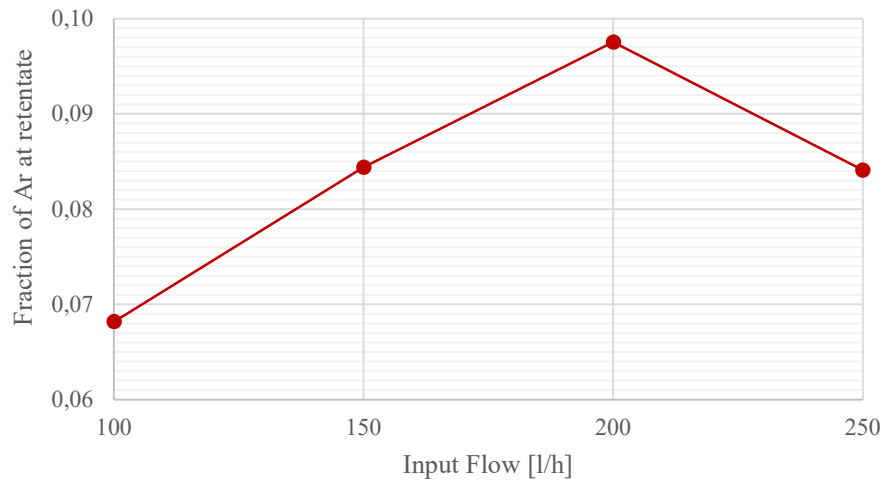


FIGURE 49: Fraction of Argon in Retentate Stream

The plot in FIGURE 49 summarizes the trend of Ar fraction (5) in retentate flow. It is visible its dependence from the input flow rate, and it has the maximum value for 200 l/h of input flow and it can be explained considering that higher flow causes minor contact time between molecules and fibers and they consequently have less time to

permeate the membrane. The membrane results to be less permeable by Ar molecules than E-type model and it is probably due to the different pores size in the polymer that increase in the outer layer of the fiber (FIGURE 50).



FIGURE 50: Schematic representation of gradient of density

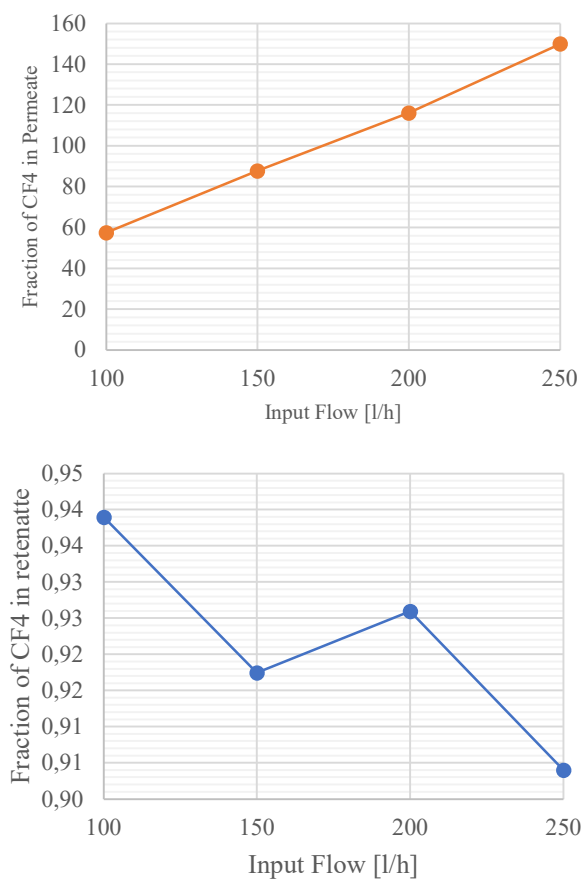


FIGURE 51: Fraction of CF_4 at Permeate (left) and Retentate (right) side

As for the E-type membrane, at higher input flow the CF_4 loss at the permeate side decreases and it is due to the combination of gradient of density and high input flow rate (FIGURE 51).

In this membrane the CF_4 loss is 100 times lower than the E-type membrane and the best CF_4 recuperation efficiency is achieved for input flow of 250 l/h.

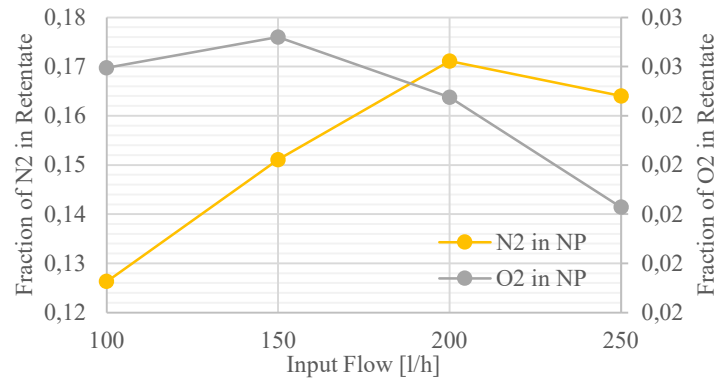


FIGURE 52: Fraction of O₂ (grey) and N₂ (yellow) in Retentate

As shown in FIGURE 52 the trend of N₂ fraction (6) in retentate side is similar to that of Ar, reaching a value > 15% for input flow value of 200 l/h. O₂ fraction at the retentate side is very low and in particular it decreases at higher input flow. The higher fraction of O₂ in retentate is for input flow of 150 l/h.

This behaviour is predictable considering the higher permeability coefficient of O₂ than N₂ as seen in previous paragraph.

Considering the average membrane flow, this membrane has a good behaviour for the flows at which it was tested and it could be taken into account as substitute of the old membrane 1.

4.2.3 Test 3: CO-C10A Membranes

The CO-C10A model is a membrane produced by the UBE Industries and it is characterized by high fibers thickness and gradient of density as the CO-C10 model³ (previous paragraph). In the CO₂ membrane module there are two membranes of this type, the membranes 2 and 3. The test were performed at nominal input flow of 100, 150 and 250 l/h at which they shown the same behaviour in terms of efficiency.

³ The CO-C10A is the old version of the CO-C10 model, but they have the same chemical-physical characteristics.

Permeate Stream							
Nominal Flow [l/h]	Measured Flow [l/h]	CF₄ [%]	CO₂ [%]	Ar [%]	CF₄ Volume [l/h]	CO₂ Volume [l/h]	Ar Volume [l/h]
100	98	0.70	57.4	41.4	0.7	56.3	40.7
150	151	0.07	57.7	42.0	0.1	87.0	63.3
250	247	0.01	58.9	41.4	0.0	145.6	102.4

Table 6: Composition of Permeate Stream for Membrane 2

Permeate Stream							
Nominal Flow [l/h]	Measured Flow [l/h]	CF₄ [%]	CO₂ [%]	Ar [%]	CF₄ Volume [l/h]	CO₂ Volume [l/h]	Ar Volume [l/h]
150	149	0.07	58.0	42.1	0.1	86.6	62.8
250	249	0.02	58.4	41.6	0.1	145.6	103.7

Table 7: Composition of Permeate Stream for Membrane 3

Retentate Stream							
Nominal Flow [l/h]	Measured Flow [l/h]	CF₄ [%]	CO₂ [%]	Ar [%]	CF₄ Volume [l/h]	CO₂ Volume [l/h]	Ar Volume [l/h]
100	9	61.3	0.47	35.0	5.5	0.0	3.1
150	13	58.4	0.12	37.0	7.8	0.0	4.9
250	24	54.1	0.03	42.0	13.1	0.0	10.2

Table 8: Composition of Retentate Stream for Membrane 2

Retentate Stream							
Nominal Flow [l/h]	Measured Flow [l/h]	CF₄ [%]	CO₂ [%]	Ar [%]	CF₄ Volume [l/h]	CO₂ Volume [l/h]	Ar Volume [l/h]
150	13	58.4	0.11	38	7.8	0.01	5.0
250	26	55.5	0.03	41	14.3	0.01	10.5

Table 9 Composition of Retentate Stream for Membrane 3

Considering the Table 6, Table 7, Table 8 and Table 9 it is visible how the different mixture components have the same behaviour in the two membranes. The CO₂ totally permeates the membranes and its contamination at the retentate side is very little, while CF₄ loss at the permeate side is low also for the input flow value of 100 l/h. Ar contamination at the retentate side is significant even if the most part goes to the permeate side. In the followings will be briefly displayed the results obtained during the tests.

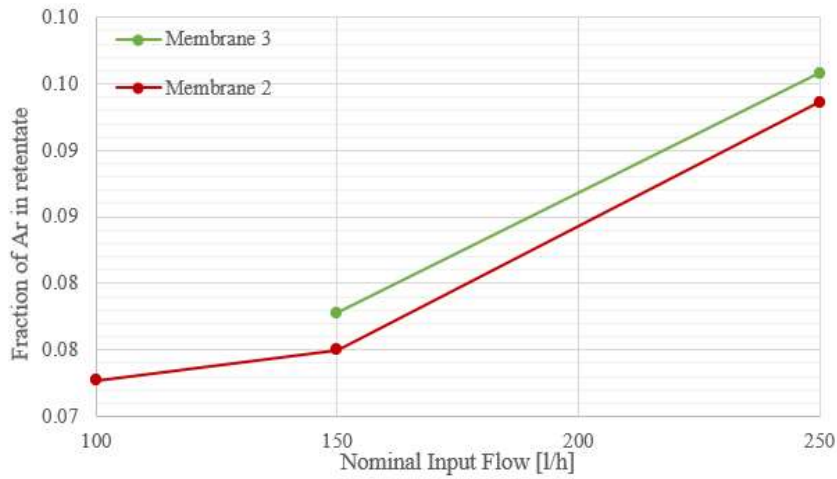


FIGURE 53: Fraction of Argon in Retentate Stream for membrane 2 (red) and membrane 3 (green)

In FIGURE 53 there are summarized the trends of Ar fraction (5) in retentate flow for the two membranes. It is visible the dependence from the input flow rate and the maximum value is reached for a nominal input flow of 250 l/h and it can be explained considering that higher flow causes minor contact time between molecules and fibers and they consequently have less time to permeate the membrane. The Ar permeance is similar to that of CO-C10 membrane.

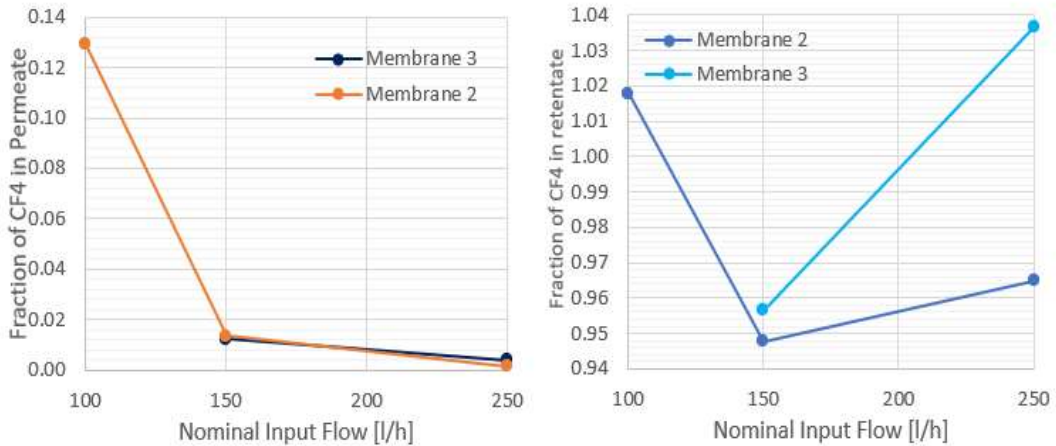


FIGURE 54: Fraction of CF₄ at Permeate (left) and Retentate (right) side for membranes 2 and 3

The graphs in FIGURE 54 show the trend of CF₄ loss and CF₄ recuperation efficiency for both membranes 2 and 3.

As regards the CF_4 loss at the permeate side, the two membranes have the same behaviour at the flow at which they were tested and specifically the CF_4 loss decreases for higher nominal input flow, showing good performance in the membrane flow range.

For what concerning the CF_4 at the retentate side, membrane 2 seems to be less performing at the flow at which tests were performed and it is visible for input flow value of 250 l/h. However, membrane 3 (and 2) shows an efficiency higher than 1 at 250 l/h and this is due to difference between nominal input flow and measured input flow and to intrinsic error of instrument used for flow measurements.

Generally, it can be considered that membranes have good performance in the flow range.

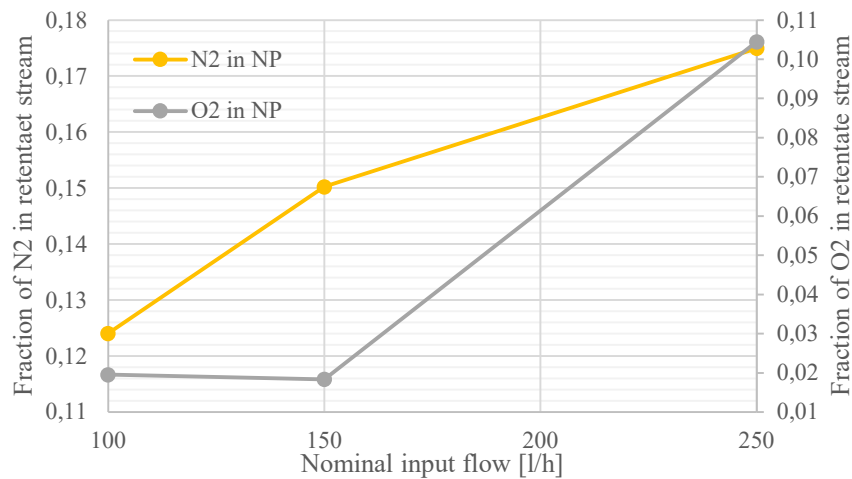


FIGURE 55: Fraction of O_2 (grey) and N_2 (yellow) in Retentate for Membrane 2

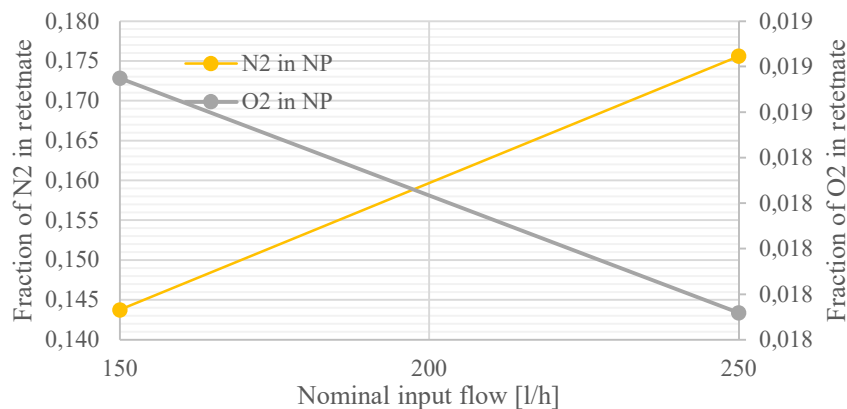


FIGURE 56: Fraction of O_2 (grey) and N_2 (yellow) in Retentate for Membrane 3

From the comparison between FIGURE 55 and FIGURE 56 the two membranes have the same rate of N₂ contamination at the retentate side while for what concerning the O₂ contamination, membrane 2 has higher O₂ content at the same flows than membrane 3.

It must be considered that even if the membranes are the same in terms of polymer (polyimide) and fibers, every membrane has unique internal structure due to production process and it justifies the differences of separation efficiency rates for each component.

4.2.4 Test 4: C07FS Membrane

The C07FS membrane was the last membrane tested which can work at flows up to 300 l/h. This is a asymmetric hollow fibers membrane and its structure is based on a gradient of density and small thickness of fibers. Among the various possible configurations of membranes in the modules, at an industrial level, asymmetric hollow fibers are preferred to others owing to their low production costs, high surface/volume ratios, reduced overall dimensions of the equipment (footprint) and excellent mechanical strength. Made up of a very thin dense layer, responsible for the separation, on a porous support made of the same material to increase the mechanical stability of the membranes against high pressure feed and with negligible mass transport resistance, this type of membrane configuration offers separation with high productivity [32].

The tests were performed to evaluate the membrane performance in order to potentially substitute the old membrane 1.

<i>Permeate Stream</i>							
<i>Nominal Flow [l/h]</i>	<i>Measured Flow [l/h]</i>	<i>CF₄ [%]</i>	<i>CO₂ [%]</i>	<i>Ar [%]</i>	<i>CF₄ Volume [l/h]</i>	<i>CO₂ Volume [l/h]</i>	<i>Ar Volume [l/h]</i>
50	43	0.0	58.4	42.3	0.0	25.3	18.3
100	99	0.0	59.3	41.6	0.0	58.9	41.3
150	143	0.0	64.7	43.9	0.0	92.5	62.7
200	190	0.0	63.4	39.6	0.0	120.5	75.3
250	223	0.0	66.0	35.4	0.0	147.1	78.9

Table 10: Composition of Permeate Stream

<i>Retentate Stream</i>							
<i>Nominal Flow [l/h]</i>	<i>Measured Flow [l/h]</i>	<i>CF₄ [%]</i>	<i>CO₂ [%]</i>	<i>Ar [%]</i>	<i>CF₄ Volume [l/h]</i>	<i>CO₂ Volume [l/h]</i>	<i>Ar Volume [l/h]</i>
50	7	53.6	5.2	41.0	4.0	0.4	3.0
100	11	61.8	0.3	47.0	6.7	0.0	5.1
150	18	49.5	0.1	57.0	9.0	0.0	10.3
200	30	37.4	0.4	62.0	11.3	0.1	18.8
250	49	28.4	1.6	68.0	13.9	0.8	33.3

Table 11: Composition of Retentate Stream

In Table 10 and Table 11 the concentration of mixture components between permeate and retentate sides are shown. The CO₂ is the main component at the permeate side as expected while the CO₂ contamination at the retentate side decrease from 50 l/h to 200 l/h and it increases again for a flow of 250 l/h. CF₄ loss at the permeate side can be considered zero also for low input flow (50 l/h) and it is due to the high selectivity of the membrane. The main Ar stream goes to the permeate side even if the contamination at the retentate side is significant and it greatly increases from 50 l/h up to 250 l/h. In the followings will be briefly displayed the results obtained during the tests.

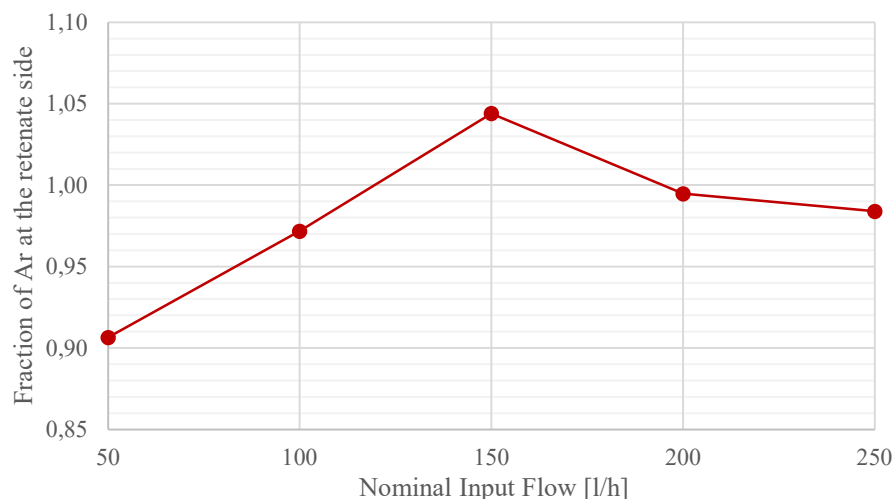


FIGURE 57: Fraction of Argon in Retentate Stream

In the graph (FIGURE 57) is shown the trend of Ar fraction (5) in retentate flow stream. It depends on the input flow rate and it decreases from 50 to 100 l/h (it is probably due to the bigger uncertainty for the low flows) and then it increases again

reaching the maximum value for a nominal input flow of 250 l/h. Ar contamination is higher than in the other tested membranes.

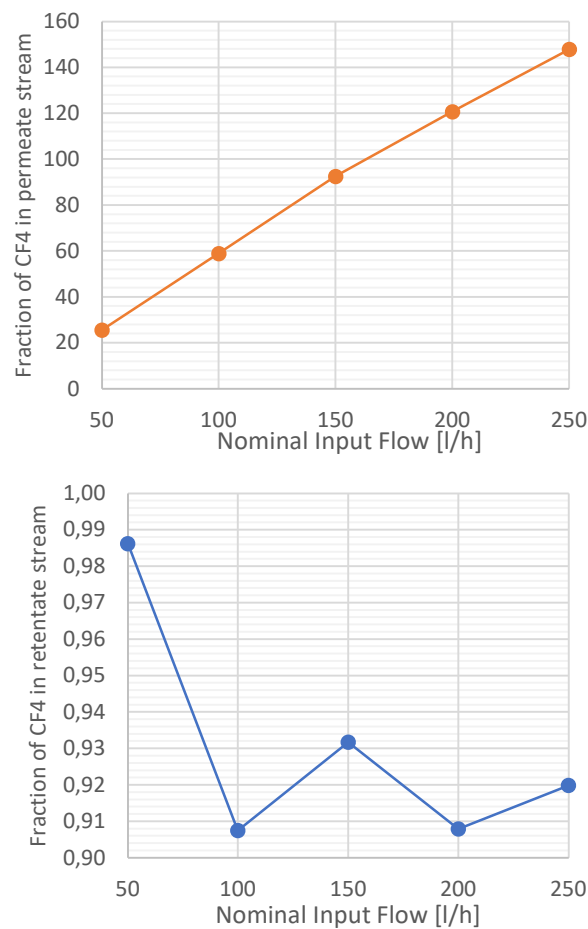


FIGURE 58: Fraction of CF_4 at Permeate (left) and Retentate (right) side

The CF_4 loss at the permeate side for this membrane model is almost zero and this is due to the polymer structure that confers it the high sensitivity. The CF_4 permeation decreases from 50 l/h to 250 l/h at which it is zero. In FIGURE 58 the recuperation efficiency is higher than 1 also for low input flow stream (50 l/h). These values of efficiency are due to difference between the values read by the flowmeters and the actual flow out of the membrane but also to the GC measures. For concentration higher than 30% the ratio concentration/area is not linear as a result of peak saturation. In this membrane the CF_4 loss is up to 1000 times lower than other membranes tested.

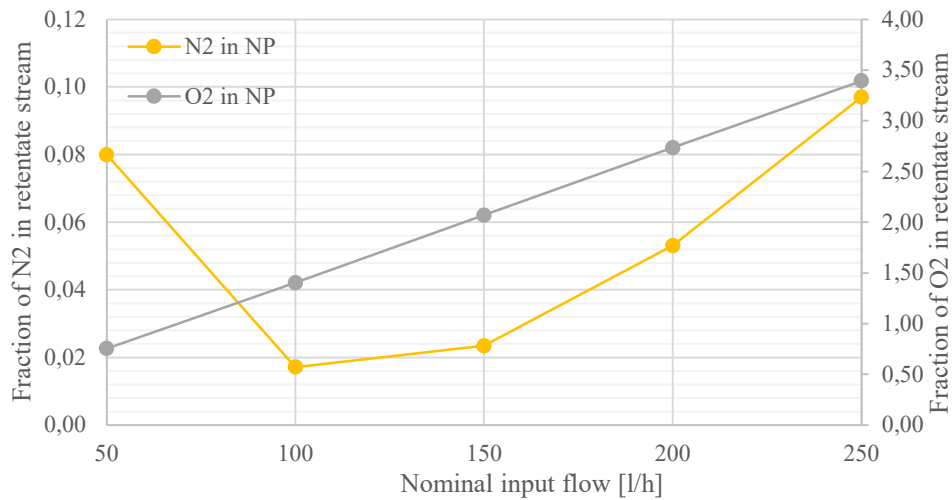


FIGURE 59: Fraction of O₂ (grey) and N₂ (yellow) in Retentate

In FIGURE 59 the trends of the two others main contaminants, O₂ and N₂, are shown. As for the Ar, their fractions decrease from 50 to 100 l/h and then they increase up to 250 l/h at which N₂ reaches a value of 50%.

Due to the high contamination of Ar and N₂ at the retentate side, this membrane cannot be used in the recuperation plant.

4.2.5 Test 5: Membrane CO-C410

The CO-C410 membrane is produced by the UBE Industries and it is characterized by high fibers thickness and gradient of density as the CO-C10A and CO-C10 models (paragraphs 4.2.2 Test 2: CO-C10 Membrane 4.2.3 Test 3: CO-C10A Membranes) but it can work at higher flows, up to 600 l/h. In the CF₄ membrane module there is a membrane of this type, the membrane 4. The tests were performed at nominal input flow of 250, 300 and 400 l/h since the membrane usually works between 250 and 350 l/h.

<i>Permeate Stream</i>							
<i>Nominal Flow [l/h]</i>	<i>Measured Flow [l/h]</i>	<i>CF₄ [%]</i>	<i>CO₂ [%]</i>	<i>Ar [%]</i>	<i>CF₄ Volume [l/h]</i>	<i>CO₂ Volume [l/h]</i>	<i>Ar Volume [l/h]</i>
250	251	0.03	58.9	42.7	0.08	147.9	107.3
300	298	0.02	58.3	42.0	0.06	173.8	125.1
400	373	0	60.1	41.9	0.00	224.1	156.3

Table 12: Composition of Permeate Stream for Membrane 4

<i>Retentate Stream</i>							
<i>Nominal Flow [l/h]</i>	<i>Measured Flow [l/h]</i>	<i>CF₄ [%]</i>	<i>CO₂ [%]</i>	<i>Ar [%]</i>	<i>CF₄ Volume [l/h]</i>	<i>CO₂ Volume [l/h]</i>	<i>Ar Volume [l/h]</i>
250	19	65.4	5.0	29.8	12.4	1.0	5.7
300	23	62.4	4.4	30.2	14.4	1.0	7.0
400	29	65.1	1.4	32.7	18.9	0.4	9.5

Table 13: Composition of Retentate Stream for Membrane 4

The results of tests performed on CO-C410 membrane are summarized in the Table 12 and Table 13 for input flows from 250 to 400 l/h. It can be considered that there is not CF₄ loss at the permeate side also for low input flow (250 l/h). For the input flow value of 300 l/h there is the best trade-off in terms of Ar and CO₂ contamination at the retentate side. The CO₂ concentration at the retentate side is higher than in the other membranes tested and it is higher for lower input flow. The achieved gas quality is good for input flow stream above 300 l/h.

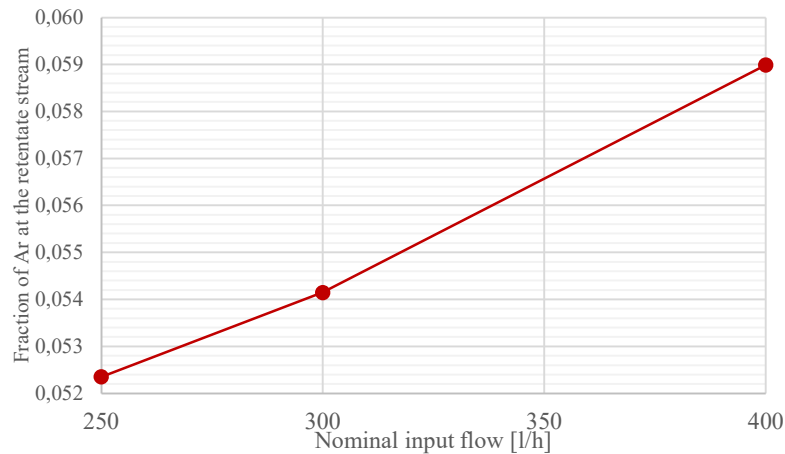


FIGURE 60: Fraction of Argon in Retentate Stream

The plot in FIGURE 60 summarize the trend of Ar fraction (5) in the retentate flow. As seen in the previous tests, it is visible the increasing of Ar fraction with the input flow rate, reaching the maximum value for 400 l/h. The Ar trend for this membrane is similar to that of CO-C10A and CO-C10 models.

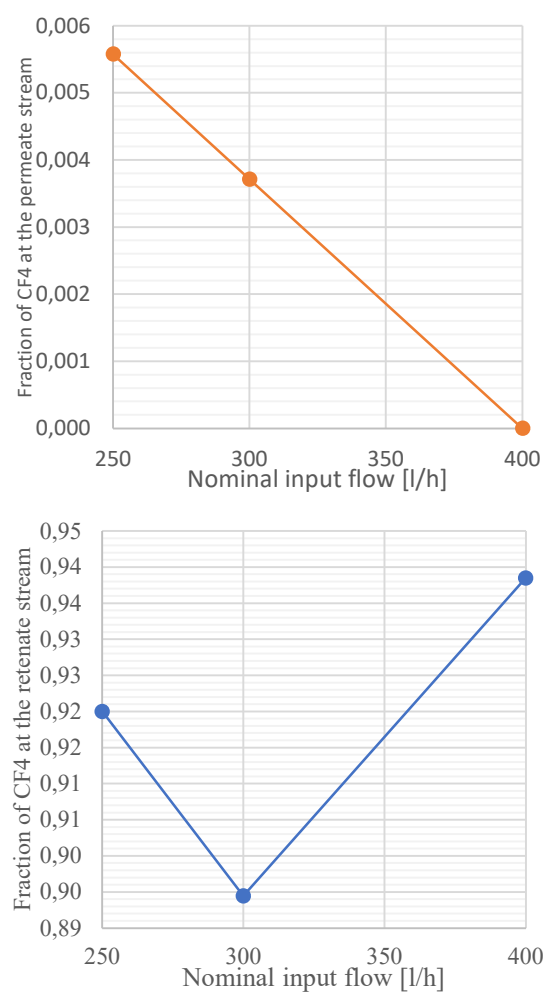


FIGURE 61: Fraction of CF_4 at Permeate (left) and Retentate (right) side

For higher input flow rate, the CF_4 loss at the permeate side decreases and it is due to the combination of gradient of density and high input flow rate.

In this membrane the CF_4 loss is 10 times lower than the membranes 2 and 3, and the best CF_4 recuperation efficiency is achieved for input flow of 400 l/h.

However, in the last months the usual input flow rate of the membrane was between 250 and 350 l/h so it did not reach the maximum efficiency.

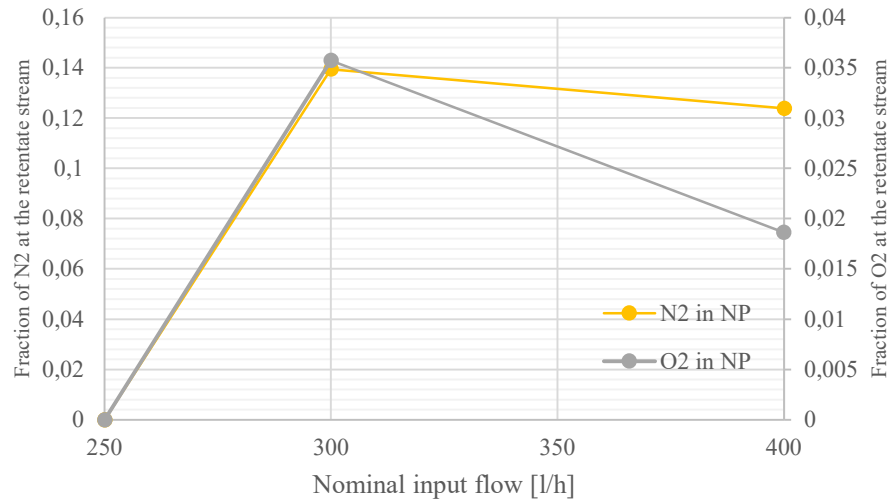
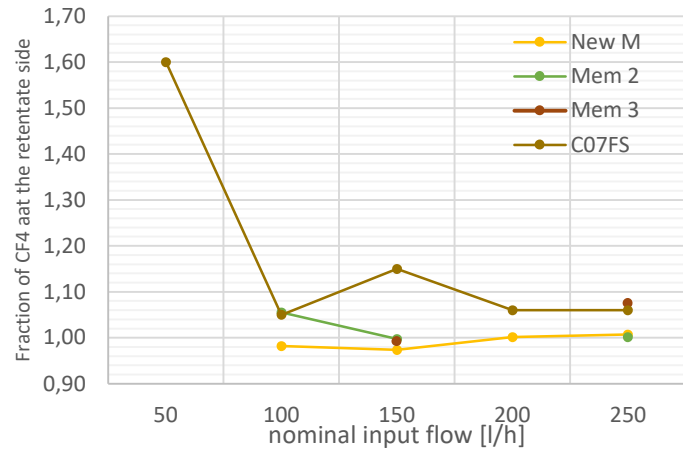


FIGURE 62: Fraction of O_2 (grey) and N_2 (yellow) in Retentate

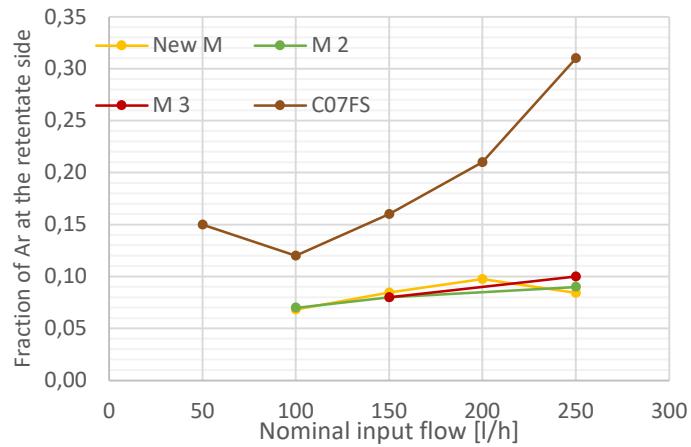
As shown in FIGURE 62, the trend of N_2 fraction (6) in the retentate side increases from 250 to 300 l/h and then it stabilizes at 400 l/h. It reaches a value ~14% for input flow value of 300 l/h and it means that for the usual input flow rate, the N_2 contamination is maximum. O_2 fraction at the retentate side is lower than that of N_2 but they have the same trend, reaching the maximum value at 300 l/h.

Considering the average membrane flow, this membrane has a quite good behaviour for the flows at which it was tested as well as the other membranes tested.

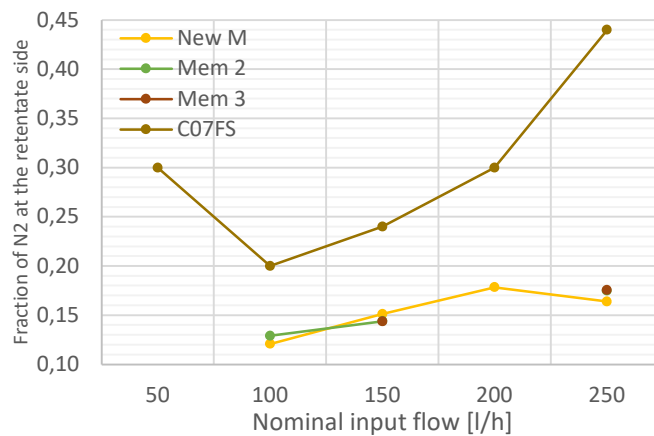
4.2.6 Membranes tests: overview



a)



b)



c)

FIGURE 63: Comparison between the membranes tested (except the E-Type and CO-C410 models); a) Fraction of CF_4 at the retentate side; b) Fraction of Ar at the retentate side; c) Fraction of N_2 at the retentate side.

The tests results show that the old membrane model E-Type has a very low efficiency as it was found during previous tests and it has confirmed that it cannot be used in the system due to the high CF₄ loss. For this reason, it was not included in the comparison with the other tested membranes. As shown in FIGURE 63, Membranes 2, 3 (CO-C10A model) and the new membrane CO-C10 have a similar behaviour in the flow range tested. A good separation of the gas mixture components is achieved with these membranes, which provide a good quality of CF₄ at the retentate side also at high input flow (200-250 l/h), with a little fraction of contaminants (Ar and N₂) that will be partially reduced in the next modules. The highly sensitive membrane CO-C07FS has a good separation efficiency even if a big fraction of Ar and N₂ (~ 30%) permeates the membrane, and consequently the recuperated CF₄ presents a high level of contamination. For this reason, this type of membrane is not the best solution for the recuperation system because it would affect the quality of the recuperated gas.

The best CF₄ membrane module configuration for the current work conditions is with the two membranes CO-C10A and the biggest one, the CO-410A. For an average input flow of 600 l/h they work, respectively, at 150 l/h and 300 l/h, flow at which the membranes have good performance.

4.3 Flow Test on the CF₄ Membrane module

One of the main problems of the CF₄ recuperation system was the difficulty to stabilize the input flow rate coming from the detector exhaust module. As a result of the tests performed, it was found that the membranes performance is influenced by the input flow rate. Several tests have been carried out at various input flow rate from 400 l/h to 800 l/h to better understand the effect of flow fluctuation on the CF₄ recovery membrane module.

Each test was realized in the membrane module in which there were three membranes: the two membranes CO-C10A and the membrane CO-C410. This configuration of the module has been tested at five different flows: 400, 500, 600, 700 and 800 l/h. The input gas flow (from the exhaust module) was set through the WinCCOA software, the gas flow rates of permeate and retentate were monitored with Mass Flow Controller devices that have a precision of 0.5% Rd ±0.1% FS, the pressure at the permeate (variable with the flow) and retentate sides were monitored through the dedicated software. Finally, the gas mixture concentration at the feed and retentate sides of the membrane

was measured using the μ Gas-Chromatograph (Paragraph 2.3) that allows to determine the concentration of the different components and to calculate the efficiency of the separation in the different conditions by combining the concentration and flow measurements. Beside the nominal input flow, also the corrected flow was calculated because the MFC was calibrated with a gas mixture of $\text{CF}_4/\text{Ar}/\text{CO}_2$ 10/40/50 and, for this reason, it was necessary to convert the flow set with the real flow sent by the MFC. Fractions and efficiency were calculated considering the *corrected flow*. In the followings the tests and their results will be explained.

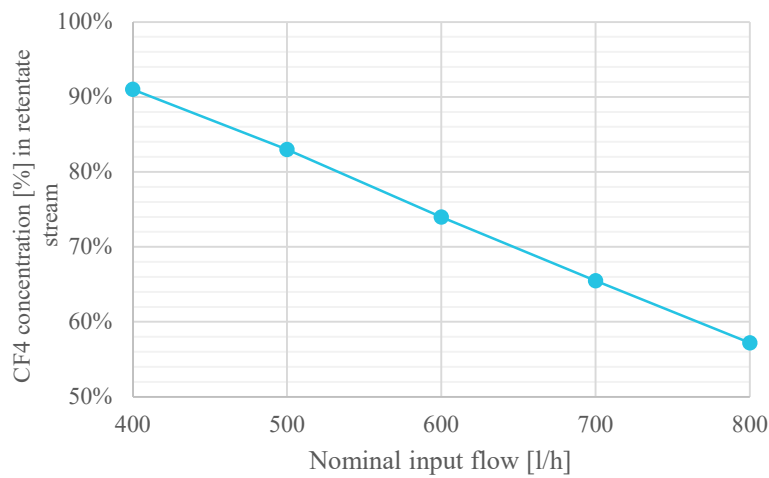


FIGURE 64: Concentration of CF_4 in retentate stream vs nominal input flow [l/h]

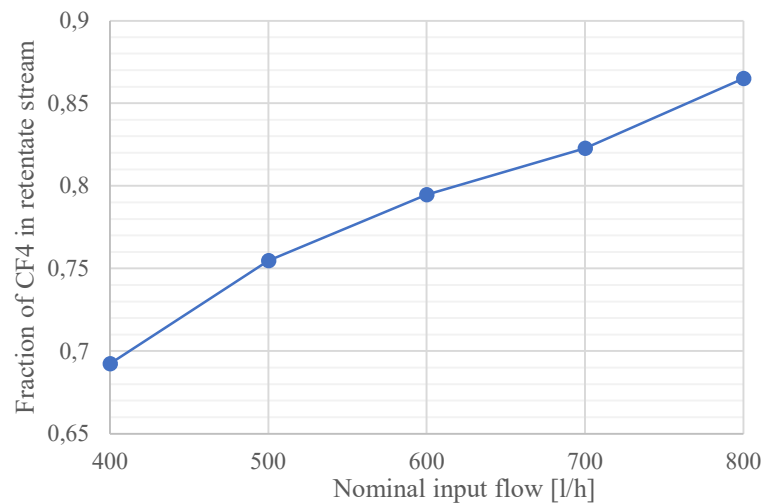


FIGURE 65: Fraction (6) of CF_4 in Retentate stream vs nominal input flow [l/h]

FIGURE 64 shows the trend of CF_4 concentration (measured by μGC) for the different values of nominal input flow and it decreases for higher input flow streams. It is probably since higher flow causes minor contact time between molecules of gas mixture and fibers and they consequently have less time to permeate the membrane, increasing their concentration at the retentate side.

On the other hand, FIGURE 65 shows the graph of the fraction of CF_4 (6) in retentate stream for the different values of nominal input flow. The higher the input flow stream, the higher the fraction of CF_4 recuperated at the retentate side and higher is the efficiency of the membrane module. The trend is not linear but increases more quickly from 700 to 800 l/h.

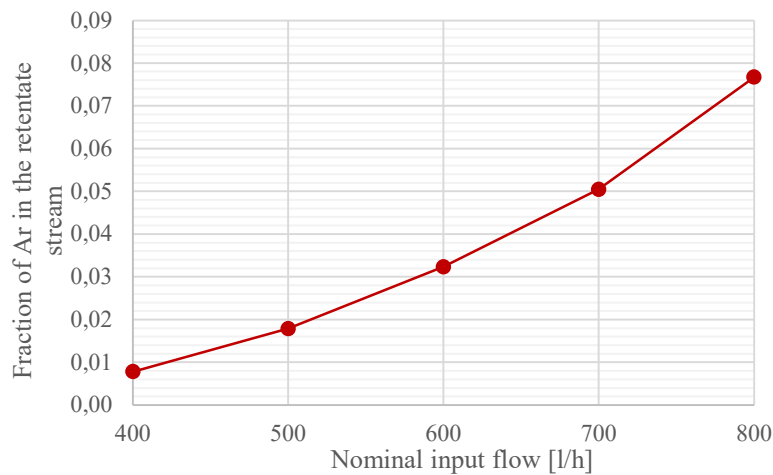


FIGURE 66: Fraction of Argon at the retentate side vs different nominal input flows

As regards the Ar contamination at the retentate side, FIGURE 66 shows the trend of Ar vs the values of nominal input flows [l/h] and it is visible that it increases for higher input flow rate. Also for the highest input flow (800 l/h) the fraction of Ar at the retentate side is less than 1% and it is acceptable for the recovery system.

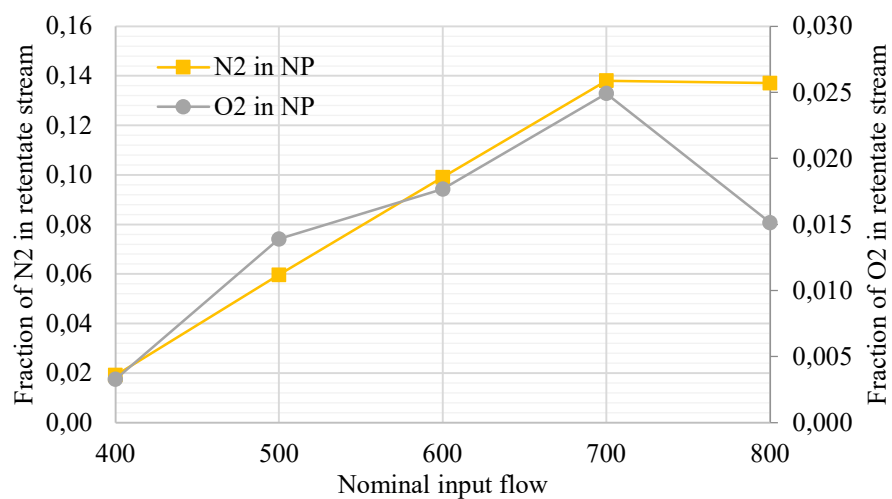


FIGURE 67: Fraction of O_2 (grey) and N_2 (yellow) in Retentate

In FIGURE 67 the trends of the two others main contaminants, O_2 and N_2 , are shown. Their fractions increase from 400 to 700 l/h and then the first one decreases for input flow value of 800 l/h while the latter one presents a plateau for nominal input value 700-800 l/h.

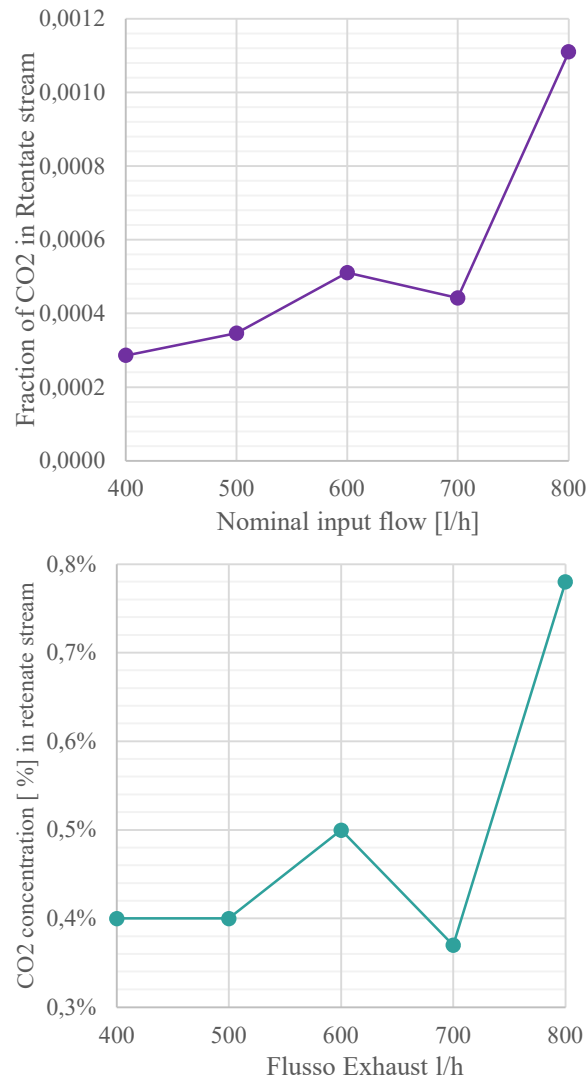


FIGURE 68: CO₂ Fraction (left) and concentration (right) in Retentate stream

Lastly, in FIGURE 68 the CO₂ fraction (left) and concentration (right) in retentate stream vs the nominal input flow [l/h] are shown. The fraction is very low also for high input flow and it increases slowly up to 700 l/h, reaching the maximum value for the nominal input flow of 800 l/h. Moreover, the concentration (right) is not negligible and it reaches the highest value for the 800 l/h.

4.3.1 Flow Test: Overview

<i>Composition of retentate stream</i>							<i>Fraction [%] at the retentate side</i>				
<i>Nom. Flow [l/h]</i>	<i>CF₄ [%]</i>	<i>CO₂ [%]</i>	<i>Ar [%]</i>	<i>O₂ ppm</i>	<i>N₂ ppm</i>	<i>P [bar]</i>	<i>CF₄</i>	<i>CO₂</i>	<i>Ar</i>	<i>O₂</i>	<i>N₂</i>
400	91.0	0.4	8.0	22	7301	-0.61	69.2	0.03	0.8	0.3	1.2
500	83.0	0.4	15.3	77	19000	-0.52	74.0	0.03	1.8	0.3	4.5
600	74.0	0.5	23.4	83	26700	-0.45	77.5	0.05	3.3	0.3	7.4
700	65.5	0.4	31.2	100	31825	-0.38	80.7	0.04	5.1	0.4	10.3
800	57.2	0.8	39.4	50	26242	-0.31	86.5	0.11	7.7	1.5	13.7

Table 14: Summary of concentration of components at the retentate side and composition of retentate stream in terms of fraction [%].

The performed tests (summarized in Table 14) have confirmed the relation between the input flow rate and the efficiency of the membranes separation. In particular, for low input flow rate all the components' fractions are low, including that of CF₄. This means that there is a big CF₄ loss rate with a consequent lower efficiency of the system, despite the good quality of the recuperated gas. For higher input flow rate, the fraction and the concentration of the CF₄ are inversely proportional and it is due to the increase in the fraction of the other components at the retentate side. The best performances of the membrane module are achieved for input flow rate between 600-700 l/h in terms of fraction of recuperated CF₄ and fractions of contaminants at the retentate side. Finally, the level of contamination given by the entire membrane module is lower than that of the single membranes and its efficiency is not affected also at higher input flow.

4.4 Pressure Test for the CF₄ Membrane module

An important parameter affecting the membranes efficiency has been noticed to be the pressure at the permeate side and for this reason several tests were performed to understand the effect of this parameter on the efficiency rate of the CF₄ membrane module. The module was tested at flows from 400 to 800 l/h and for the first it was evaluated the automatic variation of permeate pressure for each flow value and then a second pump was put into operation to increase or decrease the pressure at the permeate side. During the tests all the parameters (pressure and flow) were tuned and measured. The input gas flow (from the exhaust module) was set through the WinCCOA software,

the gas flow rates of permeate and retentate were monitored with Mass Flow Controller devices (Paragraph 4.3), the pressure at the permeate and retentate sides were set and monitored through the dedicated software. Finally, the gas mixture concentration at the feed and retentate sides of the membrane was measured using the μ Gas-Chromatograph (Paragraph 2.3) that allows to determine the concentration of the different components and allows to calculate the efficiency of the separation at the different pressures and flows.

Beside the nominal input flow, also the corrected flow was calculated because the MFC was calibrated with a gas mixture of $\text{CF}_4/\text{Ar}/\text{CO}_2$ 10/40/50 and, for this reason, it was necessary to convert the flow set with the real flow sent by the MFC. Fractions and efficiency were calculated considering the *corrected flow*.

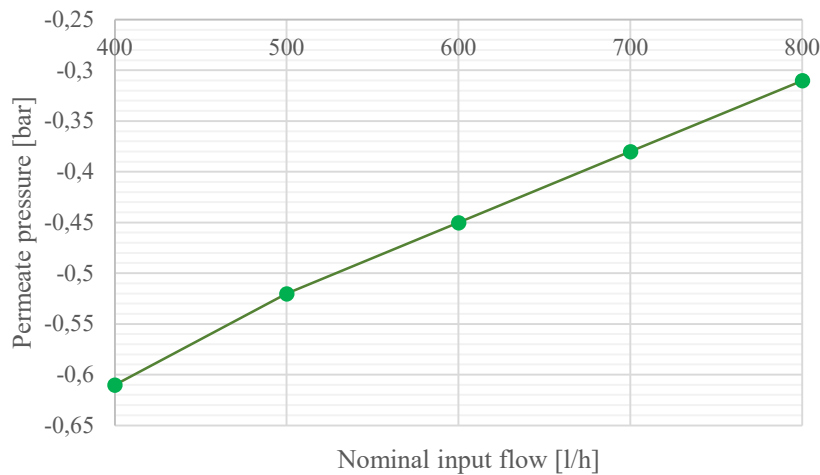


FIGURE 69: Pressure at permeate side vs nominal input flow

FIGURE 69 shows the trend of pressure at permeate side for the different values of nominal input flow and it can be noticed that the higher the flow, the higher the pressure. During these tests only one pump was in use and it was not possible to reach lower pressure.

The concentrations and fractions of each component at retentate and permeate side were the same seen in the previous paragraph and, as a result of the tests, it was noticed that at higher input flow streams also the contamination at the retentate side increases. The second pump was therefore put in use and there three sets of tests were performed at nominal input flow of 400, 600 and 800 l/h changing the pressure at the permeate side.

In the followings the results of these tests will be explained.

- **400 l/h**

For the nominal input flow stream of 400 l/h the system was tested at two different permeate pressures: -0.45 bar and -0.6 bar.

<i>Nominal Flow [l/h]</i>	<i>Corrected flow [l/h]</i>	<i>Permeate Press. [bar]</i>	<i>CF₄ [%]</i>	<i>CO₂ [%]</i>	<i>Ar [%]</i>	<i>Fraction of CF₄ [%]</i>	<i>Fraction of CO₂ [%]</i>	<i>Fraction of Ar [%]</i>
400	417.5	-0.45	79.6	1.2	17.8	70.76	0.10	2.0
400	417.5	-0.6	89.9	0.6	8.5	67.50	0.04	0.84

Table 15: Concentration and fraction of mixture components at the retentate side for different values of permeate pressure at nominal input flow of 400 l/h

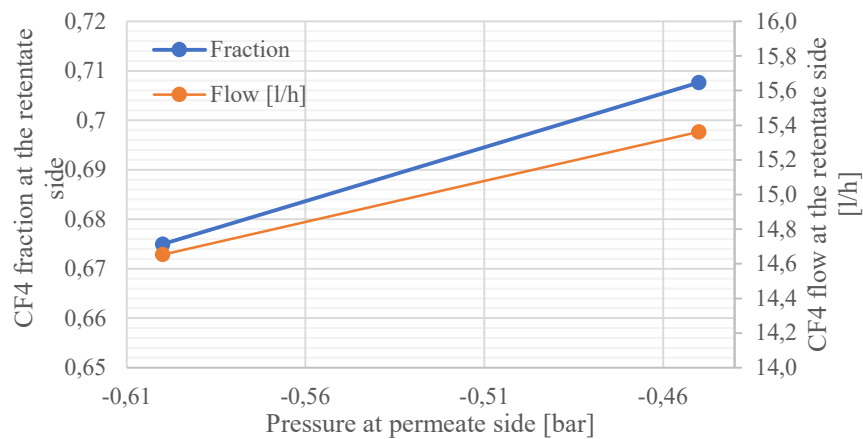


FIGURE 70: CF₄ fractions and CF₄ flows [l/h] at the retentate side vs different pressure at permeate side [bar]

In Table 15 the concentrations and the fractions (6) of the mixture components at the retentate side for the different values of pressure at the permeate side are shown. For lower pressure, the concentration of CF₄ is higher (from 80 to 90%) as the purity of recovered gas. On the other hand, the lower pressure causes higher permeate stream flow and consequently part of the CF₄ goes to the permeate side, decreasing the global efficiency of the system. In FIGURE 70 there are the trends of CF₄ fraction (blue) and

CF₄ flow stream at the retentate side and it is visible that in this case the CF₄ loss in terms of l/h is negligible with respect to the higher purity of recovered gas. Since the concentration of CF₄ in the feed stream is low, also a large variation of recovered fraction values is very small if expressed as l/h.

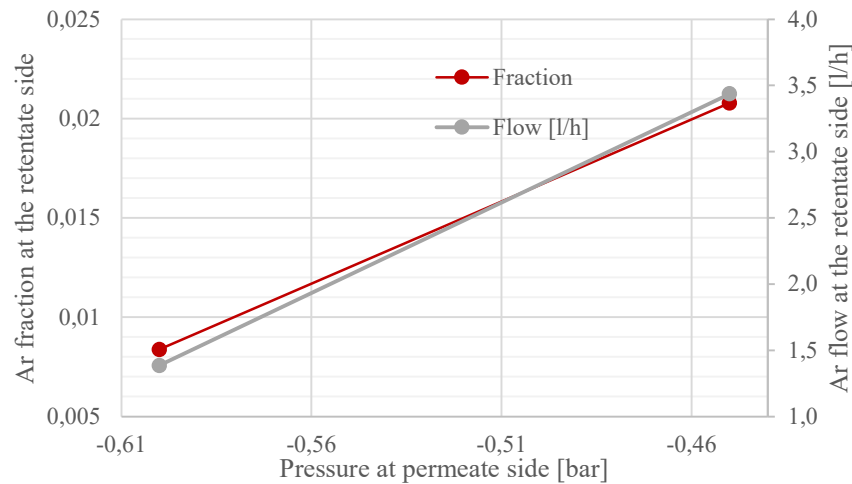


FIGURE 71: Ar fractions and Ar flows [l/h] at the retentate side vs different pressure at permeate side [bar]

As regarding the Ar contamination (FIGURE 71), the fraction and the flow stream at the retentate side decreases passing from -0.45 to -0.6 bar, confirming a better performance of the membrane at lower permeate pressure.

The membrane module achieves also a good N₂ separation quality passing from ~12500ppm to ~6500ppm for -0.45 and -0.6 bar, respectively.

- **600 l/h**

For the nominal input flow stream of 600 l/h the system was tested at three different permeate pressure: -0.35 bar, -0.44 bar and -0.6 bar

<i>Nominal Flow [l/h]</i>	<i>Corrected flow [l/h]</i>	<i>Permeate Press. [bar]</i>	<i>CF₄ [%]</i>	<i>CO₂ [%]</i>	<i>Ar [%]</i>	<i>Fraction of CF₄ [%]</i>	<i>Fraction of CO₂ [%]</i>	<i>Fraction of Ar [%]</i>
600	626.2	-0.35	64.8	0.6	33.2	82	0.1	5.5
600	626.2	-0.44	72.7	0.5	24.8	78.53	0.1	3.5
600	626.2	-0.6	86.5	0.2	12.6	75.9	0.02	1.5

Table 16: Concentration and fraction of mixture components at the retentate side for different values of permeate pressure at nominal input flow of 600 l/h

As seen for the 400 l/h tests, also in this case the concentration and the fraction have opposite behaviour: for lower pressure at the permeate side, the concentration of CF₄ increases while the one of contaminants decreases and the fraction decreases both for CF₄ and contaminants. The important parameter to evaluate is the ratio CF₄ loss/ CF₄ purity that will be discussed in the followings.

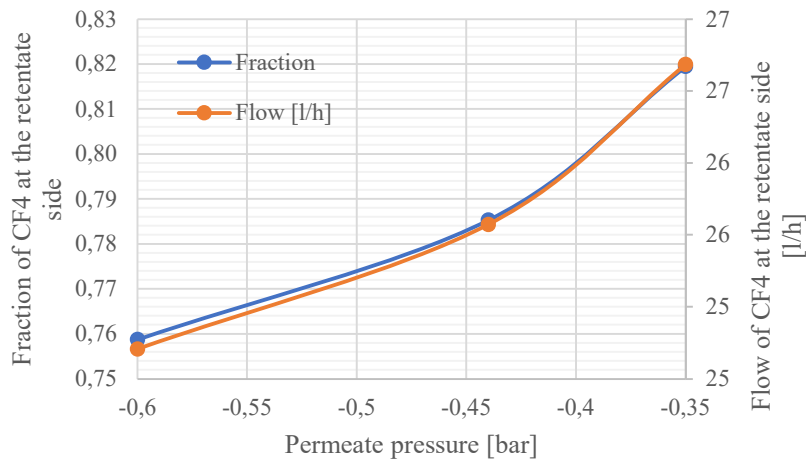


FIGURE 72: CF₄ fractions and CF₄ flows [l/h] at the retentate side vs different pressure at permeate side [bar]

The fraction and flow of CF₄ at the retentate side decrease for lower values of pressure at the permeate side. Although the fraction seems to decrease a lot, the CF₄ loss in terms of l/h is only 2 l/h and the gain in term of purity of recovered CF₄ is much higher and it can be ignored.

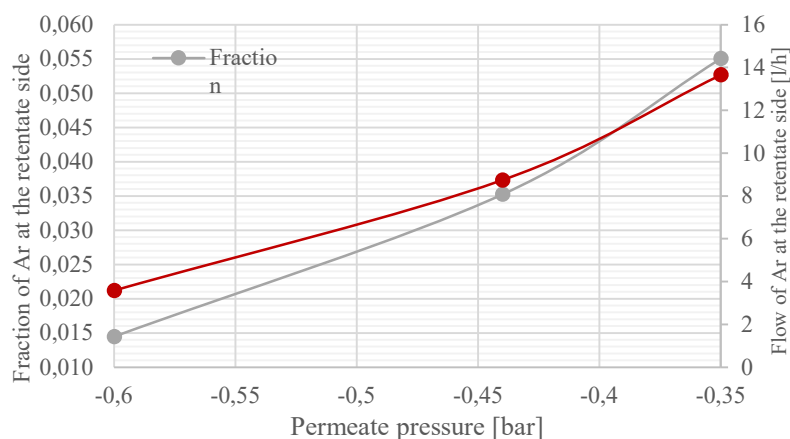


FIGURE 73: Ar fractions and Ar flows [l/h] at the retentate side vs different pressure at permeate side [bar]

The Ar fraction at the retentate side decreases of 4% passing from -0.35 bar to -0.6 bar and the decrease of flow was 10 l/h. Also in this case the loss of CF₄ is much lower than the gain in terms of purity and a lower pression at the permeate side was confirmed as the best setup for the membrane module.

Good results were also achieved for the N₂ contamination at retentate side which passed from ~22000ppm to ~10400ppm for -0.35 and -0.6 bar, respectively while the fraction of N₂ decreased by 7%.

- **800 l/h**

For the nominal input flow stream of 800 l/h the system was tested at two different permeate pressure: -0.45 bar and -0.6 bar.

<i>Nominal Flow [l/h]</i>	<i>Corrected flow [l/h]</i>	<i>Permeate Press. [bar]</i>	<i>CF₄ [%]</i>	<i>CO₂ [%]</i>	<i>Ar [%]</i>	<i>Fraction of CF₄ [%]</i>	<i>Fraction of CO₂ [%]</i>	<i>Fraction of Ar [%]</i>
800	835.0	-0.45	70.4	0.1	28.4	82.4	0.01	4.4
800	835.0	-0.6	83.9	0.1	15.3	79	0	1.9

Table 17: Concentration and fraction of mixture components at the retentate side for different values of permeate pressure at nominal input flow of 800 l/h

From Table 17 the concentration of CF_4 increases at lower pressure at the permeate side while the fraction (6) decreases. For the other components both concentration and fraction decrease for lower values of pressure at the permeate side.

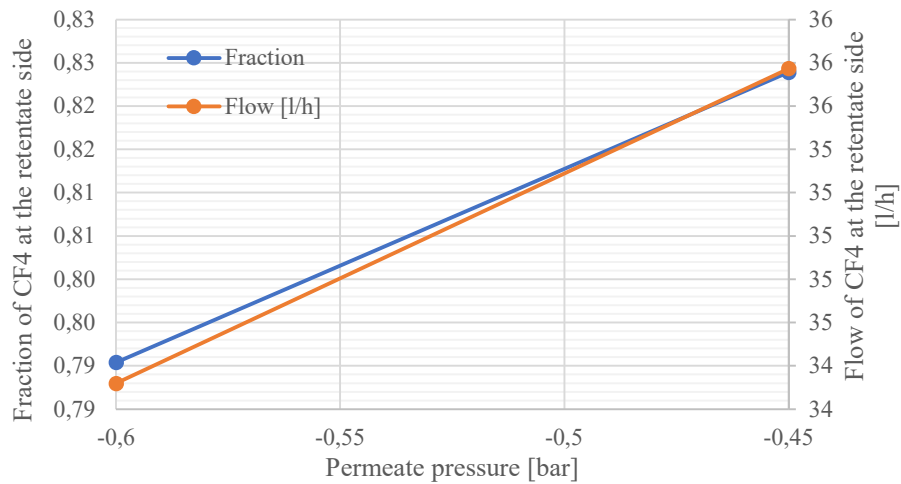


FIGURE 74: CF_4 fractions and CF_4 flows [l/h] at the retentate side vs different pressure at permeate side [bar]

The fraction of CF_4 passes from 79% to 82% for permeate pressure values of -0.6 and -0.45 bar while the CF_4 loss as flow [l/h] was 2 (FIGURE 74).

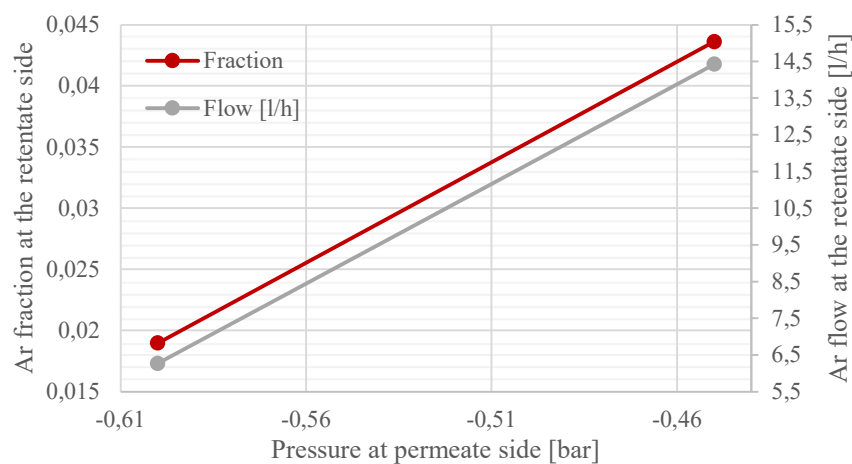


FIGURE 75: Ar fractions and Ar flows [l/h] at the retentate side vs different pressure at permeate side [bar]

The Ar fraction at the retentate side decreases of 3.5% passing from -0.45 bar to -0.6 bar and the decrease of flow was 8 l/h. The loss of CF₄ at highest input flow stream is much lower than the gain in terms of purity and a lower pressure at the permeate side. The N₂ contamination at retentate side passed from ~18000ppm to ~13500ppm for -0.45 and -0.6 bar, respectively while the fraction of N₂ decreased by 4%.

Following these tests and after evaluating the results obtained, it has been decided to leave both vacuum pumps in use to reach a lower pressure at the permeate side and to obtain a purer recovered CF₄.

4.4.1 Pressure Test: Overview

<i>Composition of retentate stream</i>						
<i>Cor- rected Flow [l/h]</i>	<i>Press P [bar]</i>	<i>CF₄ [%]</i>	<i>CO₂ [%]</i>	<i>Ar [%]</i>	<i>O₂ [ppm]</i>	<i>N₂ [ppm]</i>
418	-0.45	79.6	1.2	17.8	61	12421
418	-0.6	89.9	0.6	8.5	42	6504
626	-0.35	64.8	0.6	33.2	58	22052
626	-0.44	72.7	0.5	24.8	43	18157
626	-0.6	86.5	0.2	12.6	22	10470
835	-0.45	70.4	0.1	28.4	26	18836
835	-0.6	83.9	0.1	15.3	21	13520

<i>l/h of components at the ret. side</i>					
CF ₄	CO ₂	Ar	O ₂	N ₂	<i>CF₄ frac- tion [l/h]</i>
15	0.23	3	0.001	0.2	70.76%
15	0.10	1	0.001	0.1	67.50%
27	0.26	14	0.002	0.9	81.95%
26	0.18	9	0.002	0.6	78.53%
25	0.06	4	0.001	0.3	75.87%
36	0.07	14	0.001	1.0	82.39%
34	0.02	6	0.001	0.6	79.04%

Table 18: Summary of concentration of components at the retentate side and composition of retentate stream in terms of l/h.

The tests' results in Table 18 show that lower pressure at the Permeate side allows to obtain a higher CF₄ recuperated quality with a negligible loss of CF₄ in terms of l/h at the same side of the membrane even if there is a variation in the CF₄ fraction at the retentate side. For each input flow rate tested it has been obtained the same results:

lower pressure at the permeate side, higher quality of the recuperated CF_4 at the retentate side.

As result of this test, the second vacuum pump was switched on and the pressure at the permeate side was set at a value of ~ -0.6 bar.

Chapter 5

Optimization of the “CF₄ Absorber Module” in the CF₄ recovery plant (CMS-CSC)

5.1 CF₄ absorber module: Overview

The absorber module is the last module in which the recuperated CF₄ is purified from contaminants (N₂ and Ar). This module contains two columns of 42 l each, filled with a 13X molecular sieve that has a big affinity for both CF₄ and CO₂. For this reason, an absorber module for the CO₂ is needed before that allows to reach a CO₂ concentration of some ppm in the gas mixture arriving to the absorber module, and it does not affect the functioning of the module in trapping the CF₄.

The module was designed to work in continuous mode with one of the two columns in run and the other one in regeneration. The columns used in the LHC recuperation systems are generally heated only from outside while in this case they are heated from both inside and outside to increase the speed of regeneration and to decrease the dead time after a regeneration. At the moment, only one of the two columns is working.

The goal of this module is to absorb the CF₄ in the 13X structure leaving the contaminants out of the pores of the molecular sieve in order to release them (first contaminants and then CF₄) at different values of pressure.

The absorption is based on the Pressure Swing Adsorption method: it starts from vacuum and stops when the relative pressure inside the cartridge is equal to zero or to the pressure in the supply line. The advantage of this method is that the molecular sieve is not fully saturated and therefore the CF₄ continues to be adsorbed until the end of the cycle, leaving only Ar and N₂ in the empty space.

When the cycle is completed, the emptying of the module starts and it is divided in two phases: firstly, the pressure decreases from ~ -0.050 bar to ~ -0.450 bar releasing all the components that are in the column's empty space and which are not trapped by the molecular sieve, as N₂ or Ar, and then they are vented to the atmosphere; in the second step the pressure passes from ~ -0.450 bar to ~ -0.960 bar and during this phase all the remaining volatile components and the trapped CF₄ are released and sent to the storage module.

Until some months ago the recuperation of the CF₄ started at column pressure of -0.7 bar but it was noticed that the total efficiency of the system was very low. Consequently, it has been decided to modify the pressure parameters of the column's emptying, increasing the pressure of the start of the second phase from -0.7 bar to -0.45 bar in order to verify if the total efficiency of the system improved since one problem could be the loss of the most of CF₄ in the phase of contaminants releasing.

All the module phases are controlled by the software (FIGURE 76) through which it is possible to modify the parameters to optimize the CF₄ recuperation. This part will be treated in the next paragraphs.

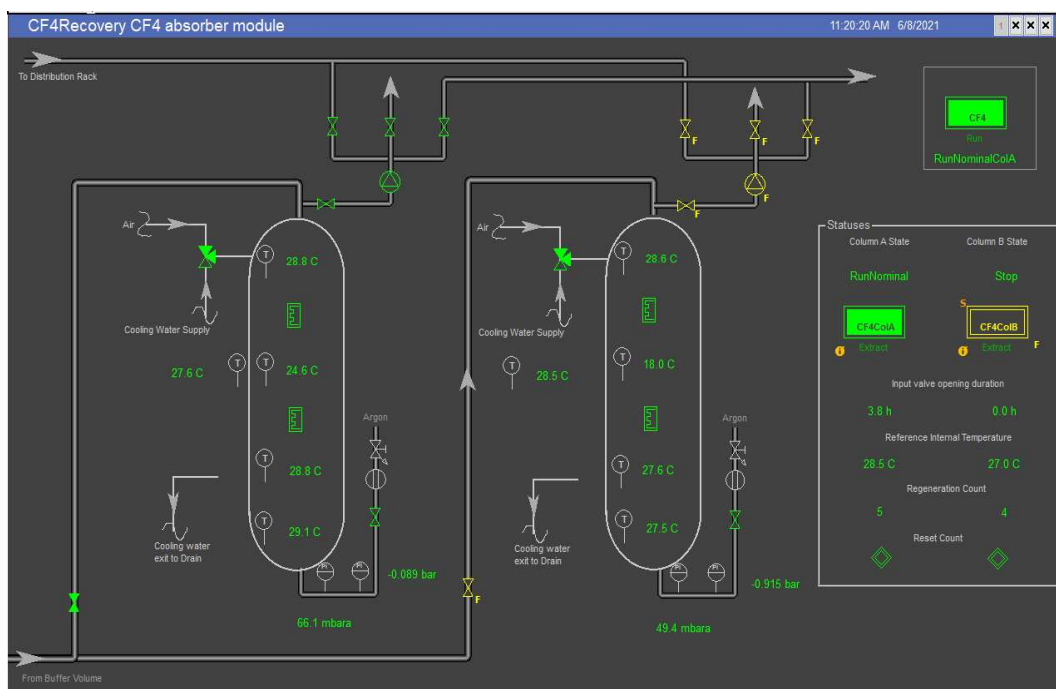
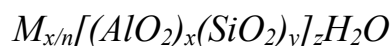


FIGURE 76: Picture of CF₄ absorber module in winCCOA software.

5.2 Structure and functioning of molecular sieve

Molecular sieve adsorbents are crystalline aluminosilicates of alkali and alkali earth elements such as sodium, potassium, and calcium, represented by the stoichiometry:



Where x and y are integers with x/y equal to or greater than 1, n is the valence of cation M, and z is the number of water molecules in each unit cell (FIGURE 31 and FIGURE 33). The skeleton has a regular structure of cages, which are usually interconnected by six windows in each cage. The size of the window apertures, which can be controlled by fixing the type and number of cations, ranges from 3Å to 10Å. These pores, or cages, have a high affinity to re-adsorb water or other polar molecules [33].

The primary structural units of zeolites are the tetrahedra of silicon and aluminium, SiO₄ and AlO₄. The units are assembled into secondary polyhedral building unit such as cubes, hexagonal prism, octahedra, and truncated octahedra. The final zeolite structure consists of assemblages of the secondary units in a regular three-dimensional crystalline framework. The inner atoms in the windows are oxygen. The size of the windows depends, then, on the number of oxygen atoms in the ring – four, five, six, eight, ten, or twelve. In the CF₄ absorber module the 13X zeolite is employed, characterized by a pore diameter of 10Å, which absorbs only CF₄ (that has a kinetic diameter of 4.8Å) while the Ar and N₂ (they respectively have a kinetic diameter of 3.4 and 3.64Å) remain volatile and are vented from the cartridge.

Aided by strong ionic forces (electrostatic fields) due to the presence of cations and by the enormous internal surface area of up to 1,000 m²/g, molecular sieves will adsorb a considerable amount of water or other fluids. If the fluid to be adsorbed is a polar compound, it can be adsorbed with high loading, even at very low concentrations of the fluid. Molecular sieves will, therefore, remove gas or liquid impurities to very low levels (ppm or less). Another feature of molecular sieve adsorbents is their ability to separate gases or liquids by molecular size or polarity. The pore, or cage, openings are the same size as many molecules, e.g., in the case of hydrocarbon paraffins, straight-

chained molecules can fit into the pores and be adsorbed, while the branched-chain molecules cannot enter the pores and pass through the molecular sieve bed unadsorbed.

5.3 Weekly analysis of the CF₄ absorber module

As a result of the test performed on the membrane module it has been possible to make a correlation between the flow rate from the exhaust module and the efficiency of the entire CF₄ recovery system. However, as seen in the previous chapter, it is not possible to stabilize the flow, but it is only possible to reduce the range in which the flow oscillates, that is also affected by environmental parameters, such as temperature or atmospheric pressure than cannot be tuned. The daily efficiency is not stable during the week, and it depends on many parameters.

For monitoring the status of the system, in addition of taking into account the parameters on the WinCCOA software, it was decided to carry out the GC analyses of the CF₄ Absorber module once a week.

The analyses of the gas exiting from the absorber module and directed towards the storage module were performed with the μ GC (Paragraph 2.3 Gas Analysis with Gas Chromatograph).

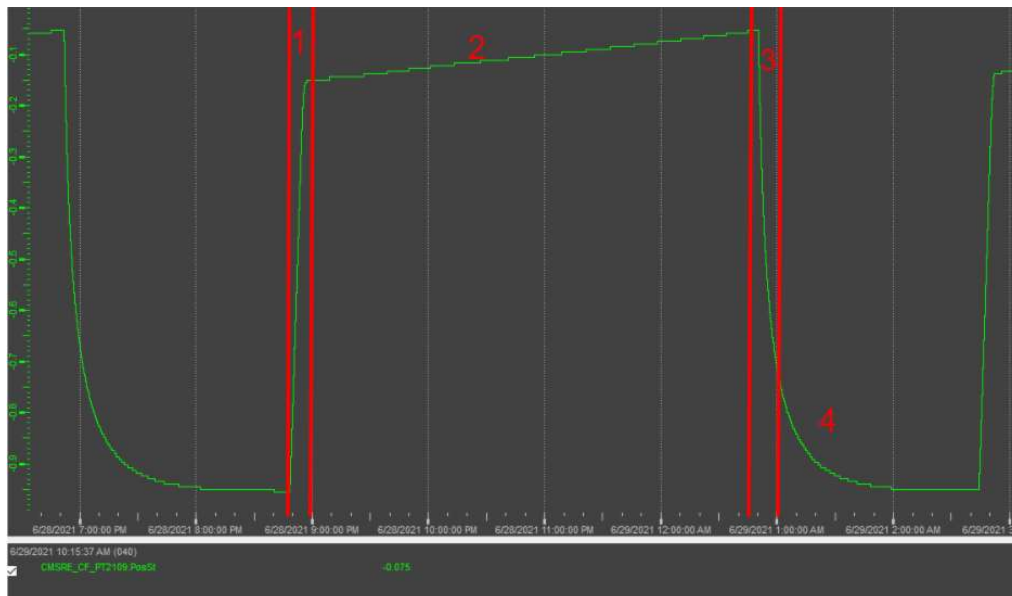


FIGURE 77: CF₄ absorber cycles graph (pressure [bar] vs time) on WinCCOA software.

In FIGURE 77 the cycle of the CF₄ absorber module is shown. It can be ideally divided in four steps:

- 1) the filling of the cartridge that correspond to the first pressure increasing (from -0.960 bar to -0.150 bar).
- 2) the separation phase (corresponding to the little increasing of the pressure in a wide time interval) during which the gas inside the cartridge is separated between the CF₄ component adsorbed by the molecular sieve and the remaining components (Ar, N₂) that occupy the free space in the cartridge and the head space in the column (from -0.150 bar to -0.055 bar).
- 3) the first phase of emptying (from -0.053 to -0.450 bar) during which the components not retained by the molecular sieve (N₂ and Ar) are released.
- 4) the last phase of emptying (before it started from -0.7 bar but now it starts from -0.451 and it ends at -0.958 bar) during which the CF₄ and a part of Ar and N₂ are released by the molecular sieve and sent to the next module.

Considering that the analysis point to the μ GC is located between the automatic valve controlling the second phase of the module emptying and the buffer before the storage battery, the right moment to perform the analyses results to be during the second phase or the fourth phase. In the first case the analyses are performed on the gas remained in the buffer from the past cycle, while in the latter case the analyses are performed on the gas that is exiting from the module at that time.

Below the analyses performed in the last months will be explained.

Date	Ar [%]	CF ₄ [%]	CO ₂ [%]	O ₂ ppm	N ₂ ppm
07/10/2020	2.22	97.23	0.016	400	3860
13/11/2020	1.13	97.41	0.066	175	2175
10/12/2020	21.03	78.00	0.054	420	24766
14/01/2021	17.14	80.95	0.014	458	37625
08/02/2021	2.09	97.38	0.020	628	4996
10/03/2021	2.88	95.37	0.004	111	4460
09/04/2021	3.85	94.49	0.019	137	5095
11/05/2021	2.05	97.67	0.016	179	2881
08/06/2021	1.78	97.16	0.006	173	2646

Table 19: Overview of CF₄ Absorber module analyses performed in the last months (October – June); the analyses have been performed during the separation phase.

In Table 19 some results of performed analyses on the CF₄ absorber module are shown. During the last months, the trend of Ar and N₂ contamination and the CF₄ % were stable except for the months of December and January (red in the table) during which the analyses showed an anomalous trend of Ar and N₂ contamination reaching the ~20%, probably due to the wide fluctuation of the flow from the exhaust module to the recuperation plant.

The concentration of Ar was calculated by deducting the concentration of N₂ from the Ar concentration, since the peak of N₂ is visible also in the PPU column where they are superposed.

It is also visible that the CO₂ and O₂ concentrations are very low, and the main contaminants remain Ar and N₂ (FIGURE 78).

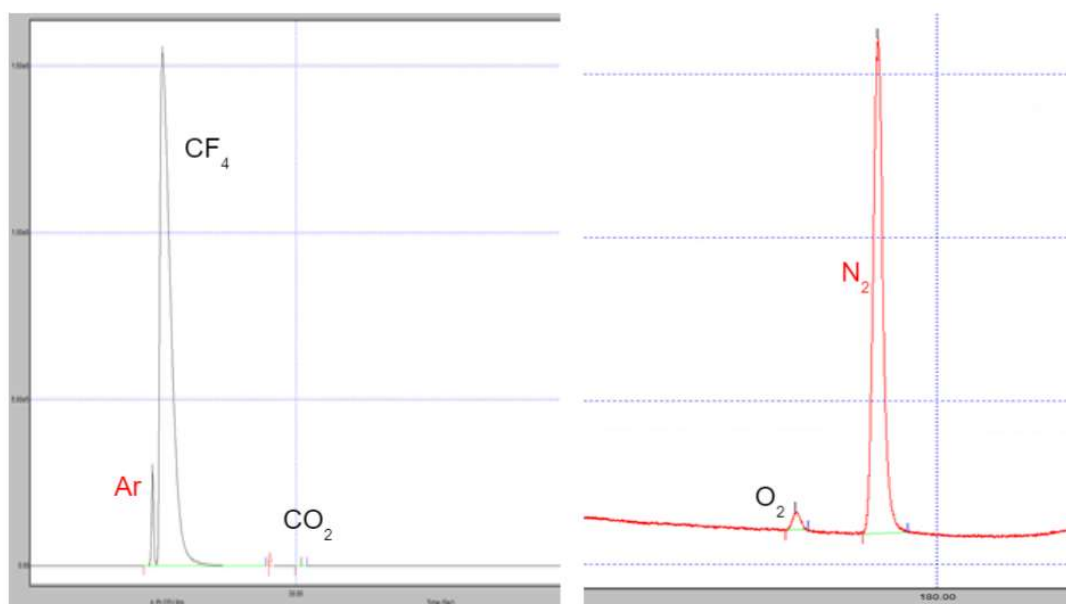


FIGURE 78: Typical peaks in the CF₄ absorber chromatogram.

Furthermore, during the μ GC analyses the CF₄ absorber parameters were monitored, and it has been noticed that there was a variation in the Ar concentration at different pressures (FIGURE 80) in the absorber column even though the automatic valve was closed at that time.

It has therefore become necessary to perform analyses during the entire CF₄ absorber module cycle to better understand the trend of CF₄ and Ar and the possible causes.

5.3.1 Analysis of complete cycle of CF₄ absorber module

The purpose of the test was to understand the phenomena occurring in the buffer module before the storage module and the causes of the fluctuation of Ar concentration during the different phases of the absorber module.

Besides the component's concentration, also some parameters were considered such as the pressure in the column at that time and the status of the automatic valves (open/closed) controlling the release of the components from the module.

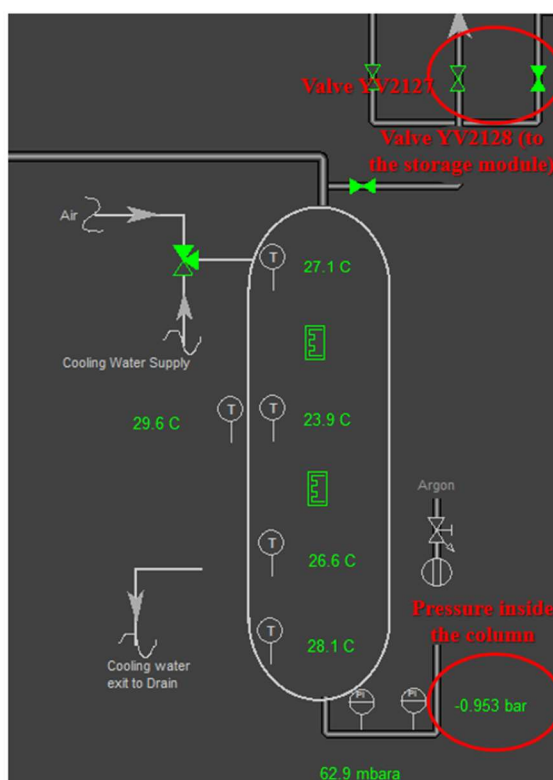


FIGURE 79: Layout of the absorber module and parameters considered during the analyses

In FIGURE 79 the absorber module and some parameters considered during the GC analyses are shown. The pressure inside the column was considered to evaluate the status of the absorber cycle during the tests how it has been shown in Paragraph 5.3 Weekly analysis of the CF₄ absorber module

The valve YV2127 is the one controlling the first phase of the column emptying, i.e. the release of the contaminants that are not trapped by the molecular sieve. It can assume the value of 1 when it is open (in the first phase of emptying) and the value of 0 when it is closed (the rest of time). The valve YV2128 is the one that connects the absorber module to the next one and, how seen for the valve YV2127, it can assume

the value of 1 when it is open (during the second phase of emptying) and the value of 0 when it is closed (for the rest of time).

Below the graphs summarizing the results obtained in these tests.

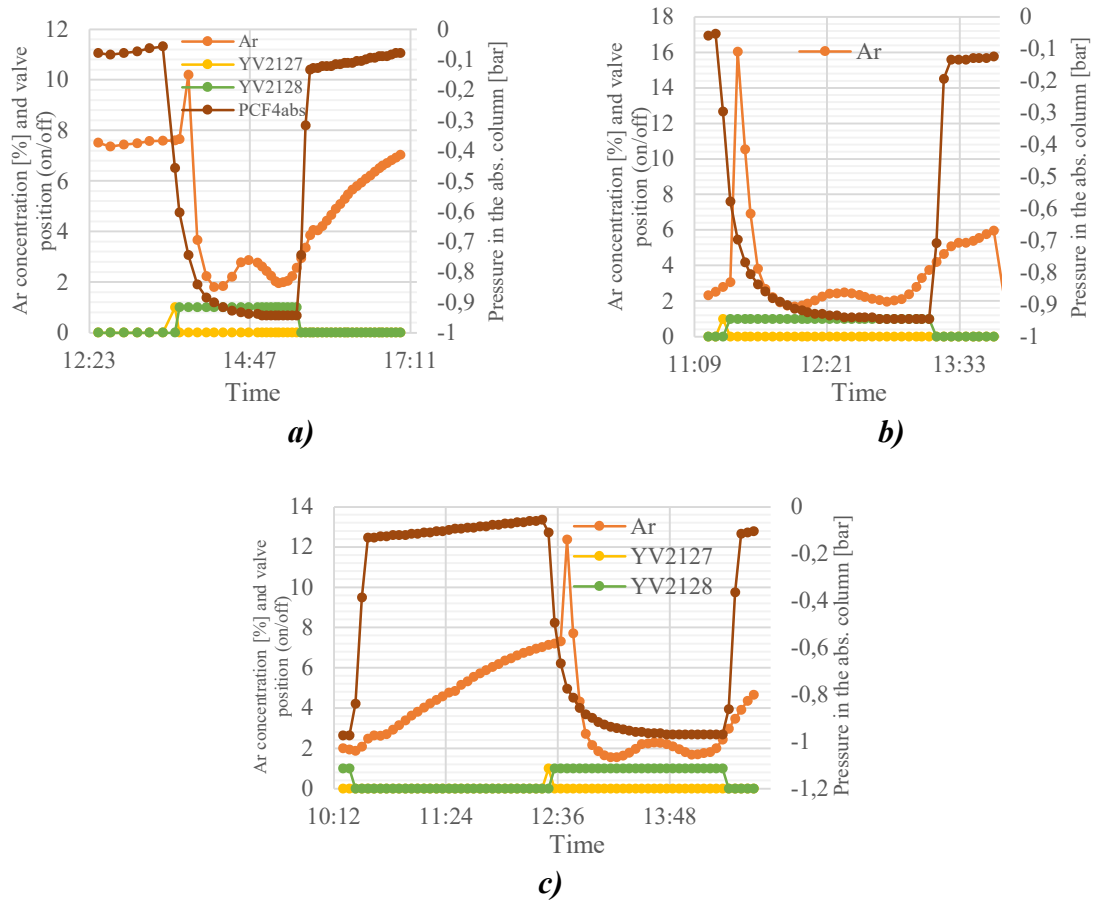


FIGURE 80: Graphs of CF_4 absorber module analyses performed during the entire cycle;
a) 09/02/2021, b) 10/02/2021, c) 25/02/2021

In the FIGURE 80 there are three graphs of the complete cycle analyses of the CF_4 absorber module. In each graph the data of Ar concentration [%], status of the valves YV2127 and YV2128, and the pressure inside the absorber column are reported. The concentration of Ar has the same behavior in all the three graphs, passing from 2% to 7.3% in the pressure range of -0.8/-0.1 bar in the absorber column. The Ar concentration has a peak at -0.7 bar (second phase of emptying) and then it decreases (FIGURE 81).

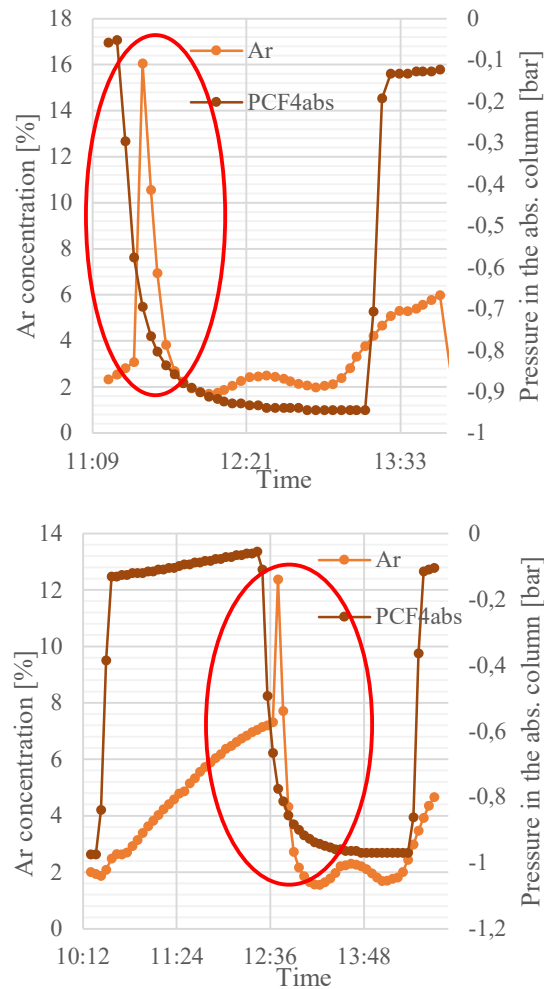


FIGURE 81: Focus on the Ar [%] trend vs pressure in the absorber column.

The first part of the trend is probably due to the motion of the gas in the buffer in which Ar cannot reach the stability, while the second part of the trend is characterized by an oscillation of the Ar concentration because of the column emptying and mixing of components in the buffer.

The peak of Ar concentration at the absorber pressure of ~ -0.7 bar is probably due to a big quantity of Ar released after the fast pressure decreasing in the column.

To better understand the trend of Ar, the possible effects of the system (as valves or leaks) on the Ar trend and to quantify the content of Ar in the CF_4 recuperated, analyses of the recuperated gas in the battery used for the mixer injection were performed and they will be explained in the next paragraph.

5.4 Analysis of the recuperated CF₄ contained in the storage batteries

The analyses of the gas in the batteries were performed with the μ GC (Paragraph 2.3 Gas Analysis with Gas Chromatograph) for monitoring the quality of the recuperated CF₄ injected in the system. Below the summary of the analyses will be shown.

Analysis	Date	Ar [%]	CF ₄ [%]	CO ₂ [%]	O ₂ ppm	N ₂ ppm
1	27/01/2021	8.6	90.4	0.002	81	9053
2	16/02/2021	8.7	90.8	0.010	86	9168
3	24/02/2021	10.3	88.9	0.012	251	13205
4	20/05/2021	7.0	92.3	0.015	99	7800
5	29/06/2021	7.0	93.9	0.020	90	7377

Table 20: Overview of CF₄ storage batteries analyses performed in the last months (January – June 2021).

In Table 20 the results N₂ of analyses performed on the recuperated CF₄ in the storage batteries are shown. The analyses 1 and 2 were performed before changing the separation parameters of the CF₄ absorber module (Paragraph 5.1 CF₄ absorber module: Overview and they are characterized by high N₂ and Ar contamination that reaches the maximum value in the third analysis (10.3% of Ar and 1.3% of N₂).

The analyses 4 and 5 were performed after changing the CF₄ absorber module parameters and the difference in terms of Ar and N₂ concentration is visible: Ar decreased from ~9% to 7% and the N₂ passed from ~1% to 0.7%. These results confirm that the new CF₄ membrane module setup and the new CF₄ absorber module parameters allow to obtain purer CF₄ without affecting the CF₄ loss and the global efficiency of the system.

As a result of these analyses, the fraction of recuperated CF₄ re-injected in the CSC system was modified from 50% to 60%, also due to the large quantity of CF₄ in the storage battery.

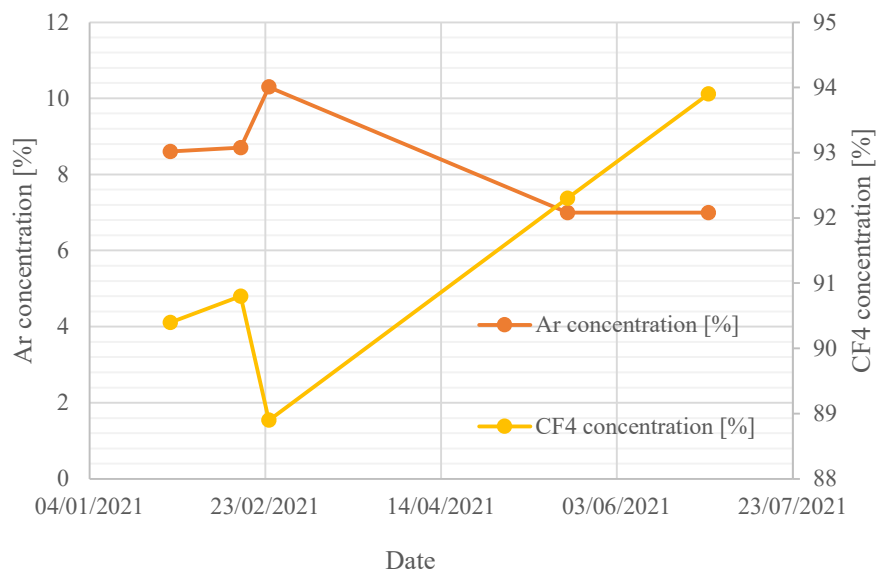


FIGURE 82: Trend of Ar and CF4 concentration vs time in the storage batteries in the period January- June 2021.

Conclusions

The experimental work presented in this thesis concerns the studies on the CF₄ recuperation system, used for the CMS CSC detector, with the final goal of optimizing the efficiency for both economic and environmental reasons. Reducing the use of GHGs is a worldwide objective to which CERN wants to contribute. The CF₄ contribution to GHG emission at CERN was about 20% during LHC Run 2 due to its use in the Cathode Strip Chambers (CSC) and Gas Electron Multiplier (GEM) detectors.

The CSC detector at the CMS experiment is a large system ($\sim 100 \text{ m}^3$) and, due to the use of the expensive and GHG CF₄ in the gas mixture (Ar/CO₂/CF₄ 40/50/10), the CF₄ recuperation plant has been developed many years ago.

The recovery system is based on warm separation process made by membranes and adsorption modules for CO₂ and CF₄. An efficient removal of the CO₂ is mandatory to reach a good CF₄ adsorption capacity, since CO₂ is easily adsorbed and more strongly retained in the CF₄ adsorption module. With these serial steps, the achieved purity of the recuperated gas can be quite high. The storage module for the recuperated CF₄ gas is made of two batteries, one used to store the recuperated gas arriving from the recuperation plant and one used for the re-injection of the recuperated gas in the CSC system. In these years, the CF₄ recuperation plant allowed significantly reducing the CSC operational cost as well as GHG emissions.

The purpose of this work was to test the membrane module and the absorber module in order to better understand the parameters affecting the proper functioning of the system and to optimize each module for increasing the total efficiency of the plant.

This work can be divided into two parts: the first part concerns the study, the characterization and the optimization of the CF₄ Membrane Module and the second part concerns the study and the optimization of the CF₄ Absorber Module.

In the first part, characterization tests were performed on each membrane of the module and some new models of membranes were also tested in order to study another module configuration. Some parameters influencing the functioning of the membranes were examined, such as the input flow stream and the pressure at the permeate side. The input, permeate and retentate streams gas analyses were performed with a μGC

while the retentate and permeate flows were measured with a flowmeter. Combining the concentration and the flow measurements, it was possible to calculate the total separation efficiency of each membrane. The tests results show that the E-type membrane (the one installed in the module but no longer in use) has a very low efficiency and it cannot be used in the system while the membrane 2, 3 of the recovery plant and the new membrane CO-C10 have a similar behaviour in the flow range tested. The highly sensitive membrane CO-C07FS has a good separation efficiency even if a big quantity of Ar permeates the membrane and consequently the recuperated CF₄ presents a high level of contamination. For this reason, this type of membrane is not the best solution for the recuperation system because it would affect the quality of the recuperated gas.

The flow test shows the dependence of the efficiency of the membranes from the feed flow and in particular, higher the feed flow (700/800 l/h) higher the efficiency in terms of CF₄ fraction recuperated

(2). Although in fact the fraction of the contaminants increases in the recuperated CF₄, it can be considered acceptable considering the very low CF₄ fraction loss in the separation process.

As result of the pressure test at the permeate side, it has been proved that lower pressure at the permeate side allows to obtain a higher CF₄ recuperated quality with a negligible loss of CF₄ fraction in the same side of the membrane. For each flow tested it has been obtained the same results: lower pressure at the permeate side, higher quality of the recuperated CF₄ at the retentate side.

Considering the current flow from the exhaust module and the test results, the best configuration of the membrane module is obtained with the two membranes CO-C10A (membranes 2 and 3) and the CO-410A membrane, in terms of recuperation efficiency and CF₄ purity at the retentate side, and a pressure at the permeate side of ~ -0.6 bar.

In the second part of this work the functioning of the CF₄ absorber module was investigated. Weekly μ GC analyses were performed for monitoring the status of the system but also to verify the effect of system's variation on the recuperation efficiency of the module. After a variation in the analyses trend, the pressure parameter controlling the column emptying was modified. At the beginning of the tests, the recuperation of the CF₄ started when the pressure in the column was about -0.7 bar. This value of pressure guaranteed the purity of CF₄ but there was a possibility that with low value of pressure,

most of the CF_4 was lost in the first phase of emptying with the contaminants releasing. Different values of pressure at which the CF_4 starts to be recuperated were tested: -0.65, -0.6, -0.55, -0.5 and -0.45 bar.

The test results show that the total efficiency of the system, calculated as the ratio of recuperated volume in the storage module and the total input volume in the system, increases at high pressure values without affecting the quality of the recuperated CF_4 .

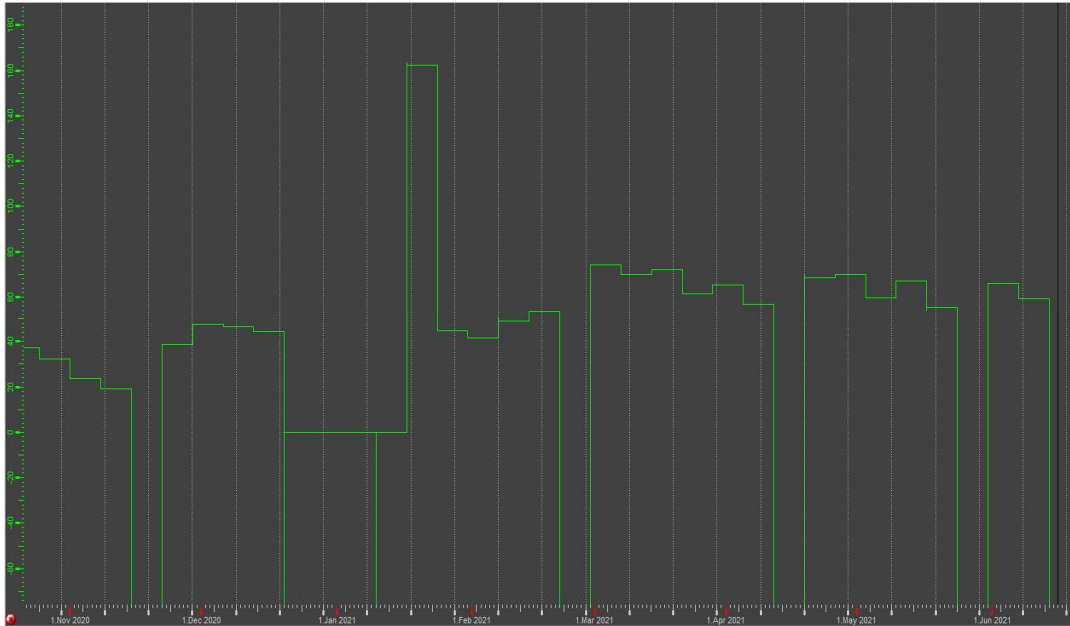


FIGURE 83: WinCCOA graph of the weekly efficiency of the CF_4 recuperation plant in the time period November-June

Finally, the new membrane module setup and the new CF_4 absorber configuration led to an increase of the total efficiency from an average weekly efficiency of $\sim 45\%$ in the period November 2020-January 2021 to an average weekly efficiency of $\sim 66\%$ in the period February-June 2021, as shown in FIGURE 83.

The analyses performed on the storage battery confirm the good results achieved: the old plant configuration provided an Ar contamination in the recuperated CF_4 of about 10%, while with the new one the Ar contamination is about 6%.

For future long-term CF_4 recuperation plant operation, it can be useful to test the membranes in series to provide purer CF_4 , in addition to new membrane technology for a better Ar and N_2 removal.

Bibliography

- [1] "CERN Accelerating Science," [Online]. Available: <https://home.cern/science/accelerators/large-hadron-collider>.
- [2] G. Martinez, "The Muon Spectrometer of the ALICE experiment," *Nuclear Physics A*, pp. 313-319, 2005.
- [3] The ATLAS Collaboration, G. Aad and E. Abat, "The ATLAS Experiment at the CERN Large Hadron Collider," *Journal of Instrumentation*, 2008.
- [4] P. Paolucci, "The CMS Muon system," CMS-CR-2006-006, Geneva, CERN, 2005.
- [5] A. A. Alves Jr and al, "Performance of the LHCb muon system," *JINST*, 2013.
- [6] F.Sauli, " "Gaseous radiation detectors: fundamentals and applications", " Vol. 36, Cambridge University Press.
- [7] W. L. Hosch, "Britannica," [Online].
- [8] M. Corbetta, "Studies on Gas Mixture and Gas Recirculation Effects on GEM " "Studies on Gas Mixture and Gas Recirculation Effects on GEM," 2018.
- [9] Buchtela and G. Steinhauser, ""Gas Ionization Detectors.", " in *Handbook of Radioactivity Analysis, Academic*.
- [10] "PROFIBUS and PROFINET International," [Online]. Available: <https://www.profibus.com/>.
- [11] The CMS Collaboration, "The CMS experiment at the CERN LHC," *Journal of Instrumentation, Volume 3*, 2008.
- [12] Y.Assran and A.Sharma, "Transport Properties of operational gas mixtures used at LHC," Suez Canal University, Suez, Egypt; CERN CH1211 Geneve, Switzerland.
- [13] M. Corbetta, "Studies on Gas Mixture and Gas Recirculation Effects on GEM Detectors Operation," in *Journees de Rencontres Jeunes Chercheurs*, 2018.
- [14] M. Corbetta, "Development of Gas System for Gaseous Detector Operation at HL-LHC," Geneve, CERN, 2021.
- [15] R. Guida, M. Corbetta, B. Mandelli and G. Rigoletti, "Strategies for reducing the use of greenhouse gases from particle detectors operation at the CERN LHC

- experiments," in *40th International Conference on High Energy physics - ICHEP2020*, Prague, Czech Republic (virtual meeting), 2020.
- [16] R. Guida and B. Mandelli, "R&D strategies for optimizing greenhouse gases usage in the LHC particle detection systems," *Nuclear Instruments and Methods in Physics Research Section A: Accelerators, Spectrometers, Detectors and Associated Equipment*, vol. Volume 958, 2020.
- [17] R. Guida, M. Capeans and B. Mandelli, "Strategies for reducing the environmental impact of gaseous detector operation at the CERN LHC experiments," *Nuclear Instruments and Methods in Physics Research A*, vol. 845, pp. 253-256, 2016.
- [18] S. Colafranceschi, L. Benussi and other, "Performance of the Gas Gain Monitoring system of the CMS RPC muon detector and effective working point fine tuning," *Journal of Instrumentation*, vol. Volume 7, 5 December 2012.
- [19] M. Capeans, R. Guida, S. Haider and F. Hahn, "Commissioning of the CF4 recuperation plant for the Cathode Strip Chambers detector at the CERN Compact Muon Solenoid experiment," in *2011 IEEE Nuclear Science Symposium Conference Record*, Valencia, Spain, 2011.
- [20] C. Anderson and V. Barashko, "Effect of gas composition on the performance of Cathode Strip Chambers for the CMS Endcap Muon System," *CMS Note*, 2004.
- [21] A. Wisecarver, "Gas Mixture Longevity Studies for the CMS Cathode Strip Chambers in Preparation for HL-LHC," in *2019 APS Meeting of the Division of Particles & Fields*, 2019.
- [22] B. Mandelli, "The CF4 Recuperation Plant for the Cathode Strip Chambers Detectors at the CMS experiment," 2012.
- [23] S. Dildick and CMS Collaboration, "Upgrade of the CMS Cathode Strip Chambers for the HL-LHC," in *ICHEP2020*, 2020.
- [24] X. Zhang, "Sensitivity Characteristic Analysis of Adsorbent-Mixed Carbon Nanotube Sensors for the Detection of SF6 Decomposition Products under PD Conditions," PubMed, 2013.
- [25] S. Sridhar, S. Bee and S. Bhargava, "Membrane-based Gas Separation: Principle, Applications and Future Potential.," *Chemical Engineering Digest.*, 2014.

- [26] M. Mazzotti, M. Gazzani, F. Milella and P. Gabrielli, "MEMBRANE SEPARATIONS - RATE CONTROLLED SEPARATION PROCESSES," Swiss Federal Institute of Technology Zurich, Zurich, 2016.
- [27] F. Bazzarelli, L. Giorno and E. Piacentini, "Dense Membranes," *Encyclopedia of Membranes*, 2016.
- [28] M. Mulder, Basic Principles of Membrane Technology, Dordrecht, The Netherlands, 1996.
- [29] X. Y. Che, N. Tien-Binh, S. Kaliaguine and D. Rodrigue, "POLYIMIDE MEMBRANES FOR GAS SEPARATION: SYNTHESIS, PROCESSING AND PROPERTIES," in *Polyimides*, Clyde Murphy, 2017.
- [30] MesaLabs, "DryCal by MesaLabs," [Online]. Available: https://drycal.mesalabs.com/wp-content/uploads/sites/5/2013/12/Defender_510_520.8.5x11-Rev-G.pdf.
- [31] E. P. Favvas and F. K. Katsaros, "A review of the latest development of polyimide based membranes for CO₂ separations," *Reactive and Functional Polymer*, vol. 120, pp. 104-130, 2017.
- [32] F. F., T. F., B. A., D. E. and B. G., "POLYIMIDE HOLLOW FIBER MEMBRANES FOR CO₂ SEPARATION FROM WET GAS MIXTURES," *Brazilian Journal of Chemical Engineering*, vol. 31, pp. 1023 - 1034, 2014.
- [33] R. T. Yang, Gas separation by adsorption processes, Boston: Imperial College Press, 1997.
- [34] L. Mondello, Gas Cromatografia, Una introduzione, Messina.
- [35] M. Maccarrone, "Metodologie biochimiche e biomolecolari," Zanichelli editore, 2019.
- [36] CERN, "CERN Accelerating Science," [Online]. Available: <https://cms.cern/detector/detecting-muons/muon-drift-tubes>.
- [37] E. Altuntas, "Long-term study of optimal gas purifiers for the RPC systems at," CERN, Geneva, 2012.
- [38] T. Wenzel, "Chemistry, LibreTexts," 9 July 2020. [Online]. Available: <https://chem.libretexts.org>.

- [39] T. Bernardi, "IMPIEGO DELLA MODERNA CROMATOGRAFIA PLANARE STRUMENTALE PER LO STUDIO DELL' AFFINITA' DI *Bifidobacterium adolescentis* MB239 PER DIVERSI SUBSTRATI GLUCIDI," Bologna, 2008.
- [40] A. G. P. Barron and R. Andrew, "Principles of Gas Chromatography," 2014.
- [41] Agilent Technologies, Fundamentals of Gas, 2002.

Acknowledgements

Al termine di questo lavoro di tesi ci tengo a ringraziare le persone che hanno reso possibile la realizzazione di tutto ciò.

In primis ci tengo a ringraziare la Professoressa Antonella Profumo, non solo per la professionalità e disponibilità che ho avuto modo di apprezzare sin dal mio primo giorno presso l'ateneo Pavese, ma soprattutto per avermi dato la possibilità di fare un'esperienza formativa come quella che ha dato origine a questo lavoro e per avermi seguito in ogni passo lungo questo percorso.

Ringrazio poi il Dott. Roberto Guida e la Dott.ssa Beatrice Mandelli, senza i quali niente di tutto ciò sarebbe stato possibile. La vostra passione e dedizione sono state per me fonte d'ispirazione, nonché insegnamento per affrontare ogni problema con spirito critico e curiosità. Vi ringrazio per avermi fornito tutti gli strumenti necessari per comprendere un mondo che mi era prima sconosciuto.

Un ringraziamento speciale lo rivolgo a Mara, per essere stata sempre presente nei momenti di difficoltà e per avermi seguita in ogni mio passo insegnandomi tutto. Ringrazio anche Gianluca, Federico, Demetrio, Fabio per avermi fatto sentire a casa sin dal primo giorno, perché senza di voi questa esperienza non sarebbe stata così bella.

Ringrazio mia madre e mio padre, non solo per avermi permesso di realizzare ogni mio sogno, ma per avermi spronato ad essere la versione migliore di me stessa, per avermi insegnato ad essere libera, indipendente e responsabile senza mai lasciarmi la mano. Vi ringrazio perché, seppur tra le tante difficoltà che abbiamo incontrato lungo la strada, non avrei mai potuto desiderare genitori migliori di voi.

Voglio ringraziare Dario, la persona che più mi conosce e mi sopporta in questo mondo, il tuo aiuto e il tuo sopporto mi hanno permesso di credere in me stessa e nelle mie possibilità, con la consapevolezza di non essere mai sola. Ti ringrazio perché mi accontenti sempre e realizzi ogni mio desiderio, facendomi sentire amata.

Ringrazio Chiara, l'amica più sincera che io abbia mai avuto, perché mi conosci e con tanta pazienza accetti tutti i miei difetti. Grazie perché cerchi di farmi vedere sempre il lato positivo delle cose ed anche in questi mesi lontane mi hai ascoltato e consolato quando ne avuto bisogno.

Infine, ringrazio tutta la mia famiglia, Vittorio e soprattutto i miei nonni, perché so quanto siete orgogliosi e felici di vedermi realizzare i miei sogni.